

Redox chemistry, solubility and hydrolysis of uranium in dilute to concentrated salt systems

Zur Erlangung des akademischen Grades eines
DOKTORS DER NATURWISSENSCHAFTEN
(Dr. rer. nat.)

der KIT-Fakultät für Chemie und Biowissenschaften
des Karlsruher Instituts für Technologie (KIT)

genehmigte

DISSERTATION

von

MSc. Nese Cevirim-Papaioannou

aus

Afyonkarahisar, Türkei

KIT-Dekan:	Prof. Dr. Reinhard Fischer
Referent:	Prof. Dr. Horst Geckeis
Korreferent:	Prof. Dr. Petra Panak

Tag der mündlichen Prüfung: 18.07.2018

Erklärung

Hiermit versichere ich, dass ich die vorliegende Arbeit selbständig verfasst und keine anderen als die angegebenen Quellen und Hilfsmittel verwendet habe. Darüber hinaus versichere ich, dass alle Stellen der Arbeit, die wörtlich oder sinngemäß aus anderen Quellen übernommen wurden, als solche kenntlich gemacht sind und die elektronische Version der Arbeit mit der schriftlichen übereinstimmt und dass die Arbeit in gleicher oder ähnlicher Form noch keiner Prüfungsbehörde vorgelegt wurde. Die Satzung des Karlsruher Instituts für Technologie (KIT) zur Sicherung guter wissenschaftlicher Praxis wurde in der jeweils gültigen Fassung beachtet.

Datum, Ort

Unterschrift

Acknowledgments

First and foremost, I would like to show my appreciation to my advisor, Prof. Dr. Horst Geckeis for trusting me and giving me the opportunity to work with him at the Institute for Nuclear Waste Management (INE) of the Karlsruhe Institute of Technology (KIT). I am very pleased to have gained precious experiences on state-of-art scientific research during my PhD studies.

I am deeply grateful for Dr. Marcus Altmaier, the head of the Radiochemistry Unit at KIT-INE for encouraging me with his support, suggestions and contributions. I appreciate his positive attitude and all the fruitful scientific discussions we have had which has made my PhD experience unique.

I especially would like to express my deepest gratitude and appreciation to my direct supervisor, Dr. Xavier Gaona, for his time despite his extremely tight schedule, his support from the very beginning, his endless patience, kindness and guidance throughout my PhD studies. I am and will always be honoured to have worked with such a great mentor and brilliant scientist.

I would like to thank my dear friend and supervisor Dr. Ezgi Yalcintas very much, for helping me to overcome every difficulty. I am sure we have had the best time that a team could ever have had.

I would like to thank Melanie Böttle for her technical support and also her lovely personality. I would also like to thank all the members of the Aquatic Chemistry and Thermodynamics group, especially Dr. Agost Gyula Tasi and Dr. David Fellhauer for their support, help when needed, and all the constructive discussions.

I am thankful to the German Ministry of Economic Affairs and Energy (BMWi) for funding my PhD study within the framework of the EDUKEM project under the contract number 02E11334.

My sincere thanks to all of my colleagues, especially Dr. Kathy Dardenne and Dr. Joerg Rothe for their support in XANES/EXAFS measurements and XAFS data evaluation at INE- and CAT-ACT beamlines KIT synchrotron source. To Ms. Corneila Walschburger and Mrs. Frank Geyer for ICP-MS measurements. To Ms. Sylvia Moisei-Rabung for ICP-OES measurements, Ms. Eva Soballa and Dr. Dieter Schild for SEM-EDS measurements, Stefanie Kraft for TG-DTA measurements and Dr. Nicolas Finck for his support in XRD measurements. I would like to thank the Radiation Protection group of INE, especially Mr. Gehrard Christill for making the work with radioactivity much easier and also for his friendliness.

I would like to thank all of my friends who live in different parts of the world for walking beside me no matter where they are. Many thanks to my friends in Karlsruhe for making me feel home. My biggest and deepest thanks to my dear parents Betul & Mustafa Cevirim and my dear sister Ebru Dogandemir for their unconditional love and trust. My lovely nephew, Batu Dogandemir for reminding me that we should keep doing our best for a better world, and my beloved husband, Dimitrios Papaioannou for being a constant source of support, and for his endless love and patience.

Abstract

Uranium is the main element present in spent nuclear fuel and accordingly contributes with the largest mass inventory to the nuclear waste. In spite of uranium being a relatively minor contributor to the overall radiological dose of the waste, it is certainly required to have an accurate knowledge on the solution chemistry and solubility phenomena of this key element. Uranium is also a redox-sensitive actinide, and accordingly its chemical behavior is strongly dependent on the redox boundary conditions of the system. Disposal of spent fuel in deep geological formations such as crystalline/granite, clay and rock salt is the option favored by international consensus. Water intrusion is a possible scenario that needs to be accounted for in the context of the long-term Safety Assessment of these repositories. The composition of the pore water contacting the waste will largely vary depending upon host-rock, backfill and other technical barriers, as well as the waste itself. Although a vast number of studies have previously investigated the solution chemistry of uranium, a number of key uncertainties remain. These affect to redox behavior, solid phases controlling solubility and hydrolysis, especially in the alkaline to hyperalkaline pH conditions of relevance in the context of nuclear waste disposal.

U(IV) and U(VI) are the most stable oxidation states of uranium controlling its solution chemistry and solubility within the stability field of water and in the absence of strong complexing ligands. The study of this redox couple in the alkaline reducing conditions relevant in certain concepts for waste disposal (*e.g.* cementitious) is challenged by the further stabilization of U(VI) in the hyperalkaline pH-region, and the high sensitivity of U(IV) towards oxidation in the presence of traces of oxygen. Accordingly, an adequate knowledge of uranium redox chemistry in the aqueous and solid phases under geochemical boundary conditions (pH, p_e , ionic strength, etc.) relevant in the context of nuclear waste disposal is important for a correct assessment of the long-term safety. For this reason, **the redox chemistry of uranium in the presence of various reducing chemical systems in dilute to concentrated NaCl solutions is investigated in acidic to hyperalkaline pH conditions**, and the results summarized in Chapter 3 of this PhD thesis. The kinetics of the reduction of U(VI) to U(IV), as well as the effect of the type and concentration of the reducing system are investigated by systematic measurements of the pH_m (with $pH_m = -\log [H^+]$ in molal units), p_e and U concentrations until attaining equilibrium conditions. Complete reduction of U(VI) to U(IV) is observed in most of the cases within the boundary conditions $(p_e + pH_m) \leq 4$, although reduction kinetics are strongly impacted by $[U(VI)]_0$, pH_m , type and concentration of the reducing system and NaCl concentration. In (oversaturated) alkaline NaCl systems, solubility data and XANES indicate

that the reduction proceeds via fast precipitation of $\text{Na}_2\text{U}_2\text{O}_7 \cdot \text{H}_2\text{O}(\text{cr})$, which slowly transforms into a $\text{UO}_2(\text{am, hyd})$ solid phase. In less favourable conditions, the completion of this process required ≈ 635 days. These results also preclude the predominance of the U(IV) anionic hydrolysis species $\text{U}(\text{OH})_5^-$ and $\text{U}(\text{OH})_6^{2-}$ below $\text{pH}_m \approx 14.5$, previously reported in the literature. Experimental data obtained within this PhD thesis indicate that previous observations reported in the literature can be possibly explained by insufficient equilibration time. Furthermore, this study confirms the key role of U(IV) in controlling the solubility and solution chemistry of uranium in reducing, alkaline systems.

Very reducing conditions are expected to develop after the closure of underground repositories for nuclear waste disposal due to the anoxic corrosion of steel and iron components. As demonstrated in Chapter 3, U(IV) is expected to control the solubility and aqueous speciation of uranium under these very reducing conditions over a broad range of pH and background electrolyte concentrations. In spite of this, key uncertainties still affect the solution chemistry of U(IV), in particular with regard to the properties of the oxo-hydroxide/s solid phases forming, the aqueous speciation in alkaline to hyperalkaline pH conditions, as well as the formation and stability of U(IV) “intrinsic colloids”. In this context, Chapter 4 of this PhD thesis focuses on the investigation of the **solubility and hydrolysis of U(IV) in reducing, dilute to concentrated NaCl, MgCl₂ and CaCl₂ solutions**. A very thorough solid phase characterization including XRD, SEM-EDS, quantitative chemical analysis, EXAFS and TG-DTA confirms that a (nano-)crystalline phase, $\text{UO}_2 \cdot \text{H}_2\text{O}(\text{ncr})$, is responsible for the control of the solubility of U(IV) in the investigated conditions. The systematic investigation of the solubility of this solid phase in dilute to concentrated, acidic to hyperalkaline pH_m conditions allows deriving comprehensive chemical, thermodynamic and SIT activity models for the system $\text{U}^{4+}-\text{Na}^+-\text{Mg}^{2+}-\text{Ca}^{2+}-\text{H}^+-\text{Cl}^- -\text{OH}^- -\text{H}_2\text{O}(\text{l})$. The investigation of supernatant solutions in solubility experiments without the use of phase separation methods gives also insight on the colloidal fraction in “equilibrium” with $\text{UO}_2 \cdot \text{H}_2\text{O}(\text{cr})$. Although a systematically increased uranium concentration (*ca.* 2–3 \log_{10} -units) is observed with respect to 10 kD ultrafiltered samples, a clear trend to decreasing $[\text{U}]_{\text{aq}}$ with longer equilibration times is also indicated in solubility experiments within $t \leq 200$ days. Hence, the contribution of U(IV) “intrinsic colloids” to the solubility is evident in all salt systems investigated in this work, but the long-term stability of such species remains unclear.

Uranium is mostly found as U(VI) under mildly reducing to oxidizing conditions. In the close vicinity of spent nuclear fuel surfaces, radiolysis effects can also promote the formation of

U(VI) even in the presence of $H_2(g)$. Under alkaline pH conditions and in the absence of complexing ligands (*e.g.* carbonate, phosphate, silicate), the solubility of U(VI) is expectedly controlled by M–U(VI)–OH uranate solid phases (with M = Na, K, Ca, among others). In contrast to Ca- and Na-uranates, very little is known on the solubility of K–U(VI)–OH phases in spite of the abundance of K^+ in many types of groundwaters and, in particular, the key role of this alkali ion in cementitious systems. In this context, Chapter 5 of this PhD is dedicated to the study of **U(VI) solubility in alkaline, dilute to concentrated KCl solutions**. Comprehensive solubility experiments with systematic variation of pH_m and ionic strength, in combination with an extensive solid phase characterization (XRD, SEM–EDS, quantitative chemical analysis, TG-DTA) resulted in thermodynamic and activity models for the system UO_2^{2+} – K^+ – Na^+ – H^+ – Cl^- – OH^- – $H_2O(l)$. Sensitivity analysis conducted using this updated thermodynamic model confirms that K- and Na-uranates ($K_2U_2O_7 \cdot 1.5H_2O(cr)$ and $Na_2U_2O_7 \cdot H_2O(cr)$, respectively) are responsible of controlling the solubility of U(VI) under boundary conditions defined by cementitious systems. The absence of these solid phases in the corresponding thermodynamic databases leads to a very large overestimation (2 – $6 \log_{10}$ -units, depending upon pH_m and alkali concentration) of U concentration in the underlined conditions. This work provides improved fundamental understanding of uranium solution chemistry, including redox processes, solubility phenomena and hydrolysis of both +IV and +VI redox states. Thermodynamic constants derived in the standard state and (SIT) ion interaction coefficients obtained can be implemented in thermodynamic databases and used in geochemical calculations under a variety of boundary conditions. This covers dilute to concentrated salt systems, thus allowing thermodynamic calculations under conditions representative of the different host-rocks foreseen for repositories for nuclear waste disposal, from crystalline and clay to salt-rock.

Table of Contents

Acknowledgments	i
Abstract	iii
1 Introduction	1
1.1 Background of the work	1
1.2 Basic knowledge and aquatic chemistry of uranium	3
1.2.1 Fundamental chemistry of uranium.....	3
1.2.2 Uranium redox chemistry	5
1.2.2.1 Definition of redox equilibrium	5
1.2.2.2 Redox chemistry of uranium.....	7
1.2.3 Solubility and hydrolysis.....	10
1.2.3.1 Solubility and hydrolysis reactions: definition and equilibrium constants .	10
1.2.3.2 Activity models	13
1.2.3.3 Solubility and hydrolysis of U(IV) in the absence of complexing ligands .	14
1.2.3.4 Solubility and hydrolysis of U(VI) in the absence of complexing ligands .	19
1.3 Thermodynamic data selection of uranium	22
1.4 Aim of the present work	26
2 Experimental	29
2.1 Chemicals and analytical work.....	29
2.1.1 Chemicals	29
2.1.2 ²³⁸ U	30
2.1.3 pH measurements	30
2.1.3.1 pH measurements in saline solutions	32
2.1.4 pH measurements in this work	33
2.1.5 <i>E_h</i> measurements	34
2.1.6 Determination of total concentration and redox speciation of uranium in aqueous systems	35
2.1.6.1 Inductively coupled plasma mass spectrometry (ICP-MS).....	35
2.1.6.2 Solvent extraction (SX).....	36
2.1.7 Solid phase characterization.....	36
2.1.7.1 X-Ray diffraction	36
2.1.7.2 Quantitative chemical analysis.....	37
2.1.7.3 Scanning electron microscopy with energy dispersive X-Ray spectroscopy (SEM-EDS)	37
2.1.7.4 Thermogravimetric-differential thermal analysis (TG-DTA).....	37

2.1.8	X-ray absorption near edge structure (XANES) and extended X-Ray absorption fine structure (EXAFS) spectroscopy.....	38
2.1.8.1	Sample preparation	38
2.1.8.2	XANES/EXAFS measurements.....	39
2.1.8.3	Data evaluation	40
2.2	Uranium redox experiments in the presence of reducing agents.....	40
2.3	U(IV) solubility experiments.....	42
2.3.1	U(IV) solid phase preparation	42
2.3.2	Sample preparation.....	43
2.4	U(VI) solubility experiments in KCl solutions.....	47
2.4.1	U(VI) solid phase preparation	47
2.4.2	Sample preparation.....	47
3	Redox chemistry of uranium in reducing systems	51
3.1	Reduction of U(VI) in 0.1 and 5.0 M NaCl solutions using a Sn(II) redox buffer....	51
3.2	Reduction of U(VI) in 0.1 M NaCl solutions using a Na ₂ S ₂ O ₄ redox buffer	56
3.3	Reduction of U(VI) in 0.1 M NaCl solutions using a Sn(II) + TiO ₂ redox buffer.....	58
3.4	Reduction of U(VI) in 0.1 M NaCl solutions using Sn(II) + Fe(0) and Sn(II) + Fe ₃ O ₄ (cr) redox buffers	59
3.5	Redox speciation of uranium in the aqueous and solid phases.....	62
3.5.1	Solvent extraction.....	62
3.5.2	XANES analysis.....	63
3.6	Discussion of kinetic aspects of U(VI) reduction to U(IV) and comparison with literature data	66
4	Solubility and hydrolysis of U(IV) in reducing, dilute to concentrated NaCl, MgCl₂ and CaCl₂ solutions	71
4.1	Solubility data of U(IV) in reducing, dilute to concentrated NaCl, MgCl ₂ and CaCl ₂ solutions.....	71
4.1.1	Solubility data of U(IV) in reducing, dilute to concentrated NaCl solutions.....	71
4.1.2	Solubility data of U(IV) in reducing, dilute to concentrated MgCl ₂ solutions...	77
4.1.3	Solubility data of U(IV) in reducing, dilute to concentrated CaCl ₂ solutions....	79
4.2	U(IV) solid phase characterization	81
4.2.1	XRD, SEM-EDS, quantitative chemical analysis and TG-DTA.....	81
4.2.2	EXAFS	87
4.3	Chemical, thermodynamic and SIT activity models of the system U ⁴⁺ -Na ⁺ -Mg ²⁺ -Ca ²⁺ -H ⁺ -OH ⁻ -Cl ⁻ -H ₂ O(l)	90
4.3.1	Application of the thermodynamic model derived to CaCl ₂ systems	95
4.3.2	Systematic trends on An(IV) solubility: new insights arising from the present work	96

5 Solubility and hydrolysis of U(VI) in alkaline, dilute to concentrated KCl solutions	103
5.1 U(VI) solubility in dilute to concentrated KCl–KOH solutions.....	103
5.2 Solid phase characterization	106
5.3 Chemical, thermodynamic and SIT activity models for the system UO_2^{2+} – H^+ – K^+ – Na^+ – Cl^- – OH^- – $\text{H}_2\text{O}(\text{l})$	111
5.3.1 Thermodynamic data derived using U(VI) solubility experiments in alkaline, dilute to concentrated KCl solutions	111
5.3.2 Re-evaluation of $\log^* K_{s,0}^{\circ}\{1/6 \text{K}_2\text{U}_6\text{O}_{19}\cdot 11\text{H}_2\text{O}(\text{cr})\}$ (compreignacite) in 1 m KCl reported in the literature.....	113
5.3.3 Summary of the improved thermodynamic model for the system UO_2^{2+} – H^+ – K^+ – Na^+ – Cl^- – OH^- – $\text{H}_2\text{O}(\text{l})$	115
5.3.4 Role of ternary Na-U(VI)-OH and K-U(VI)-OH solid phases in cementitious systems	118
6 Summary and conclusions	121
References	125

1 Introduction

1.1 Background of the work

Radioactive waste is generated in a number of anthropogenic activities, including production of nuclear energy, medical applications, nuclear research or production / dismantling of nuclear weapons, among others. Radioactive waste contains highly toxic radioactive elements including long-lived isotopes, which need to be handled very carefully and disposed of safely to isolate from humans and the environment for a very long time. With regard to radioactive waste generated in the context of nuclear energy production, uranium (^{235}U and ^{238}U), plutonium and minor actinides (^{239}Pu , ^{237}Np , ^{241}Am , etc.) generated by neutron capture of ^{238}U , as well as fission (^{99}Tc , ^{79}Se , ^{135}Cs , ^{129}I , etc.) and activation products (^{14}C , ^{36}Cl , ^{59}Ni , etc.) deserve special attention.

The internationally favored option for the disposal of radioactive waste involves the use of deep underground repositories, which are designed in deep underground geological formations especially crystalline, clay and rock salt. Different geological formations feature different properties with regard to heat conductivity and resistance, permeability, strength, deformation, dissolution and absorption behaviour, etc., which are thoroughly evaluated in the context of nuclear waste disposal. Crystalline formations are characterized by their stability, low heat sensitivity and very low solubility. However, they are prone to become fractured which may facilitate the transport of radionuclides [1]. The known favorable properties of argillaceous rock (clay, claystone) for hosting repositories are in particular the very low permeability, low solubility and high sorption capacity. On the other hand, underground repositories in clay formations require additional reinforcement during the construction phase [1]. Rock salt is highly impermeable to gases and liquids, has very high heat conductivity and visco-plastic properties that enable underground cavities to seal up. Nevertheless, it expectedly shows lower intrinsic retention capacities due to weaker sorption properties*.

The concept of multi-barrier systems is usually considered in the context of nuclear waste disposal to minimize the potential radionuclide release and mobilization into the biosphere. The first barrier is the fuel itself, which is sealed by corrosion-resistant metallic cladding (Zircaloy

* Sorption on rock salt is usually considered negligible, although recent studies at KIT-INE have shown that strong sorption on other minerals can also be observed in highly saline environments.

or stainless steel) materials. The spent nuclear fuel is placed in the waste canister made from iron inserted stainless steel or copper. The canisters are encased by engineered barriers with very significant properties like mechanical stability, high sorption capacity, etc. depending on the host-rock formation and type of waste. The geological formation where the repository is constructed is considered as the final barrier preventing the mobilization of the radionuclides into the biosphere.

Water intrusion is one of the scenarios that are considered in the Safety Assessment of repositories for radioactive waste disposal. This scenario can lead to aqueous systems interacting with the waste. The composition of such aqueous systems is highly dependent on the geochemical boundary conditions, and is mostly given by the groundwater and host rock formation, technical barriers and construction materials (*e.g.* cement), the canister and the waste itself. This imposes a variety of boundary conditions, which range from dilute systems (in granite and most repository concepts in clay) to concentrated brines ($I > 5 \text{ mol}\cdot\text{kg}^{-1}$, containing mainly Na^+ , Mg^{2+} , K^+ , Cl^- and SO_4^{2-} and lower concentrations of Ca^{2+} , HCO_3^- , F^- and Br^-) as those expected in salt-rock-based repositories [2-5]. Note that although the composition of granitoids and argillities pore waters are usually characterized by low ionic strength ($I < 0.1 \text{ mol}\cdot\text{kg}^{-1}$), formation waters with intermediate ionic strengths are also found in some sedimentary bedrocks such as Canadian Shield [6] and Cretaceous argillites in Northern Germany [7]. Cementitious materials are used for the stabilization of the waste (especially for low- and intermediate level wastes), for the construction of vaults containing the waste (in some concepts also for high-level waste) and for general construction purposes. In the early degradation phase of cement (stage I), K_2O and Na_2O dissolve buffering the pH at ≈ 13.3 , setting also relatively high concentrations of Na and K (0.1 – 0.2 M). In the degradation stage II and after washing out the alkali content of cement, portlandite ($\text{Ca}(\text{OH})_2$) buffers the porewater composition at $\text{pH} \approx 12.5$ and $[\text{Ca}]_{\text{tot}} \approx 20 \text{ mM}$. The non-congruent dissolution of calcium silicate hydrates (C-S-H phases) with Ca:Si ratio 0.8 – 1.5 controls the porewater composition of cement in the degradation stage III, buffering the pH within $10 \leq \text{pH} \leq 12.5$ [8-11].

Reducing conditions are expected to develop after the closure of the repository due to the anoxic corrosion of iron and steel components present in the repository and consequent generation of hydrogen. Such reducing conditions can importantly affect the chemical behavior of redox-sensitive radionuclides, which accordingly needs to be thoroughly evaluated. The corrosion of metallic Fe results in the formation of secondary phases such as magnetite and green-rust, which

can actively participate in redox phenomena but offer also surfaces potentially participating in the sorption / retention of radionuclides.

1.2 Basic knowledge and aquatic chemistry of uranium

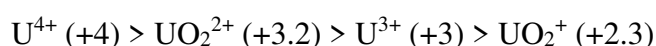
1.2.1 Fundamental chemistry of uranium

Uranium was discovered in 1789 by the German chemist Martin Heinrich Klaproth who named this element after the planet “Uranus” [12]. At the beginning, the only significant use of uranium was to color the glasses and ceramics. In 1896, Henri Becquerel noticed a penetrating radiation emitted by a uranium salt, $K_2UO_2(SO_4)_2(s)$. In 1939, Otto Hahn and Fritz Strassmann discovered the nuclear fission of uranium with the support of Lise Meitner [13]. The use of nuclear power began in 1942 with the first self-sustaining nuclear chain reaction of natural uranium in the first nuclear reactor, “Chicago Pile-1”, which was assembled at University of Chicago by the team lead by Enrico Fermi [14].

Uranium ($Z= 92$) is the heaviest natural element present on earth with an electronic configuration of $[Rn] 5f^36d^17s^2$. In the periodic table, it is located in the actinides series (An), between protactinium (Pa) and plutonium (Pu). The most abundant uranium mineral is uraninite (UO_2). However, a large number of other uranium minerals are known resulting from the interaction with other metal cations and inorganic ligands depending on the geological environment (*e.g.* autunite $Ca(UO_2)_2 \cdot 10-12H_2O$, clarkeite $(Na,K)_{2-2x}(Ca,Pb)_xU_2O_7 \cdot yH_2O$, saleeite, $Mg(UO_2)_2(PO_4)_2 \cdot 8-10H_2O$, coffinite $U(SiO_4)_{1-x}(OH)_{4x}$, among many others) [15]. In aqueous systems, uranium can be found in four oxidation states: U(III), U(IV), U(V), U(VI). +VI and +IV are known to be the most stable oxidation states of uranium. While U(III) and U(IV) can exist in acidic solutions as aquo-ions, U^{3+} and U^{4+} , U(V) and U(VI) form the oxocations UO_2^+ and UO_2^{2+} due to the strong attraction of oxygen atoms by the highly charged hypothetical bare cations and formation of stable covalent bondings [16-18]. Although U(V) disproportionates rapidly to U(IV) and U(VI), it is stabilized in the presence of strong complexing ligands such as carbonate [19, 20] or some chelating ligands [21-24]. U(VI) is predominating under mildly reducing and oxidizing conditions. In the absence of other complexing ligands, its solubility is mostly controlled by $UO_3 \cdot 2H_2O(cr)$ and $M-U(VI)-OH(s)$ solid phases with $M = Na^+, K^+, Ca^{2+}$, under acidic and alkaline conditions, respectively. It

hydrolyses strongly forming polymeric species in acidic conditions where U(VI) shows enhanced solubility. Monomeric anionic hydrolysis species dominate in near-neutral to hyperalkaline pH conditions. U(IV) prevails under strongly reducing systems and forms sparingly soluble $\text{UO}_2(\text{s})$, under weakly acidic to alkaline conditions. The aquo-ion U^{4+} is only stable in very acidic conditions and readily hydrolysis at $\text{pH} \geq 1$.

The solution chemistry of a given element is strongly dependent on its oxidation state. Uranium (and actinides in general) are hard Lewis acids that tend to interact strongly with hard Lewis bases such as hydroxide or carbonate. Accordingly, the magnitude of this ionic interaction is mostly affected by the charge of the metal cation (z). In the case of uranium and because of the actinyl moieties formed by U(V) and U(VI), the effective charge (Z_{eff}) provides a more accurate representation of the complexation strength with a given ligand [18] (Z_{eff} provided in brackets):



For a given oxidation state of uranium, the strength of the complexes forming with different ligands can be qualitatively classified as [17]:

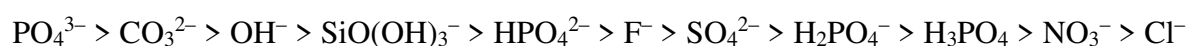


Table 1.1 shows the ionic radii and the most common coordination numbers of hexavalent and tetravalent uranium complexes as summarized by Shannon [25].

Each metal complex or compound has a specific coordination chemistry depending on the number, type and arrangement of the ligands as well as the central metal atom properties. Therefore, coordination chemistry of uranium shows a great variety due to its several different oxidations states and the relatively large size of the respective cations, which allows accommodating a large number of ligands. Note however that the geometries of U(V) and U(VI) complexes / compounds are in most of the cases constricted by the linear actinyl moiety. Hence, U(VI) compounds usually show pentagonal [26, 27], hexagonal [28-30] and square bipyramidal [31-33] coordination geometries. Some uranates and oxides are known to have distorted octahedral or pentagonal pyramidal structures [34, 35]. The U^{4+} coordination geometries tend to be more variable due to its relatively large ionic radii and the less restricted coordination sphere. There are reported structures as octahedron [36], triangular dodecahedron [37], and pentagonal bipyramid [38] for U^{4+} compounds [35]. Note that Table 1.1 does not show some exceptional coordination numbers described in the literature (*e.g.* CN = 2 for U(VI) [25]).

Table 1.1 Coordination numbers and corresponding ionic radii reported in Shannon [25] for U(IV) and U(VI).

Oxidation State	Coordination	Ionic Radii [Å]
4	VI	0.89
	VII	0.95
	VIII	1
	IX	1.05
6	VI	0.73
	VII	0.81
	VIII	0.86

All isotopes of uranium are unstable, and decay via emitting α particles. In the environment, uranium isotopes are present mainly as ^{238}U (99.27 %, $t_{1/2} \sim 4.47 \cdot 10^9$ y), ^{235}U (0.72 %, $t_{1/2} \sim 7.04 \cdot 10^8$ y) and a very small amount of ^{234}U (0.0054 %, $t_{1/2} \sim 2.46 \cdot 10^5$ y). The fissile ^{235}U is generally used as nuclear fuel and, accordingly, uranium is a very relevant part of the so-called “nuclear fuel cycle”. Resulting from its contribution in different steps of the “nuclear fuel cycle”, uranium needs to be disposed of as one of the main components of high level waste (HLW, e.g. matrix in spent nuclear fuel), but also as a part of low- and intermediate wastes (L/ILW). Therefore, an accurate knowledge of the solution chemistry of uranium is of great importance for a correct, comprehensive assessment on the behaviour of the waste under repository-relevant conditions.

1.2.2 Uranium redox chemistry

1.2.2.1 Definition of redox equilibrium

The mobility and migration behaviour of a radionuclide in a deep geological repository is strongly dependent on its solubility, aqueous speciation (including complexation) and sorption properties. In this frame, the oxidation state plays a very important role due to its direct impact on these three phenomena. Redox reactions are defined as electron transfer reactions between oxidized and reduced counterparts. The equilibrium reaction of a half-cell is generally defined as:



The Nernst equation is related to the reduction potential of an electrode (half-cell), explaining the correlation of the redox potential for a medium of interest (E), and the redox potential under standard conditions (E°) according to the equation:

$$E = E^\circ + \frac{RT}{nF} \ln\left(\frac{a_{\text{ox}}}{a_{\text{red}}}\right) \quad (1.2)$$

where n is number of electrons exchanged in the electrochemical reaction, R is universal gas constant, T is the temperature in Kelvin and F is the Faraday constant.

The electrode potential is identified as redox potential and is quoted as E_h . E_h values refer to the standard hydrogen electrode (SHE) potential, which is used as reference on half-cell potential reactions and equals zero per definition. For a given system, the redox potential quantifies the tendency of the system to gain/lose electrons. The redox potential can be also defined as the negative logarithm of electron activity:

$$pe = -\log a_{e^-} \quad (1.3)$$

The relationship between pe and E_h values is given in equations (1.4) and (1.5) (at $T = 25^\circ\text{C}$):

$$E_h = -\frac{RT}{nF} \ln(a_{e^-}) \quad (1.4)$$

$$pe = 16.9E_h[\text{V}] \quad (1.5)$$

The stability field of different redox species can be evaluated using systematized pH- E_h measurements of an aqueous system in combination with *Pourbaix* (predominance) diagrams. In such diagrams, the predominance area of different (redox) species are separated by (redox) borderlines calculated as 50:50% distribution between two species. These borderlines are calculated using equilibrium constants for the corresponding chemical reactions at standard state or in a given medium. The borders of water reduction and oxidation are also calculated and provided in *Pourbaix* diagram to constrain the region of interest / relevance in aqueous systems, although in specific cases experimentally measured redox potentials in aqueous system may overcome these upper and lower limits (for a given period of time).

The reduction to $\text{H}_2(\text{g})$ and oxidation to $\text{O}_2(\text{g})$ define the lower and upper stability limits of water, respectively, according to the reactions:



with the equilibrium constants:

$$\log K^\circ(\text{red}) = 0.5 \log P(\text{H}_2(\text{g})) + \text{pH} + \text{pe} = 0 \quad (1.8)$$

$$\text{pH} + \text{pe} = -0.5 \log P(\text{H}_2(\text{g})) \quad (1.9)$$

and

$$\log K^\circ(\text{ox}) = 0.25 \log P(\text{O}_2(\text{g})) - 0.5 \log a_w - \text{pH} - \text{pe} = -20.77 \quad (1.10)$$

$$\text{pH} + \text{pe} = 20.77 + 0.25 \log P(\text{O}_2(\text{g})) - 0.5 \log a_w \quad (1.11)$$

where a_w is the activity of water and P is the partial pressure. Since the $P(\text{H}_2(\text{g})) = 1$ bar and $P(\text{O}_2(\text{g})) = 1$ bar, the upper and lower limits of water are calculated from Eq (1.9)-(1.10) as $(\text{pe} + \text{pH}) = 0$ and $(\text{pe} + \text{pH}) = 20.77$, respectively, at $T = 25^\circ\text{C}$ and $I = 0$.

The “redox neutral line” [39] for redox-neutral solutions in the absence of reducing and oxidizing agents can be theoretically calculated as:



$$\log K^\circ = \log P(\text{H}_2(\text{g})) + 0.5 \log P(\text{O}_2(\text{g})) = -41.55 \quad (1.13)$$

with hypothetical partial pressures of $\log P(\text{H}_2(\text{g})) = -27.6$ and $\log P(\text{O}_2(\text{g})) = -27.9$ equivalent to $(\text{pe} + \text{pH}) = 13.8$. This definition is analogous to a pH-neutral aqueous solution at $\text{pH} = 7$, with $[\text{H}^+] = [\text{OH}^-] = 10^{-7}$ M (at $I = 0$, with $\text{p}K_w^\circ = 14$). The redox potentials of inert background solutions (NaCl, HCl, NaOH, etc.) under Ar atmosphere are usually close to this “redox neutral line” in pe-pH diagrams [39]. The redox neutral line is often included in the *Pourbaix* diagrams, providing insight on the oxidation / reducing character of a given system.

1.2.2.2 Redox chemistry of uranium

Considering the great impact of the oxidation state on the solution chemistry of the early actinides, the investigation of uranium redox chemistry is of high interest from the perspective of fundamental research, but also in view of the relevant role of uranium as matrix in most of the HLW to be directly disposed of in deep geological repositories.

The thermochemical database (TDB) project of the Nuclear Energy Agency (NEA) [40, 41] provides the most extensive and accurate thermodynamic data selection available for uranium, which includes thermodynamic quantities of redox reactions, solubility phenomena, hydrolysis

and complexation. Figure 1.1 shows the *Pourbaix* diagrams of uranium calculated for $I = 0.1$ M NaCl and $[U]_{\text{tot}} = 3 \cdot 10^{-5}$ M, a) indicating only aqueous species and b) including also solid phases. Calculations are performed using thermodynamic data reported in NEA-TDB [40, 41], complemented with data reported in Neck and Kim (2001) [42] and Altmaier *et al.* (2017) [43] for U(IV) and U(VI), respectively (see also Table 1.2 and 1.3). Both figures give a clear insight on the multifold and complex solution chemistry of uranium.

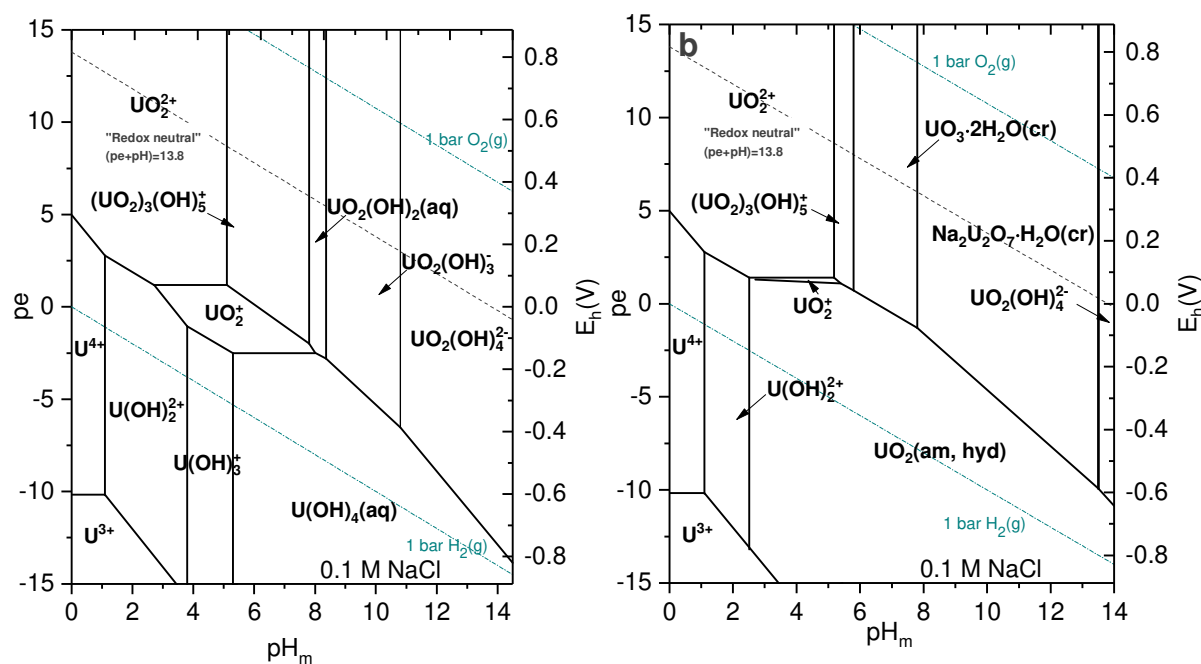


Figure 1.1. Pourbaix diagrams of uranium calculated for $I = 0.1$ M NaCl and $[U]_{\text{tot}} = 3 \cdot 10^{-5}$ M considering a. only aqueous species of uranium, and b. including solid phases forming. Calculations are performed using thermodynamic data reported in NEA-TDB, Neck and Kim (2001) and Altmaier *et al.*, 2017. Black lines correspond to the 50:50 distribution borderlines between different species. The dark cyan and grey dash lines indicate the borders of water oxidation, water reduction, and redox neutral line. Precipitation of $UO_3 \cdot 2H_2O(cr)$, $Na_2U_2O_7 \cdot H_2O(cr)$ and $UO_2(am, hyd)$ is allowed in calculations in Figure a, accordingly resulting in the variation of $[U]_{aq}$ as a function of $(pe + pH_m)$.

U(IV) has been scarcely investigated due to the difficulties in retaining the oxidation state (especially under hyperalkaline conditions), the formation of the sparingly soluble $UO_2(s)^\dagger$ phase limiting the application of many experimental techniques, as well as the strong impact of the solid phase properties (particle size, degree of hydration, surface alteration, crystallinity) on

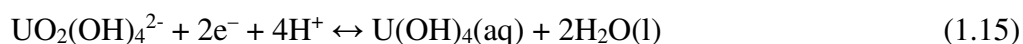
[†] A generic notation for solids, (s), is used here. This accounts for the different degrees of crystallinity of the solids used in the solubility experiments, ranging from amorphous (am) to crystalline (cr) and very likely including colloidal phases (col).

solubility. Such challenges are likely behind the discrepant results reported in many of the solubility studies using $\text{UO}_2(\text{s})$, especially under alkaline conditions [5, 42, 44-52].

The formation of anionic hydrolysis species of U(IV) ($\text{U}(\text{OH})_5^-$ and $\text{U}(\text{OH})_6^{2-}$) at $\text{pH} > 12$ is reported in some studies [44-46, 52], due to the increase of [U] concentrations under alkaline conditions. On the other hand, a larger number of experimental studies support the predominance of $\text{U}(\text{OH})_4(\text{aq})$ from weakly acidic to hyperalkaline conditions [42, 47, 49, 53]. It appears thus unclear whether the increase in solubility in the former studies corresponds to the formation of anionic hydrolysis species of U(IV), or can be rather attributed to redox processes, *e.g.* oxidative dissolution of $\text{UO}_2(\text{s})$. The NEA-TDB update book [41] disregarded the selection of tetravalent $\text{U}(\text{OH})_5^-$ and $\text{U}(\text{OH})_6^{2-}$, but large uncertainties were assigned to thermodynamic quantities of $\text{U}(\text{OH})_4(\text{aq})$ due to the scattered data in the alkaline pH region.

Indeed, partial oxidation in experiments with U(IV) has been reported in some cases due to the increasing trend of U concentration under alkaline conditions. This is in spite of the use of reducing systems in most of the studies, including $\text{H}_2(\text{g})$, $\text{Na}_2\text{S}_2\text{O}_4$, Zn, Fe(0), EuCl_2 , hydrazine, among others [47, 49, 51-56]. This behaviour is possibly related to the decreased stability field of U(IV) with increasing pH, as shown in Figure 1.1.

The reduction of U(VI) to U(IV) requires a rearrangement of the primary coordination sphere in combination with the multielectron transfer between two structurally different moieties, see reactions (1.14) and (1.15) [18, 57-59]. Multielectron transfer processes are known to be affected by slow kinetics [60], which accordingly should be also expected for redox transformations between U(VI) and U(IV).



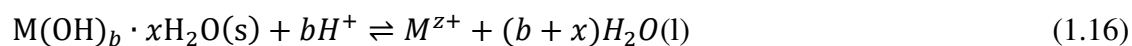
Because of the presence of hydrogen expected under repository conditions as a result of the anoxic corrosion of iron, a number of studies were carried out to assess the reduction behaviour of U(VI) in the presence of carbonate and $\text{H}_2(\text{g})$ [61, 62]. In these experiments, $\text{UO}_2(\text{s})$ was either initially present, or introduced to the system containing U(VI) after at a given time. A decrease of the U(VI) concentration ($\approx 8 \cdot 10^{-6}$ M) was observed only when $\text{UO}_2(\text{s})$ was present, thus supporting the partial reduction of U(VI) to U(IV). The authors concluded that the surface of $\text{UO}_2(\text{s})$ was responsible of activating / catalysing the redox reaction, which did not occur in the presence of $\text{H}_2(\text{g})$ but absence of this solid phase.

Several studies reported on U redox chemistry in the presence of iron-containing materials. Among others, the reduction of U(VI) to U(IV) in the presence of magnetite (Fe₃O₄) was widely investigated. This type of studies is motivated by the identification of magnetite as one of the main corrosion products of iron under reducing conditions [63-72]. Diverging observations were reported, including fast and complete reduction [69-71], partial reduction with slow kinetics [64, 65, 67, 73, 74], or even no reduction to U(IV) [63]. Such variation in the experimental results can be rationalized by the strong impact of several factors on the reducing capacity of Fe₃O₄, namely pH, composition of ionic media, presence of oxidants (*e.g.* traces of O₂), initial concentration of uranium and the ratio Fe(II)/Fe(III) in magnetite (ideally 0.33) [68]. The reduction of U was also investigated in the presence of zero valent iron based upon its reducing properties (Fe(0) ⇌ Fe²⁺ + 2e⁻), which resulted in a reductive precipitation [75] or partial reduction [76, 77] to U(IV). Note that most of the studies have been performed under near-neutral pH-range, leaving aside the alkaline to hyperalkaline pH conditions of relevance in cementitious systems.

1.2.3 Solubility and hydrolysis

1.2.3.1 Solubility and hydrolysis reactions: definition and equilibrium constants

For an adequate quantitative description of the solution chemistry of a given actinide system, it is necessary to derive thermodynamic constants related to solid-aqueous phase equilibria, complexation reactions and ion interaction processes that represent the actinide solubility and aqueous speciation of the given actinide. In general terms, the solubility of metal hydroxides/oxides are defined according to the dissolution equilibrium with a conditional solubility constant, $K'_{s,(x,y)}$ in a selected medium (ionic strength) and a solubility constant, $K^{\circ}_{s,(x,y)}$ at standard state ($I = 0$). When the dissolution equilibrium occurs between the solid and the bare, non-hydrolyzed cation of the metal (M^{z+}), the equilibrium constant is defined as $K'_{s,0}$ at $I > 0$ and $K^{\circ}_{s,0}$ at $I = 0$. This solubility equilibrium can be described according to:



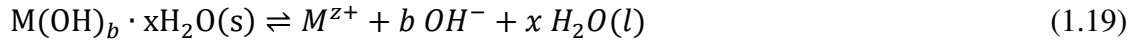
with

$$\log {}^*K'_{s,0} = \log [M^{z+}] - b \log [H^+] \quad (1.17)$$

and

$$\log {}^*K'_{s,0} = \log {}^*K'_{s,0} + \log \gamma_{M^{z+}} + (b+x) \log a_w - b \log \gamma_{H^+} \quad (1.18)$$

or



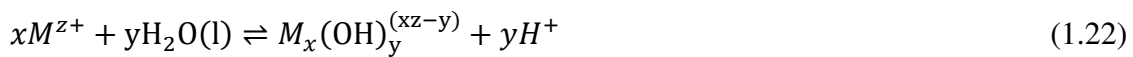
with

$$\log K'_{s,0} = \log [M^{z+}] + b \log [OH^-] \quad (1.20)$$

and

$$\log K'_{s,0} = \log {}^*K'_{s,0} + \log \gamma_{M^{z+}} + x \log a_w + b \log \gamma_{OH^-} \quad (1.21)$$

In the absence of complexing ligands, hard Lewis acids such as actinides tend to react with water to accordingly form hydrolysis species. The formation reactions of hydrolysis species can be described involving the participation of $H^+/H_2O(l)$ or OH^- , and considering the reaction $H_2O(l) \rightleftharpoons H^+ + OH^-$ with $pK'_w = 14$. The hydrolysis constants ${}^*\beta'_{(x,y)}$ referring to formation constant in a given medium and ${}^*\beta^\circ_{(x,y)}$ to standard state conditions are defined by:



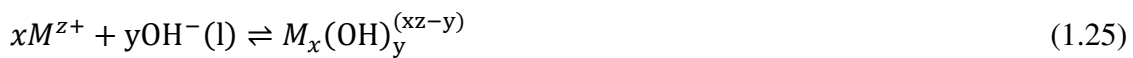
with

$$\log {}^*\beta'_{(x,y)} = \log [M_x(OH)_y^{(xz-y)}] + y \log [H^+] - x \log [M^{z+}] \quad (1.23)$$

and

$$\log {}^*\beta^\circ_{(x,y)} = \log {}^*\beta'_{(x,y)} + \log \gamma_{M_x(OH)_y^{(xz-y)}} + y \log \gamma_{H^+} - x \log \gamma_{M^{z+}} - y \log a_w \quad (1.24)$$

or



with

$$\log \beta'_{(x,y)} = \log [M_x(OH)_y^{(xz-y)}] - y \log [OH^-] - x \log [M^{z+}] \quad (1.26)$$

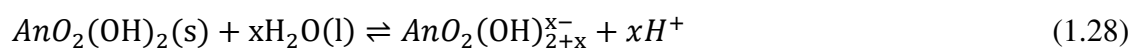
and

$$\log \beta^\circ_{(x,y)} = \log \beta'_{(x,y)} + \log \gamma_{M_x(OH)_y^{(xz-y)}} - y \log \gamma_{OH^-} - x \log \gamma_{M^{z+}} \quad (1.27)$$

where γ_i is the activity coefficient of a species i and a_w is the water activity. The value of $K'_{s,(x,y)} / K^\circ_{s,(x,y)}$, namely the dissolution equilibrium between the solid and a hydrolyzed aqueous species of the metal can be calculated as the sum of the hydrolysis constant $\beta'_{(x,y)} / \beta^\circ_{(x,y)}$ and the solubility constant $K'_{s,0} / K^\circ_{s,0}$.

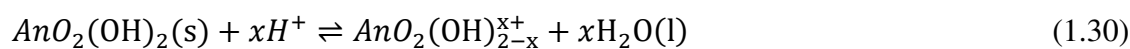
Conditional solubility constants, $K'_{s,(x,y)}$, are determined experimentally in a given medium. The extrapolation of $\log^* K'_{s,(x,y)}$ (or $\log K'_{s,(x,y)}$) to the standard state ($I = 0$) allows to derive the solubility constant $\log^* K^{\circ}_{s,(x,y)}$ (or $\log K^{\circ}_{s,(x,y)}$) whilst gaining insight in the ion interaction coefficients of the charged aqueous species prevailing in solution. Along this PhD thesis, the specific ion interaction theory (SIT) model is used for activity corrections (see section 1.2.3.2). SIT is also the model favored within the NEA-TDB project [41].

The trend (slope) followed by the solubility curve of a given metal cation with varying pH can be evaluated to gain insight on the stoichiometry of the prevailing equilibrium reaction. For example, according to reactions (1.28) and (1.30) corresponding to the equilibrium between a typical hexavalent actinide solid phase and hydrolysis species, a given number of H^+ will be exchanged as a function of the aqueous speciation:



$$\log[AnO_2(OH)_{(2+x)}^-] = -x \log[H^+] + \log^* K'_{(1,2+x)} \quad (1.29)$$

and



$$\log[AnO_2(OH)_{(2-x)}^+] = x \log[H^+] + \log^* K'_{(1,2-x)} \quad (1.31)$$

Considering the Eq (1.29) and Eq (1.31), the experimental data (as measured An total concentration) is expected to follow a well-defined slope as a function of pH ($y = mx + n$, where $y = \log[AnO_2(OH)_{(2-x)}^+]$ and $x = \log[H^+]$) if the following conditions are fulfilled:

- thermodynamic equilibrium has been attained;
- the solid remains unaltered along the investigated pH-range;
- only one species prevails in the aqueous phase;
- solubility experiments are performed under the principle of constant activity coefficients.

If this principle is fulfilled, conditional equilibrium constants can be correctly described assuming only concentration terms and ignoring any activity coefficient. For this purpose, a constant (and sufficiently high) background electrolyte concentration must be used in the experiments.

If the four conditions above apply, the slope of the solubility curve corresponds to the number of exchanged protons in the solubility reaction. This is a necessary information for the definition of the chemical model defining a given aqueous system, and thus a key contribution in the development of correct thermodynamic and activity models.

1.2.3.2 Activity models

Activity models based on the Debye-Hückel theory are used for the recalculation of the thermodynamic data obtained in systems with $I > 0$ to the standard state ($I = 0$). The Debye-Hückel term only accounts for electrostatic, non-specific long-range interactions between ions of opposite charge. On the other hand, short range, non-electrostatic interactions are important in the case of concentrated ionic media. The Debye-Hückel expression can be accordingly extended with ionic strength-dependent terms. Pitzer and SIT (specific ion interaction theory) two of the most commonly used methods for ionic strength corrections based on the extended Debye-Hückel theory. Pitzer is very accurate for highly concentrated systems and applicable to single and mixed electrolytes, at the cost of requiring many fitting / input parameters. The SIT method is favored in the present study and can be used for the correction of the ionic strength effects up to $I = 3.5$ m [78]. Recent studies have reported the successful application of SIT to very high concentrations of background electrolyte, *e.g.* concentrated MgCl_2 and CaCl_2 systems with $I_m \approx 15$ mol·kg⁻¹ [79-81], however this should be seen as an exception to the rule.

SIT model

The specific ion interaction theory [82] is the method adopted by the NEA–TDB [40, 41] for the correction of ion interaction processes and ionic strength effects for the systems at $I > 0$. The basic formulism in SIT considers:

$$\log y_j = -z_j^2 D + \sum_k \varepsilon(j, k, I_m) m_k \quad (1.32)$$

with

$$D = \frac{A\sqrt{I_m}}{1+Ba_j\sqrt{I_m}} \quad (1.33)$$

where z_j is the charge of the ion j , D is the Debye-Hückel term, m_k is the molality of the oppositely charged ion k , and $\varepsilon(j, k, I_m)$ is the specific ion interaction parameter. A and B in the

Debye-Hückel terms are temperature and pressure dependent constants, whereas a_j is an ion size parameter for the hydrated ion j . At 25°C and 1 bar, the terms A and Ba_j have a value of $0.509 \text{ kg}^{0.5} \cdot \text{mol}^{-0.5}$ and $1.5 \text{ kg}^{0.5} \cdot \text{mol}^{-0.5}$, respectively. The ionic strength is expressed as:

$$I = 1/2 \sum m_i z_i^2 \quad (1.34)$$

The Debye-Hückel term in SIT accounts for electrostatic, non-specific long-range interactions that prevail in dilute systems. At higher concentrations of background electrolyte, the term $\sum_k \varepsilon(j, k, I_m) m_k$ represents short range, non-electrostatic interactions that consider also differences between ions of the same charge but different size.

1.2.3.3 Solubility and hydrolysis of U(IV) in the absence of complexing ligands

U(IV) is characterized by a low solubility and strong hydrolysis. Figure 1.2 exemplifies the solubility of $\text{UO}_2(\text{am, hyd})$ (thick solid line in the figure) and underlying hydrolysis scheme (thin solid lines in the figure) calculated using thermodynamic data summarized in Table 1.2. Although most of the available experimental studies support the predominance of the neutral hydrolysis species $\text{U}(\text{OH})_4(\text{aq})$ from weakly acidic to hyperalkaline pH conditions, the formation of the anionic hydrolysis species $\text{U}(\text{OH})_5^-$ and $\text{U}(\text{OH})_6^{2-}$ (dashed lines in Figure 1.2) is also proposed in a number of studies. Note that the amphoteric character (formation of cationic and anionic hydrolysis species) has not been confirmed for any other An(IV). This section summarizes the main experimental and theoretical studies available in the literature dealing with U(IV) solubility and hydrolysis.

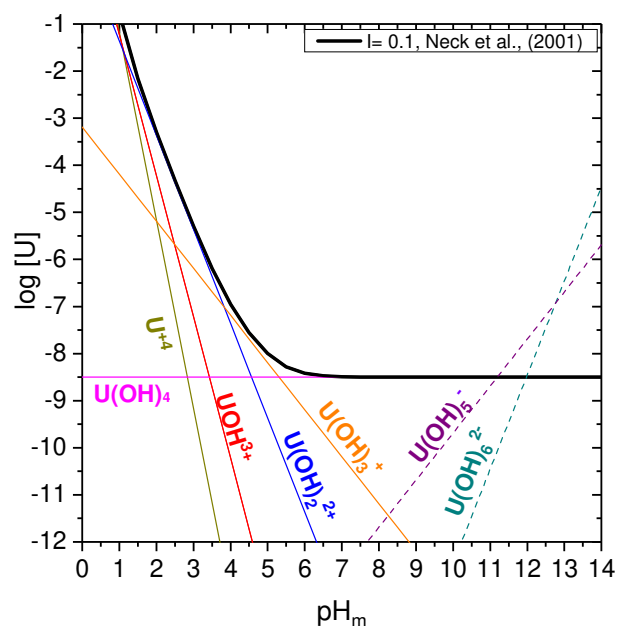


Figure 1.2. Solubility curve of $UO_2(am,hyd)$ and underlying hydrolysis scheme calculated at $I = 0$ using thermodynamic data available in the literature (see text) [41, 42]. Dashed lines correspond to $U(OH)_5^-$ and $U(OH)_6^{2-}$ species as calculated using thermodynamic data reported by Fujiwara *et al.* (2005) [52]. Intrinsic colloids are not considered.

Kraus and Nelson (1950) [83] performed a spectroscopic study on the hydrolysis of U(IV) in acidic solutions. The authors reported that U^{4+} predominates in very acidic solutions (1 M $HClO_4$), whereas UOH^{3+} was observed under less acidic conditions ($\sim 10^{-3}$ M $HClO_4$). The hydrolysis constant of UOH^{3+} derived in this study ($\log^* \beta_{(1,1)}^\circ = -0.54 \pm 0.06$) was later selected in the NEA-TDB [40, 41]

Gayer and Leider (1957) [44] studied the solubility of U(IV) from undersaturation conditions. The authors used a freshly precipitated solid phase, $U(OH)_4(s)$, whose solubility was investigated under alkaline conditions (up to 0.63 M NaOH) in the absence of reducing systems. The increase in solubility observed with increasing NaOH concentration was interpreted as with the formation of the anionic species $H_3UO_4^-$. Galkin and Stepanov (1960) [45] performed undersaturation solubility experiments with $U(OH)_4(s)$ within a larger range of NaOH concentrations (up to 7.0 M) in order to confirm the accuracy of the results derived by Gayer and Leider [44]. Consistent solubility data were obtained to the previous ones [44] up to 1.0 M NaOH. At higher hydroxide concentrations, the authors observed a slight decrease in the concentration of uranium, which was attributed to the transformation of $U(OH)_4(s)$ into $NaH_3U^{IV}O_4(s)$. The solubility of $UO_2(s)$ was investigated by Tremaine *et al.* (1981) [46] at

different temperatures (25 – 300 °C) under alkaline conditions set by LiOH. The experiments were performed in a flow system in the presence of H₂(g) to prevent the oxidation of U(IV) to U(VI). A lower solubility limit ($\sim 10^{-7}$ M) was obtained at pH = 12.5 and T = 25 °C compared to the solubility data reported by Gayer and Leider [44], even though Tremaine and co-workers determined by XPS analysis a surface composition of the solid phase controlling the solubility as U(VI)/U(IV) = 0.2. Above pH \approx 12.5, the authors observed an increase of the solubility that was attributed to the formation of the anionic species U(OH)₅⁻.

Ryan and Rai (1983) [47] performed an oversaturation solubility study with U(IV) in the alkaline pH range in the presence of Na₂S₂O₄ and Zn as reducing systems. The reported solubility data was about 10⁻⁸ M, at least four orders of magnitude lower than the results determined by Gayer *et al.* [44]. Thus, no evidence on the formation of anionic hydrolysis species was obtained in this study. The solubility of amorphous and crystalline UO₂(s) was studied by Bruno *et al.* (1986) [56] in NaClO₄ solutions in the pH range 2 to 10. The measured solubility was approximately 10⁻⁴ M at 5.5 \leq pH \leq 10, as high as reported previously by Gayer and Leider [44] and Galkin and Stepanov [45]. The authors explained the difference between their results and those obtained by Ryan and Rai [47] with the differences in the crystallinity of the used solid phases. Parks and Pohl (1988) [49] investigated the solubility of UO₂(cr) at 1.0 \leq pH \leq 10.4 in dilute NaCl solutions (up to 0.1 M), at elevated T (100–300 °C) and P (500 bar H₂). The authors observed a steep decrease in the solubility with pH in very acidic solutions (pH < 2), whereas very low and pH-independent uranium concentrations ($\approx 10^{-10}$ M) were measured at pH \geq 2. No significant dependence of the solubility on the temperature was observed either. This solubility study supports again the predominance of the neutral U(OH)₄(aq) in the pH-range investigated by the authors. Rai *et al.* (1990) [50] conducted oversaturation solubility experiments (starting from a U(IV) solution) in the presence of EuCl₂ and Fe powder to maintain the reducing conditions in a wide pH range (2 \leq pH \leq 12). A steep decrease of the solubility was observed under acidic to weakly acidic pH conditions, whereas low and pH-independent U(IV) solubility ($\sim 10^{-8}$ M) was observed in the alkaline pH range. An increasing trend of U solubility was observed for some samples in the alkaline pH range, which Rai and co-workers interpreted as the partial oxidation of U(IV) to U(VI). Yajima *et al.* [53] performed a series of undersaturation solubility experiments with UO₂(cr), and compared the results with oversaturation experiments using a U(IV) stock solution. Experiments were performed in 0.1 M NaClO₄ solutions at 2 \leq pH \leq 12. Na₂S₂O₄ was used to retain uranium in the +IV redox state. Very similar uranium concentrations were measured in both approaches in the complete pH-range investigated. Significantly low solubility ([U]_{aq} $\approx 10^{-9}$ M) was observed

under alkaline conditions. Based on their experimental observations, the authors derived a thermodynamic model including only U^{4+} and $U(OH)_4(aq)$ as aqueous species in equilibrium with $UO_2(s)$. Rai *et al.* (1997) [84] conducted undersaturation solubility experiments with freshly precipitated $UO_2(am,hyd)$ in dilute to concentrated NaCl and $MgCl_2$ solutions at $1.5 \leq pH \leq 5.5$. The authors used $EuCl_2$ and Fe powder to retain uranium as +IV redox state. Based on their experimental data, Rai and co-workers reported thermodynamic and Pitzer activity models including only the hydrolysis species UOH^{3+} and $U(OH)_4(aq)$ in the hydrolysis scheme of U(IV).

In 2001, Neck and Kim [42] published the most extensive thermodynamic data set on the solubility products and hydrolysis constants of An(IV) based on a critical review of the reported experimental studies. The authors evaluated the existing experimental $UO_2(s)$ solubility data in terms of differences in the solid phases (amorphous/crystalline and fresh/aged) and possible oxidation to U(VI). The solubility data under well-controlled reducing conditions [50, 53, 84] were selected by the authors at acidic and alkaline conditions. The selected data under weakly acidic to alkaline conditions indicate $[U]_{aq} = \sim 10^{-8} - 10^{-9}$ M according with the chemical equilibrium $UO_2 \cdot xH_2O(s) \Leftrightarrow U(OH)_4(aq) + (x-2) H_2O(l)$ at $pH > 5$ independent of the age of the solid phase and the temperature. The chemical, thermodynamic and (SIT) activity models for U(IV) were derived including the hydrolysis species UOH^{3+} , $U(OH)_2^{2+}$, $U(OH)_3^+$ and $U(OH)_4(aq)$. The authors based their selections in the available experimental data but also considering the systematics and consistency along the tetravalent actinide series. Furthermore, the authors proposed that the solubility of $UO_2(cr)$ in neutral to alkaline is controlled by an amorphous $UO_2(am, hyd)$ layer growing on the surface of $UO_2(cr)$, in contrast to the solubility control of $UO_2(cr)$ observed in acidic conditions.

Fujiwara *et al.* (2003) [52] investigated the solubility and hydrolysis of U(IV) in a combined approach using solubility experiments and solvent extraction with TTA in acidic $NaClO_4$ solutions (0.1, 0.5 and 1.0 M). The equilibrium constants reported by the authors for UOH^{3+} , $U(OH)_2^{2+}$ and $U(OH)_3^+$ are in line (within the uncertainties) with those selected in Neck *et al.* (2001). The same authors performed oversaturation solubility experiments with U(VI) in alkaline to hyper-alkaline pH conditions and using $Na_2S_2O_4$ for the in-situ reduction to U(IV), which precipitated as $UO_2(am, hyd)$ [52]. The authors observed a steep increase of the solubility above $-\log [H^+] \approx 12$, which was interpreted with the formation and predominance of anionic U(IV) hydrolysis species, namely $U(OH)_5^-$ and $U(OH)_6^{2-}$. Based on their solubility data, the

authors reported the hydrolysis constants and SIT ion interaction parameters for the indicated anionic species.

In 2010, Fellhauer *et al.* [79] investigated the hydrolysis of Np(IV) and Pu(IV) in dilute to concentrated CaCl₂ solutions. Based on the steep increase of the solubility at pH_m above ≈ 11 , the authors reported the formation of the ternary complex Ca₄[An(OH)₈]⁴⁺ and determined the corresponding equilibrium constant and (SIT, Pitzer) ion interaction coefficients. Combining these data with the previous study by Altmaier and co-workers with Th(IV) [81, 85], the authors estimated the equilibrium constant for the complex Ca₄[U(OH)₈]⁴⁺ using linear free energy relationships (LFER).

The formation and stability of the hyperstoichiometric phase UO_{2+x}(s) has been investigated in a number of experimental studies, especially in the context of spent fuel corrosion under anoxic and oxic conditions [55, 86, 87]. The increase of the solubility and solubility rate with increasing x or oxygen diffusion was observed in most of the cases. Note that PuO_{2+x}(s) has been reported to play a key role in the solubility and redox chemistry of Pu in the presence of traces of oxygen [39, 88-90].

On the basis of the discussion above, the most critical points to account for with regard to the solubility of U(IV) can be summarized as follows:

- The particle size/degree of the crystallinity in most of the solubility experiments with UO₂(s) remains ill-defined. Particle size is expectedly related with $\Delta_f G^\circ_m$ of the solid phase (and accordingly with its $\log^* K^\circ_{s,0}$) through the Schindler equation [91]. Such differences are qualitatively reflected in the literature with different nomenclature descriptions of the solid phase controlling the solubility, UO₂(cr), UO₂(am), UO₂(am, hyd), etc.
- Indeed, the number of hydration waters in UO₂· x H₂O(s) solid phases is rarely discussed in the literature. Although for a crystalline structure the number of hydration waters often has a minor impact on the stability of the solid phase (*e.g.* $\Delta_f G^\circ_m / \log^* K^\circ_{s,0}$), it is expectedly related to the particle size/degree of the crystallinity in amorphous phases. An accurate knowledge of this parameter can thus provide relevant information when dealing with amorphous phases.
- A pH-dependency of the surface properties was proposed by Neck and Kim [42]. For crystalline phases, although UO₂(cr) is effectively controlling the solubility in acidic conditions, experimental data tends to reach the solubility limit of UO₂(am,hyd) under

neutral to alkaline conditions. Neck and Kim (and others later on) explained these observations with the formation of an amorphous layer on the crystalline solid. The amorphous solid phase would be then responsible of the solubility-control in the alkaline pH-region.

- The amphoteric character of U(IV) involving the formation of anionic hydrolysis species under hyperalkaline pH conditions remains undefined. Controversial results indicating the predominance of either $\text{U}(\text{OH})_4(\text{aq})$ or $\text{U}(\text{OH})_5^- / \text{U}(\text{OH})_6^{2-}$ in this pH range are available in the literature.

1.2.3.4 Solubility and hydrolysis of U(VI) in the absence of complexing ligands

In the absence of complexing ligands, the solubility of U(VI) is controlled by oxo-hydroxides compounds, whose stoichiometry mostly depends upon pH and background electrolyte concentration. Metaschoepite ($\text{UO}_3 \cdot 2\text{H}_2\text{O}(\text{cr})$) is expected to control the solubility of U(VI) under acidic to near neutral pH range, whereas ternary M–U(VI)–OH solid phases form in alkaline solutions with $\text{M} = \text{Na}^+, \text{K}^+$ and Ca^{2+} [92-99]. A number of studies dealing with the solution chemistry of U(VI) under various conditions (temperature, background electrolyte, pH etc.) are available in the literature. Those studies were critically reviewed in the NEA-TDB [40, 41, 100] providing a very comprehensive knowledge on the chemical thermodynamics of solid and aqueous uranium compounds and complexes. The equilibrium constants of U(VI) hydrolysis species are selected as (n,m) (as $(\text{UO}_2)_n(\text{OH})_m^{2n-m}$): (1,1), (1,2), (1,3), (1,4), (2,1), (2,2), (2,3), (3,4), (3,5), (3,7) and (4,7) in the updated book of the NEA-TDB, based on the experimental data up to 2002. Figure 1.3 shows the solubility of $\text{UO}_3 \cdot 2\text{H}_2\text{O}(\text{cr})$ and $\text{Na}_2\text{U}_2\text{O}_7 \cdot \text{H}_2\text{O}(\text{cr})$, together with the underlying hydrolysis scheme as calculated for $I = 0.1 \text{ M}$ NaCl using currently accepted thermodynamic data. The main experimental and theoretical studies available in the literature dealing with U(VI) solubility and hydrolysis are summarized in the following.

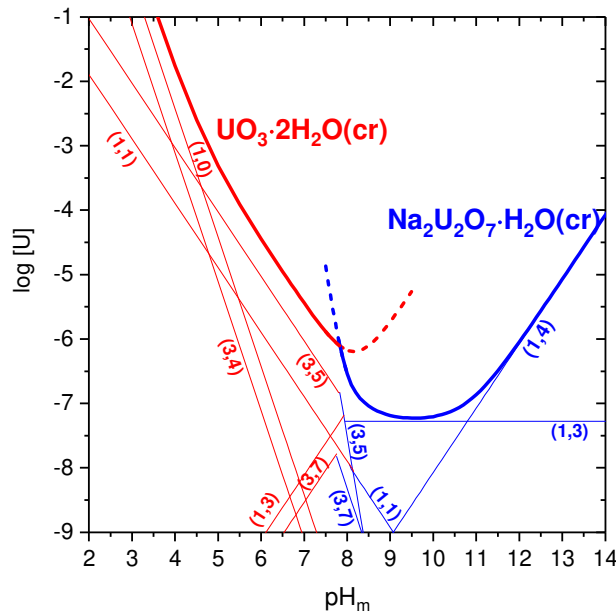


Figure 1.3. Solubility of $\text{UO}_3 \cdot 2\text{H}_2\text{O}(\text{cr})$ and $\text{Na}_2\text{U}_2\text{O}_7 \cdot \text{H}_2\text{O}(\text{cr})$ (thick red and blue lines, respectively), and underlying aqueous speciation (thin red / blue lines) calculated with thermodynamic data reported in Altmaier *et al.* [43]. Calculations performed for $I = 0.1 \text{ M NaCl}$. Change in slope of the thin (n,m) lines at $\text{pH}_m \approx 8$ are caused by the change in the solubility-controlling phase ($\text{UO}_3 \cdot 2\text{H}_2\text{O}(\text{cr})$ and $\text{Na}_2\text{U}_2\text{O}_7 \cdot \text{H}_2\text{O}(\text{cr})$), and the different stoichiometry $\text{UO}_2^{2+} : \text{OH}^-$ in both solid phases (1:2 and 1:3, respectively).

The solubility and hydrolysis of U(VI) in acidic systems has been extensively studied in the literature, possibly due to the relatively high concentrations of uranium retained in solution and the rather large number of experimental techniques available for its characterization. In combination with their own solubility and spectroscopic data in dilute to concentrated NaCl solutions, Altmaier *et al.* (2017) [43] critically reviewed the available data and proposed updated chemical, thermodynamic and (SIT) activity models for this system. On the other hand, the solubility and hydrolysis of U(VI) in near-neutral to hyperalkaline systems has been far less investigated. This is probably due to the relatively low concentration of uranium imposed by metaschoepite and ternary M-uranates in this pH-region. Consistent with previous findings reported in literature, Altmaier and co-workers reported a solubility control by $\text{Na}_2\text{U}_2\text{O}_7 \cdot \text{H}_2\text{O}(\text{cr})$ in alkaline NaCl solutions, with a solution chemistry dominated by the formation of the negatively charged species $\text{UO}_2(\text{OH})_3^-$ and $\text{UO}_2(\text{OH})_4^{2-}$. The authors reported solubility and hydrolysis constants for the formation of this solid phase and aqueous species, and provided the SIT ion interaction coefficients for the corresponding ionic species.

In contrast to NaCl-systems, the solubility and hydrolysis of U(VI) in potassium-containing systems has been far less investigated. Yamazaki *et al.* [98] studied the solubility of U(VI) following both oversaturation (starting with $\text{UO}_2(\text{NO}_3)_2$) and undersaturation approaches. Solubility samples were prepared in near-neutral to alkaline conditions at $\text{pH} = 6.4 - 12.4$, in a synthetic brine system representative of those in the WIPP repository site (1.71 M NaCl, 0.767 M KCl and 1.44 M MgCl_2 , containing also 0.044 M Na_2SO_4 , 0.011 M NaHCO_3 , 0.005 M NaBr and 0.015 M CaCl_2). After attaining equilibrium conditions, the solid phases controlling the solubility were characterized as $\text{UO}_3 \cdot 2\text{H}_2\text{O}(\text{cr})$ and $\text{K}_2\text{U}_2\text{O}_7(\text{cr})$ by XRD measurements at $\text{pH} = 8.4$ and 10.4, respectively. Sandino and Grambow [99] investigated the solubility of compreignacite ($\text{K}_2\text{U}_6\text{O}_{19} \cdot 11\text{H}_2\text{O}$) using two different initial solid phases: (i) compreignacite synthesized by reacting stoichiometric amounts of KOH with $\text{UO}_2(\text{NO}_3)_2$ first at room temperature, then exposed to 60 °C for a month to accelerate the precipitation (run K1), and (ii) $\text{UO}_3 \cdot 2\text{H}_2\text{O}(\text{cr})$ (run K2). The experiments were performed in 1 m KCl solutions at $3 \leq \text{pH} \leq 6$. After 3 months of contact time, the solid phases collected from both series were characterized as compreignacite by XRD and SEM–EDX. The solubility constants of compreignacite were determined as $\log^* K^\circ_{s,0} = (38.19 \pm 0.23)$ and $\log^* K^\circ_{s,0} = (40.53 \pm 0.21)$ from run K1 and run K2, respectively. The authors attributed the differences between the values to differences in crystallinity of the solid phases due to the use of different approaches for solid phase preparation (starting with compreignacite *vs.* solid phase transformation from $\text{UO}_3 \cdot 2\text{H}_2\text{O}(\text{cr})$). The lower solubility constant (run K2), $\log^* K^\circ_{s,0} = (37.1 \pm 0.5)$ was re-calculated and selected by NEA–TDB [41]. Gorman-Lewis *et al.* [101] investigated the solubility of compreignacite (quoted by the authors as $\text{K}_2(\text{UO}_2)_6\text{O}_4(\text{H}_2\text{O})_7$) under weakly acidic conditions at $4.3 \leq \text{pH} \leq 4.6$. The starting material was synthesized by reacting $\text{UO}_2(\text{CH}_3\text{COO})_2(\text{H}_2\text{O})_2$ and K_2CO_3 in a Teflon vial at $\text{pH} = 5$, at 373 K for 24 hours. The solid phase was characterized by using XRD, FT–IR, TGA and chemical analysis techniques before and after solubility experiments. The solid phase was identified as compreignacite, although a decrease in the degree of crystallinity was observed during the experiments. The authors derived the solubility product as $\log^* K^\circ_{s,0} = (40.5 - 1.4 / +0.2)$ in agreement with the value reported by Sandino and Grambow (1994) [99].

Besides the solubility studies conducted at room temperature, a number of calorimetric studies dealing with ternary K–U–O(cr) phases synthesized at very high T are also available in the literature. O'Hare and Hoekstra [102] synthesized $\text{K}_2\text{UO}_4(\text{cr})$ by the reaction of U_3O_8 and K_2CO_3 at $T = 1100$ K and determined the standard enthalpy of formation $\Delta H_f^\circ = -(1886.98 \pm 3.5)$ $\text{kJ} \cdot \text{mol}^{-1}$ (original value reported in $\text{kcal} \cdot \text{mol}^{-1}$) by calorimetric measurements. Cordfunke and Ouweltjes [103] determined the standard enthalpy of formation of $\text{KUO}_3(\text{cr})$, which was

synthesized by reacting UO_2 and a stoichiometric amount of K_2UO_4 at $T = 1073 \text{ K}$ in a solution containing H_2SO_4 and $\text{Ce}(\text{SO}_4)_2$. The authors reported $\Delta H_f^\circ = -(1522.9 \pm 1.6) \text{ kJ}\cdot\text{mol}^{-1}$. Fuger [104] measured the standard enthalpy of formation of a $\text{K}_2\text{U}_2\text{O}_7(\text{cr})$ phase obtained by stoichiometric reaction of uranium oxides and alkali metal (K) at high temperature, and reported $\Delta H_f^\circ = -(3250.7 \pm 4.5) \text{ kJ}\cdot\text{mol}^{-1}$.

A very comprehensive investigation on the crystal structure of potassium uranate phases with K:U atomic ratios 2.0, 1.0, 0.5 and 0.286 (*i.e.* K_2UO_4 , $\text{K}_2\text{U}_2\text{O}_7$, $\text{K}_2\text{U}_4\text{O}_{13}$ and $\text{K}_2\text{U}_7\text{O}_{22}$ compounds, respectively) was performed by Van Egmond and Cordfunke [105]. XRD diffractograms were collected for these solids during the continuous heating at $T = 700 \text{ }^\circ\text{C}$. The authors reported $\text{K}_2\text{U}_4\text{O}_{13}$ as the only stable potassium uranate phase. Besides the identified U(VI) compounds, the authors reported also the formation of a U(V) uranate (KUO_3) at low oxygen pressures.

In spite of the data summarized above, no comprehensive study dealing with the solubility of U(VI) in alkaline KCl solutions is available so far. Based on the analogy with the Na-system, the formation of ternary compounds of the like $\text{K}_2\text{U}_2\text{O}_7\cdot x\text{H}_2\text{O}(\text{cr})$ will expectedly be responsible of controlling the solubility in alkaline K-containing systems. Such phases may accordingly become relevant in cementitious systems (especially during the degradation stage I), where the porewater composition is buffered at hyperalkaline pH conditions and relatively high concentrations of potassium ($\approx 0.2 \text{ M}$).

1.3 Thermodynamic data selection of uranium

Thermodynamic calculations performed in this work for uranium are mostly based on the NEA-TDB thermodynamic selection [40, 41], which includes equilibrium constants for redox transformations, solubility, hydrolysis and complexation reactions. In some cases, this selection has been extended with available estimated data (note that NEA-TDB selection only accepts experimental data) or experimental data published after the NEA-TDB update book (released in 2003).

In the case of U(IV), the NEA-TDB selection does only include the hydrolysis species UOH^{3+} and $\text{U}(\text{OH})_4(\text{aq})$. This selection is extended in this work with the very comprehensive study by Neck and Kim on the estimation of equilibrium constants for An(IV) hydrolysis species [42]. The authors developed two estimation methods, but only the second (method B in the original

publication) provided accurate estimates for all hydrolysis species. Estimation method (B) is a semi-empirical method (developed in a previous publication by the same authors [106]), which describes the inter-ligand electrostatic repulsion for the mononuclear complexation constants $\log \beta^{\circ}_{(1,y)}$ of a certain actinide with a given ligand. Based on combination of these estimation methods, available experimental data [50, 84] and expected trends along the An(IV) series, the authors derived a complete thermodynamic model for the hydrolysis of U(IV). The authors estimated also ion interaction coefficients of charged U(IV) hydrolysis species with chloride. These estimates were obtained by correlation between ion interaction coefficients available for Cl^- and ClO_4^- , as well as considering the known values of analogous tetravalent actinides with same charge.

After the last update volume of NEA-TDB [41], Altmaier *et al.* [43] reported the equilibrium constants and ion interaction coefficients of the U(VI) solubility and hydrolysis species based on a very comprehensive experimental study in dilute to concentrated NaCl systems. The work by Altmaier and co-workers has been considered as main reference for thermodynamic calculations involving U(VI).

The formation constants and ion interaction coefficients summarized in Table 1.2 and Table 1.3 are used in this work for the thermodynamic calculations including *Pourbaix* and solubility diagrams. The data selection is mainly based on NEA-TDB [41], although extended for U(IV) and U(VI) using data reported by Neck *et al.* [42] and Altmaier *et al.* [43], respectively, as discussed above.

Table 1.2. Equilibrium constants for redox, solubility and hydrolysis reactions of uranium considered for thermodynamic calculations in the present study.

Reaction	log *K°	Reference
Redox		
$U^{4+} + e^- \leftrightarrow U^{3+}$	(9.353 ± 0.07)	[41]
$UO_2^{2+} + 4H^+ + 2e^- \leftrightarrow U^{4+} + 2H_2O(l)$	(9.04 ± 0.04)	[41]
$UO_2^{2+} + e^- \leftrightarrow UO_2^+$	(1.49 ± 0.02)	[41]
Solubility		
$UO_2(am, hyd) + 4H^+ \leftrightarrow U^{4+} + 4H_2O(l)$	(1.50 ± 1.00)	[41]
$UO_3 \cdot 2H_2O(cr) + 2H^+ \leftrightarrow UO_2^{2+} + 3H_2O(l)$	(5.35 ± 0.13)	[43]
$0.5 Na_2U_2O_7 \cdot H_2O(cr) + 3H^+ \leftrightarrow Na^+ + UO_2^{2+} + 2H_2O(l)$	(12.20 ± 0.20)	[43]
$1/6K_2U_6O_{19} \cdot 11H_2O(cr) + 7/3H^+ \leftrightarrow 1/3K^+ + UO_2^{2+} + 3H_2O(l)$	(6.7 ± 0.20)	[41, 99]
U(IV) hydrolysis		
$U^{4+} + H_2O(l) \leftrightarrow UOH^{3+} + H^+$	$-(0.40 \pm 0.20)$	[41]
	$-(0.54 \pm 0.06)$	[42]
$U^{4+} + 2H_2O(l) \leftrightarrow U(OH)_2^{2+} + 2H^+$	$-(1.10 \pm 1.00)$	[42]
$U^{4+} + 3H_2O(l) \leftrightarrow U(OH)_3^+ + 3H^+$	$-(4.70 \pm 1.00)$	[42]
$U^{4+} + 4H_2O(l) \leftrightarrow U(OH)_4(aq) + 4H^+$	$-(10.00 \pm 1.40)$	[41, 42]
U(VI) hydrolysis		
$UO_2^{2+} + H_2O(l) \leftrightarrow UO_2OH^+ + H^+$	$-(5.25 \pm 0.24)$	[41]
$UO_2^{2+} + 2H_2O(l) \leftrightarrow UO_2(OH)_2(aq) + 2H^+$	$-(12.15 \pm 0.17)$	[41]
$UO_2^{2+} + 3H_2O(l) \leftrightarrow UO_2(OH)_3^- + 3H^+$	$-(20.70 \pm 0.42)$	[43]
$UO_2^{2+} + 4H_2O(l) \leftrightarrow UO_2(OH)_4^{2-} + 4H^+$	$-(31.90 \pm 0.33)$	[43]
$2UO_2^{2+} + H_2O(l) \leftrightarrow (UO_2)_2OH^{3+} + H^+$	$-(2.70 \pm 1.00)$	[41]
$2UO_2^{2+} + 2H_2O(l) \leftrightarrow (UO_2)_2(OH)_2^{2+} + 2H^+$	$-(5.62 \pm 0.06)$	[41]
$3UO_2^{2+} + 4H_2O(l) \leftrightarrow (UO_2)_3(OH)_4^{2+} + 4H^+$	$-(11.90 \pm 0.30)$	[41]
$3UO_2^{2+} + 5H_2O(l) \leftrightarrow (UO_2)_3(OH)_5^+ + 4H^+$	$-(15.55 \pm 0.12)$	[41]
$3UO_2^{2+} + 7H_2O(l) \leftrightarrow (UO_2)_3(OH)_7^- + 7H^+$	$-(32.20 \pm 0.80)$	[41]
$4UO_2^{2+} + 7H_2O(l) \leftrightarrow (UO_2)_4(OH)_7^+ + 7H^+$	$-(21.90 \pm 1.00)$	[41]
Ternary Ca(II)–U(IV)–OH complexes		
$4Ca^{2+} + U^{4+} + 8H_2O(l) \leftrightarrow Ca_4[U(OH)_8]^{4+} + 8H^+$	$-(58.7 \pm 1.0)$	[79]

Table 1.3. SIT ion interaction coefficients (in $\text{kg}\cdot\text{mol}^{-1}$) of U(IV), U(V) and U(VI) aqua-ions and hydrolysis species in NaCl media at 25°C considered for activity corrections in the present study.

	j	$\epsilon(i,j)$	Reference
U(III) species			
U^{3+}	Cl^-	$(0.18 \pm 0.05)^a$	[41]
U(IV) species			
U^{4+}	Cl^-	(0.36 ± 0.10)	[42]
UOH^{3+}	Cl^-	(0.20 ± 0.10)	[42]
$\text{U}(\text{OH})_2^{2+}$	Cl^-	(0.10 ± 0.10)	[42]
$\text{U}(\text{OH})_3^+$	Cl^-	(0.05 ± 0.10)	[42]
$\text{Ca}_4[\text{U}(\text{OH})_8]^{4+}$	Cl^-	$-(0.01 \pm 0.10)$	[79, 85]
$\text{U}(\text{OH})_4(\text{aq})$	Na^+, Cl^-	0^b	[107]
U(V) species			
UO_2^+	Cl^-	$(0.09 \pm 0.05)^a$	[41]
U(VI) species			
UO_2^{2+}	Cl^-	(0.21 ± 0.02)	[43]
$\text{UO}_2(\text{OH})^+$	Cl^-	(0.10 ± 0.10)	[43]
$\text{UO}_2(\text{OH})_2(\text{aq})$	Na^+, Cl^-	0^a	[107]
$\text{UO}_2(\text{OH})_3^-$	Na^+	$-(0.24 \pm 0.09)$	[43]
$\text{UO}_2(\text{OH})_4^{2-}$	Na^+	(0.01 ± 0.04)	[43]
$(\text{UO}_2)_2(\text{OH})_2^{2+}$	Cl^-	(0.30 ± 0.06)	[43]
$(\text{UO}_2)_3(\text{OH})_4^{2+}$	Cl^-	$-(0.07 \pm 0.17)$	[43]
$(\text{UO}_2)_3(\text{OH})_5^+$	Cl^-	(0.24 ± 0.15)	[43]
$(\text{UO}_2)_3(\text{OH})_7^-$	Na^+	$-(0.24 \pm 0.09)$	[43]
$(\text{UO}_2)_4(\text{OH})_7^+$	Cl^-	(0.17 ± 0.18)	[43]

a. estimated considering $\epsilon(\text{M}^{z+}, \text{Cl}^-) = 0.38 \cdot \epsilon(\text{M}^z, \text{ClO}_4^-)$; b. by definition in SIT.

1.4 Aim of the present work

This PhD thesis aims at a comprehensive description of three main aspects of the solution chemistry of uranium, namely redox processes, solubility phenomena and hydrolysis. The study covers very acidic to hyperalkaline pH conditions, tackles oxidizing to very reducing chemical systems and extends from dilute to highly concentrated salt systems. Although the work is mostly intended to contribute to an improved fundamental understanding of these main aspects / processes, some of the investigated systems cover boundary conditions of high relevance in different repository concepts for nuclear waste disposal, thus providing insight on the retention and potential migration behaviour of uranium under such conditions. The combination of fundamental research with an applied character is highlighted throughout the discussion of the three main chapters of the thesis. The main objectives of this work can be summarized as follows:

- I. The redox behaviour of U(VI/IV) is investigated in 0.1–5.0 M NaCl solutions in the presence of individual and mixed reducing chemical systems. E_h , pH_m and uranium concentration were measured at periodic time intervals and evaluated using *Pourbaix* and solubility diagrams. Solid phase characterization (XANES) and aqueous speciation (XANES, solvent extraction) were also performed. This study targets the reduction process of U(VI) to U(IV), with focus on the kinetics and the role of U(VI) and U(IV) solid phases in the overall reduction process. Following the controversy in the literature on the existence of anionic hydrolysis species of U(IV), special attention is dedicated to assess the aqueous speciation under hyperalkaline conditions. As a general goal, this part of the PhD thesis aims at evaluating the reliability of ($\text{pe} + \text{pH}_m$) measurements as input for an accurate characterization of U redox distribution under conditions relevant for nuclear waste disposal (Chapter 3).
- II. The solubility of U(IV) is investigated in dilute to concentrated NaCl, MgCl₂ and CaCl₂ systems. Based on the knowledge gained in Chapter 3, Sn(II) is used to retain reducing conditions throughout the timeframe of the solubility experiments. Systematic pH_m and uranium concentration measurements were complemented with solid phase characterization (XRD, XANES/EXAFS, SEM-EDS, TG-DTA and quantitative chemical analysis). The extensive solid phase characterization aims at providing a very accurate description of the UO₂(am, hyd) solid phase controlling the solubility of U(IV)

in these conditions. The ultimate goal of this study is to derive complete chemical, thermodynamic and activity models for the system U^{4+} - Na^+ - Mg^{2+} - Ca^{2+} - H^+ - Cl^- - OH^- - $H_2O(l)$. These models can be implemented in thermodynamic databases and geochemical calculations used in the Safety Case of nuclear waste repositories (Chapter 4).

- III. The solubility of U(VI) is investigated in alkaline, dilute to concentrated KCl systems. Systematic measurements of pH_m and uranium concentration are combined with a comprehensive solid phase characterization (XRD, XANES/EXAFS, SEM-EDS, TG-DTA and quantitative chemical analysis). In combination with data available in literature, this study aims at deriving comprehensive chemical, thermodynamic and activity models for the system UO_2^{2+} - K^+ - Na^+ - H^+ - Cl^- - OH^- - $H_2O(l)$. Special focus is given to the ternary K-U(VI)-OH(s) solid phases forming in alkaline conditions, and to assess the possible role of such phases in controlling the solubility of U(VI) in cementitious systems (Chapter 5).

2 Experimental

2.1 Chemicals and analytical work

2.1.1 Chemicals

All solutions were prepared with ultrapure water purified with a Milli-Q-academic apparatus (Millipore Milli-Q Advantage A10 with Millipore Millipak® 40 0.22 µm; 18.2 MΩ·cm at 25°C, 4 ppb TOC) and purged with Ar during 1 hour before use. All sample/solid preparation steps were carried out in an Ar-glove box (< 1 ppm O₂) at $T = (22 \pm 2) ^\circ\text{C}$. The pH electrode was calibrated using pH standard buffer solutions (pH= 2-12) (Merck).

Table 2.1. List of chemicals used in this study.

Name	Chemical formula	Molar weight (g.mol ⁻¹)	Provider
1-phenyl-3-methyl-4-benzoyl-2-pyrazolin-5-one (PMBP)	C ₁₇ H ₁₄ N ₂ O ₂	278.31	Fluka (≥99.0%)
2-Amino-2-(hydroxymethyl)propan-1,3-diol (TRIZMA, TRIS)	C ₄ H ₁₁ NO ₃	121.14	Sigma-Aldrich (99.9%)
Ammonium iron(II) sulfate hexahydrate	(NH ₄) ₂ Fe(SO ₄) ₂ ·6H ₂ O	392.14	Sigma-Aldrich (99.8%)
Ammonium hydroxide	NH ₄ OH	35.05	Sigma-Aldrich (30%)
Calcium chloride -dihydrate	CaCl ₂ ·2H ₂ O	147.02	Merck (p.a.)
Calcium hydroxide	Ca(OH) ₂	74.10	Merck (p.a.)
Iron powder	Fe (10 µm)	55.85	Merck (99.5.)
Ethanol (absolute)	CH ₃ CH ₂ OH	46.07	VWR Chemicals (99.9%)
Hydrochloric acid	HCl	36.46	Merck Titrisol©
Magnesium chloride hexahydrate	MgCl ₂ ·6H ₂ O	203.30	Merck (p.a.)
Magnesium hydroxide	Mg(OH) ₂	58.32	Merck
2-(N-morpholino)ethanesulfonic acid (MES)	C ₆ H ₁₃ NO ₄ S	195.24	Sigma-Aldrich
Nitric acid (65%)	HNO ₃	63.01	Merck (suprapure) Merck (ultrapure)
Potassium chloride	KCl	74.55	Merck (EMSURE®)
Potassium hydroxide	KOH	56.11	Merck Titrisol©
Sodium chloride	NaCl	58.44	Merck (p.a.)
Sodium dithionite	Na ₂ S ₂ O ₄	174.11	Merck (>87%)
Sodium hydroxide	NaOH		Merck Titrisol©
Tin(II) chloride	SnCl ₂	189.60	Sigma-Aldrich (98%)
Titanium dioxide (rutile)	TiO ₂	79.87	Merck (≥99.5%)

Table 2.1 summarizes the list of chemicals used in the experiments. Magnetite (α -Fe₃O₄(cr), 60-120 nm) used in this work was prepared hydrothermally at KIT–INE following the protocol previously described in the literature [108].

2.1.2 ²³⁸U

A pure, nitrate-free 0.42 M ²³⁸UO₂Cl₂ stock solution was used to prepare samples in all experiments. For redox experiments (Chapter 3), a calculated amount of solution was directly added to pre-equilibrated matrix solutions aiming at an initial uranium concentration of 3.0·10⁻⁵ M and 4.2·10⁻⁴ M. An aliquot of U(VI) stock solution was electrochemically reduced and precipitated as UO₂(am, hyd) in reducing and alkaline conditions. The resulting solid was aged for 3 months and used in U(IV) undersaturation solubility experiments (see section 2.3.1 and Chapter 4). The solid phase K₂U₂O₇·xH₂O(cr) was synthesized by slow addition of the nitrate-free U(VI) stock solution to a 2.43 M KCl + 0.07 M KOH solution (see section 2.4.1). The resulting potassium uranate was used in a series of undersaturation solubility experiments summarized in Chapter 5.

2.1.3 pH measurements

The pH was originally defined by Sørensen and Linderstørm as the negative logarithm of hydrogen concentration in molar units ($-\log [H^+]$) [109]. This definition was afterwards updated referring to the hydrogen ion activity, a_{H^+} , instead of concentration [110-112]:

$$\text{pH} = -\log(a_{H^+}) = \log \left[\left(\frac{m_{H^+} \gamma_{H^+}}{m^0} \right) \right] = \quad (2.1)$$

where m_{H^+} is the molal concentration of H⁺ and γ_{H^+} is the corresponding molal activity coefficient. m^0 is an arbitrary constants representing the standard amount of concentration equal to 1 mol·kg⁻¹. Note that Eq (2.1) can also be used on the molar scale by considering the term $\left(\frac{c_{H^+} \gamma_{H^+}}{c^0} \right)$. In spite of the clear definition, the activity of H⁺ cannot be experimentally measured. Therefore, a consensual pH scale was introduced after international agreement in

order to measure and compare the acidity of dilute solutions with $I \leq 0.1$ m. In this context, the International Union of Pure and Applied Chemistry (IUPAC) recommended the use of H⁺ sensitive electrodes (Harned cell) without junction potential as the primary method [112], to provide the absolute measurement of standard buffer solutions of certain pH values. The Harned cell is defined by:



and contains standard buffers, S, and Cl⁻ ions in the form of NaCl or KCl. The overall reaction occurring spontaneously in the cell is:



and the potential difference of the cell is given by the Nernst equation:

$$E = E^0 - \left(\frac{RT}{F} \ln 10 \right) \log[(m_{\text{H}^+} \gamma_{\text{H}^+})(m_{\text{Cl}^-} \gamma_{\text{Cl}^-})] \quad (2.4)$$

where E^0 corresponds to the standard potential difference of the Ag/AgCl electrode, which is determined from the Harned cell containing pure HCl at a fixed molality as filling solution. The single-ion activity coefficient γ_{Cl^-} cannot be quantified experimentally and it is therefore calculated using the Bates-Guggenheim convention as derived from the Debye-Hückel theory:

$$\log \gamma_{\text{Cl}^-} = -A I^{1/2} / (1 + Ba I^{1/2}) \quad (2.5)$$

where A is the Debye-Hückel temperature-dependent constant, a is the ion size parameter (the distance of closest approach of the ions), Ba is equal to 1.5 mol kg^{-1} at all temperatures in the range 5-50°C, and I is the ionic strength of the buffer ($I = 1/2 \sum m_i z_i^2$).

In addition to primary methods, the use of secondary methods including also a liquid junction contribution to the potential difference allows also the determination of pH. Absolute potential difference cannot be measured by secondary methods, but pH can be determined as long as a calibration with standard buffer solutions is performed prior to the measurement. The electrochemical cell used for the measurement consists of a H⁺ sensitive glass electrode and a reference electrode with a salt bridge. These two electrodes are combined in a single glass unit in order to avoid a separate external reference electrode and connected with a cable to a sensitive electrometer for the measurements of potential difference between these two electrodes. The potential of the electrode is defined as:

$$E = E^0(\text{REF}) - E^0(\text{GE}) - E_{\text{AS}} + RT \ln(10) / F \log a_{\text{H}^+} + E_j \quad (2.6)$$

where $E^\circ(\text{REF})$ and $E^\circ(\text{GE})$ are the temperature dependent potential of reference and the glass electrode, respectively. $RT \ln(10) / F$ is equal to 59.16 mV at 25°C and corresponds to the Nernst slope which is used when the glass electrode is perfectly reversible to hydrogen ions. This is a good approximation for the measurement of solutions with $\text{pH} < 12$ using commercial glass electrodes. The asymmetry potential, E_{AS} , is the potential difference of a symmetrical cell with identical solutions and reference electrodes on each side of the glass membrane. It depends on the internal and external hydrated ion exchange layers of the glass membrane. E_j is the liquid junction potential, which depends on the diffusion rates of anions and cations present in reference and sample solutions.

The measured electron potentials (mV) of a standard buffer (S) of a known pH and the unknown sample (X) are expressed as:

$$E(\text{S}) = E(\text{REF}) - E(\text{GE}) - E_{\text{AS}} + RT \ln(10) / F \cdot \log a_{\text{H}^+}(\text{S}) + E_j(\text{S}) \quad (2.7)$$

$$E(\text{X}) = E(\text{REF}) - E(\text{GE}) - E_{\text{AS}} + RT \ln(10) / F \cdot \log a_{\text{H}^+}(\text{X}) + E_j(\text{X}) \quad (2.8)$$

Therefore, since the $E^\circ(\text{REF})$, $E^\circ(\text{GE})$ and E_{AS} do not change in the calibration and the measurement of sample, the unknown pH of the sample can be calculated using the difference between $E(\text{X})$ and $E(\text{S})$:

$$\text{pH}(\text{X}) = \text{pH}(\text{S}) + [E(\text{S}) - E(\text{X})] \cdot F / RT \ln(10) + [E_j(\text{S}) - E_j(\text{X})] \cdot F / RT \ln(10) \quad (2.9)$$

The difference between the liquid junction potential contributions to both measurements is negligible at low and similar ionic strengths ($I \leq 0.1 \text{ m}$) [113].

2.1.3.1 pH measurements in saline solutions

At high ionic strengths ($I \geq 0.1 \text{ m}$), the activity coefficient of H^+ and liquid junction potential of the electrode are largely affected by ion interaction processes, and the use of $\text{pH}_m / \text{pH}_c$ (concentration scale, in molal or molar units) instead of pH (activity scale) is required for the correct evaluation of unknown systems [114]:

$$\text{pH}_m = -\log(m_{\text{H}^+}) \text{ and } \text{pH}_c = -\log(c_{\text{H}^+}) \quad (2.10)$$

Experimentally measured pH values (pH_{exp}) include the combined contribution of the activity coefficient of H^+ and the liquid junction potential of the electrode. Therefore, an empirical correction factor, $A_{m/c}$ is used to calculate $\text{pH}_{m/c}$ from the operational pH_{exp} :

$$\text{pH}_m = \text{pH}_{\text{exp}} + A_m \text{ and } \text{pH}_c = \text{pH}_{\text{exp}} + A_c \quad (2.11)$$

$A_{m/c}$ values can be calculated according to:

$$A_m = \log^m \gamma_{\text{H}^+} + E_j \frac{RT}{F} \ln 10 \text{ and } A_c = \log^c \gamma_{\text{H}^+} + E_j \frac{RT}{F} \ln 10 \quad (2.12)$$

$A_{m/c}$ values depend upon salt type and concentration, and they can be empirically determined by measuring a set of reference sample solutions with different concentrations of background electrolyte and known H^+ concentrations.

2.1.4 pH measurements in this work

In the present study, the hydrogen ion concentration (as pH_{exp}) was measured using a ROSS combination pH electrode (Orion). The standard buffer solutions at $\text{pH} = 2\text{-}12$ were used for calibration prior to the measurements. pH adjustments were performed using HCl–NaCl–NaOH, HCl–KCl–KOH, HCl–MgCl₂ and HCl–CaCl₂ solutions with ionic strength adjusted to the corresponding sample. Mg(OH)₂(s) and Ca(OH)₂(s) solid phases were also used to adjust the pH in the alkaline range in MgCl₂ and CaCl₂ systems, respectively. MES and TRIS (with total concentrations in the samples ranging from 5 to 25 mM) were used to buffer the pH_m of selected samples at ≈ 6 and ≈ 8 , respectively. The values of A_m were taken from Altmaier *et al.* [85, 115] for NaCl, MgCl₂ and CaCl₂ systems, and from Baumann *et al.* [116] for KCl systems. Table 2.2 shows the A_m values used within this work. In those systems with $[\text{H}^+] > 0.01 \text{ M}$ or $[\text{OH}^-] > 0.01 \text{ M}$, pH_m values were calculated from the initial $[\text{H}^+]$ and from the known hydroxide concentration and the conditional ion product (K'_w) of water, respectively. In MgCl₂ and CaCl₂ solutions, the maximum pH_m values (pH_{max}) are fixed at ~ 9 and ~ 12 , respectively, by the precipitation of Mg(OH)₂(s) and Ca(OH)₂(s) (or corresponding hydroxochlorides at Ca/Mg concentrations above $\sim 2 \text{ m}$) [115].

Table 2.2. A_m values used in this study as reported in Altmaier et al. [85, 115] (NaCl, MgCl₂ and CaCl₂ systems) and Baumann et al. [116] (KCl systems).

Background electrolyte	A_m^a
0.10 m NaCl	-0.08
0.51 m NaCl	-0.01
1.02 m NaCl	0.08
5.61 m NaCl	0.90
0.25 m MgCl ₂	0.03
2.11 m MgCl ₂	0.95
5.15 m MgCl ₂	2.77
0.25 m CaCl ₂	-0.01
2.11 m CaCl ₂	0.83
5.25 m CaCl ₂	2.41
0.10 m KCl	-0.11
0.51 m KCl	-0.16
1.04 m KCl	-0.13
3.26 m KCl	0.15
4.50 m KCl	0.32

a: ± 0.04

2.1.5 E_h measurements

Measurements of redox potential were performed with Pt combination electrodes with a Ag/AgCl reference system (Metrohm). The measured values in mV were converted to E_h versus the standard hydrogen electrode (SHE) using the correction for the potential of reference electrode according with the reaction $\text{AgCl(s)} + \text{e}^- \rightleftharpoons \text{Ag(s)} + \text{Cl}^-$:

$$E = E^\circ_{\text{Ag/AgCl}} + \frac{RT \ln(10)}{F} \cdot \log a_{\text{Cl}^-} \quad (2.13)$$

where $E^\circ_{\text{Ag/AgCl}} = 0.2222$ V and $(RT / F) = 0.02569$ V at $T = 25$ °C. Equation (2.13) results in $E = 0.208$ V for a 3.0 M KCl filling solution. The apparent electron activity ($\text{pe} = -\log a_{\text{e}^-}$) was calculated using the relation between pe and E_h shown in Section 1.2.2.1 ($\text{pe} = 16.9 E_h$, with E_h

in [V]). All samples were measured under constant agitation for 5-15 min until stable E_h readings were obtained.

2.1.6 Determination of total concentration and redox speciation of uranium in aqueous systems

2.1.6.1 Inductively coupled plasma mass spectrometry (ICP-MS)

The determination of the total uranium concentration in the aqueous phase of all investigated systems was performed using ICP-MS. This instrumental technique is the combination of a high-temperature ICP and a mass spectrometer. First, the elements are ionized by the inductively coupled plasma source, and then detected and quantified by the mass spectrometer. An aliquot of the aqueous sample is converted to an aerosol by a nebulizer, and subsequently injected in the plasma. The detection capability of ICP-MS is highly affected by the concentrated matrix solution of the sample due to the possible formation of salt crusts in the thin pipes used for the injection of samples and the cone of the plasma. Therefore, samples were accordingly diluted to a salt content below ≈ 50 ppm before the measurement.

In selected samples with less concentrated NaCl (0.1 and 0.5 M NaCl), a μ -injection technique was used in order to quantify very low uranium concentrations. This technique allows the injection of a significantly lower sample volume, compared to the standard ICP-MS technique. This minimizes the risk of salt deposition, allows the injection of more concentrated samples and consequently decreases the detection limit.

For sample preparation, an aliquot of the supernatant (50 to 800 μ L) of each sample was centrifuged at 12000 g with 10 kD filters (2–3 nm cut-off Nanosep® centrifuge tubes, Pall Life Sciences) for 2-10 minutes to separate colloids or suspended particles. Then, the filtrate was diluted using 2% HNO₃, depending on the salt and uranium concentration of the sample (1:100 – 1:5000). Different detection limits, quantified as 3 times the standard deviation of repeated blank measurements (ranging between $\approx 10^{-6}$ and $\approx 10^{-11}$ M), were observed due to the dilution factors required for different concentrations of background electrolyte. Uranium concentrations determined in molar units were converted to molal units using the conversion factors reported in the NEA-TDB [40, 41].

2.1.6.2 Solvent extraction (SX)

A solvent extraction approach was used to determine the oxidation state of U (+4 or +6), in the aqueous phase of samples containing $[U] \geq 10^{-5}$ M.

After attaining equilibrium conditions (constant pH_m , E_h and $[U]$ measurements), 250 μ L of the supernatant solution of selected samples were acidified with 250 μ L of 2 M HCl after ultrafiltration with 10 kD filters. Afterwards, the acidified samples were contacted with 0.025 M PMBP prepared in 500 μ L xylene [117, 118]. The mixture was vigorously shaken for 3–5 minutes and centrifuged at 12000 g for 5 minutes. The aqueous phase was carefully separated from the organic phase using thin tip Pasteur pipettes. Concentration of uranium in the aqueous phase was quantified by ICP-MS and attributed to presence of U(VI). PMBP is known to strongly complex An(IV) under acidic conditions [119], which are accordingly quantitatively extracted in the organic phase.

2.1.7 Solid phase characterization

Solid phase characterization of starting solid phases and selected solubility samples (after attaining equilibrium conditions) were performed using different methods as described in Sections 2.1.6.1 to 2.1.6.4.

2.1.7.1 X-Ray diffraction

An aliquot of the solid phase of each selected sample (~ 1 mg) was washed 5–6 times with 1 mL ethanol to remove the salt content in the matrix solution. After the last cleaning step, the solid was re-suspended in ethanol and deposited on an XRD sample plate. The sample was dried under Ar atmosphere for a few minutes, and the sample holder was transferred outside the glovebox for the collection of the XRD diffractogram. XRD measurements were performed on a Bruker AXS D8 Advance X-Ray powder diffractometer at measurement angle $2\theta = 5\text{--}100^\circ$ with incremental steps of $0.02^\circ\text{--}0.04^\circ$ and a measurement time of 1.5–37 seconds per step. The collected diffractograms were compared to reference data reported in the Joint Committee on Powder Diffraction Standard (JCPDS, [120]). For those solid phases with well-defined / known

structures, XRD patterns were also used for the evaluation of the particle size using Rietveld analysis.

2.1.7.2 Quantitative chemical analysis

After XRD analysis, the solid deposited on the sample holder was dissolved in 1 mL of 2% HNO₃. ICP-OES technique (inductively coupled plasma–optical emission spectroscopy, Perkin–Elmer 4300 DV) was used for the quantification of the concentrations of U, Na, Mg, Ca and K (depending upon the investigated salt system). This information was considered to identify the presence of impurities (sorbed cations, salt remains from insufficient washing of the solid) or, in the case of ternary K–U(VI)–OH compounds, to establish the ratio U:K in the solid phase controlling the solubility of uranium.

2.1.7.3 Scanning electron microscopy with energy dispersive X-Ray spectroscopy (SEM-EDS)

A second fraction of the solid phase washed for XRD analysis was characterized by SEM-EDS (FEI Quanta 650 FEG equipped with Noran EDS unit). SEM images were considered for a qualitative assessment of particle size, crystallinity and morphology, whereas EDS provided additional insights on the atomic composition of the investigated solid phase. Note that EDS is a surface sensitive technique gathering information from the upper layer of the solid, whilst quantitative chemical analysis gives information on the bulk. Therefore, differences on the atomic ratios determined for a given solid phase may arise between both experimental techniques.

2.1.7.4 Thermogravimetric-differential thermal analysis (TG-DTA)

The number of hydration waters in the solid phases controlling the solubility of uranium was quantified by TG-DTA using a Netzsch STA 449C equipment. Solid phases collected from selected solubility samples were washed 5 times with ethanol to remove the matrix solution. The washed samples were transferred in tightly closed vials to the glovebox where TG-DTA

measurements were performed. Typically, 5–20 mg of uranium solid phase were used in the measurements. Samples were heated to $T = 900\text{ }^{\circ}\text{C}$ at a rate of 10 K min^{-1} , and the number of hydration waters was calculated using the mass loss with respect to the original weight.

2.1.8 X-ray absorption near edge structure (XANES) and extended X-Ray absorption fine structure (EXAFS) spectroscopy

XANES and EXAFS measurements of selected solid and aqueous phases were recorded at the INE- and CAT-ACT beamlines at the KIT synchrotron source [121]. Measurements and data evaluation were carried with close supervision / indications by the beamline scientists.

XANES was used to determine the oxidation state of uranium in selected aqueous / solid samples investigated in the redox study. XANES spectra of solid phases were collected at the INE-beamline, whereas the ACT-beamline (with a significantly higher flux of photons) was used for the characterization of dilute aqueous samples with $[\text{U}]_{\text{aq}} \geq 3 \cdot 10^{-5}\text{ M}$. EXAFS was considered to gain structural information of the solid phases used in U(IV) solubility experiments. All EXAFS spectra were collected at the INE-beamline.

2.1.8.1 Sample preparation

Approximately 300 μL of a suspension (containing *ca.* 1 mg of solid) of the selected solubility samples were transferred to a 400 μL polyethylene vial and centrifuged at 4020g for 10 minutes under an Ar atmosphere. This approach resulted in a compacted solid at the bottom of the vial well-separated from the supernatant solution, which allowed the distinct measurement of aqueous phase, solid or both (depending upon investigated system, see Table 2.3). The vials were mounted inside the Ar-glovebox in a gas-tight cell with Kapton® (polyimide) film windows. The cell was transported to INE- or ACT-beamlines, and samples were measured under continuous flow of Ar gas within a few hours after preparation. Table 2.8 summarizes all reference and unknown samples investigated by XANES/EXAFS within this PhD thesis.

Table 2.3. *References and unknown samples measured using XANES and EXAFS.*

Study	Sample description	Technique	Beamline
Redox	0.1 M NaCl, $pH_m = 10.9$, 20 mM Sn(II) + 15 mg Fe(0)		
	Solid	XANES	INE
Redox	5.0 M NaCl, at $pH_m = 11.9$, 20 mM Sn(II)		
	Solid	XANES	INE
Reference	UO ₂ (s, hyd)	XANES	INE
Reference	Na ₂ U ₂ O ₇ ·H ₂ O(cr)	XANES	INE
Redox	0.1 M NaCl, at $pH_m = 2.1$, 20 mM Sn(II)		
	Aqueous	XANES	ACT
Reference	U(IV) in 1.0 M HCl	XANES	ACT
Reference	U(VI) in 1.0 M HCl	XANES	ACT
U(IV) solubility	UO ₂ (s, hyd), $pH_m = 12.1$, 10 mM Na ₂ S ₂ O ₄ “starting material”	EXAFS	INE
U(IV) solubility	UO ₂ (s, hyd), 0.1 M NaCl, $pH_m = 8.5$, 5 mM Sn(II)	EXAFS	INE

2.1.8.2 XANES/EXAFS measurements

Uranium L_{III}-edge (17166 eV) XANES/EXAFS spectra (5–8 replicates per sample) were collected at room temperature under a continuous flow of Ar. The INE-Beamline [122] is equipped with a Ge(422) double crystal monochromator (DCM) coupled with a collimating and a focusing Rh coated mirrors before and after the DCM, respectively. The beam spot size on the sample is below 1mm diameter. The DCM-crystals were detuned at 70% and the incident beam intensity was held constant by means of a piezo driven feedback system to the second crystal. The incident and transmitted beam intensities were measured by argon-filled ionization chambers. U L_{III} EXAFS signal was recorded in fluorescence mode using simultaneously 4-elements and 1-element Silicon drift Vortex detectors. The ACT-Beamline [123] is equipped with a pair of Si(311) crystals in the double crystal monochromator (DCM, FMB Oxford, Oxford, United Kingdom). The monochromatic radiation delivered by the DCM is focused by an Rh-coated toroidal mirror into a spot-size below 1 mm diameter at the sample position. A five pixel LGe solid state detector (Canberra, Olen, Belgium) is used for collecting U L_{III} fluorescence radiation. In both beamlines, the energy calibration was performed by assigning the energy of 17038 eV to the first inflection point of the K-edge absorption spectrum of the Y metal foil, recorded simultaneously in transmission geometry.

2.1.8.3 Data evaluation

XANES/EXAFS data reduction and analysis were performed with the ATHENA/ARTEMIS programs of the Demeter 0.9.26 package following standard procedures [124].

2.2 Uranium redox experiments in the presence of reducing agents

The redox behaviour of uranium was investigated in 0.1 and 5.0 M NaCl solutions in the presence of individual and mixed reducing chemical systems (2, 10 and 20 mM Sn(II), 20 mM Na₂S₂O₄, 20 mM Sn(II) + 10 mg TiO₂, 20 mM Sn(II) + 15 mg Fe(0), 20 mM Sn(II) + 10 mg Fe₃O₄). Experiments were performed covering a wide pH range, $2 \leq \text{pH}_m \leq 14.5$. In a first step, the inactive background solutions were equilibrated until attaining the targeted, stable pH_m and *E*_h readings. A nitrate-free UO₂Cl₂ stock solution was added to the equilibrated background solutions to obtain initial uranium concentrations of $3.0 \cdot 10^{-5}$ and $4.2 \cdot 10^{-4}$ M, resulting in 40 independent batch samples (see Table 2.3). The values of *E*_h, pH_m and uranium concentration were monitored at periodic time intervals for up to 635 days. After attaining equilibrium conditions (assumed after constant *E*_h, pH_m and [U]_{aq} measurements), aqueous and solid phases of selected samples were characterized as described above. The initial experimental conditions before the addition of uranium are summarized in Table 2.4.

Table 2.4. Initial pH_m and E_h values of uranium redox experiments in NaCl systems and presence of different reducing chemicals.

Background electrolyte		0.1 M NaCl		5.0 M NaCl	
Reducing chemicals	Initial U concentration (M)	pH_m^a	E_h (mV) ^b	pH_m^a	E_h (mV) ^b
2 mM Sn(II)	$4.2 \cdot 10^{-4}$	12.9	-847		
10 mM Sn(II)	$4.2 \cdot 10^{-4}$	10.1	-580		
10 mM Sn(II)	$4.2 \cdot 10^{-4}$	10.8	-629		
10 mM Sn(II)	$4.2 \cdot 10^{-4}$	12.1	-768		
10 mM Sn(II)	$4.2 \cdot 10^{-4}$	12.8	-939		
20 mM Sn(II)	$3.0 \cdot 10^{-5}$	11.8	-839		
20 mM Sn(II)	$3.0 \cdot 10^{-5}$	12.9	-895		
20 mM Sn(II)	$3.0 \cdot 10^{-5}$	2.1	-207	3.2	-253
20 mM Sn(II)	$3.0 \cdot 10^{-5}$	3.6	-281	7.7	-603
20 mM Sn(II)	$3.0 \cdot 10^{-5}$	6.0	-411	11.9	-817
20 mM Sn(II)	$3.0 \cdot 10^{-5}$	8.1	-542	13.1	-896
20 mM Sn(II)	$3.0 \cdot 10^{-5}$	9.5	-674	14.4	-998
20 mM Sn(II)	$3.0 \cdot 10^{-5}$	10.9	-775		
20 mM Sn(II)	$3.0 \cdot 10^{-5}$	11.8	-841		
20 mM Sn(II)	$3.0 \cdot 10^{-5}$	12.9	-921		
20 mM Na ₂ S ₂ O ₄	$3.0 \cdot 10^{-5}$	12.1	-843		
20 mM Na ₂ S ₂ O ₄	$3.0 \cdot 10^{-5}$	12.9	-921		
20 mM Sn(II) + 10 mg TiO ₂	$3.0 \cdot 10^{-5}$	2.2	-220		
20 mM Sn(II) + 10 mg TiO ₂	$3.0 \cdot 10^{-5}$	3.6	-297		
20 mM Sn(II) + 10 mg TiO ₂	$3.0 \cdot 10^{-5}$	6.0	-433		
20 mM Sn(II) + 10 mg TiO ₂	$3.0 \cdot 10^{-5}$	8.1	-561		
20 mM Sn(II) + 10 mg TiO ₂	$3.0 \cdot 10^{-5}$	9.5	-647		
20 mM Sn(II) + 10 mg TiO ₂	$3.0 \cdot 10^{-5}$	10.9	-765		
20 mM Sn(II) + 10 mg TiO ₂	$3.0 \cdot 10^{-5}$	11.8	-835		
20 mM Sn(II) + 10 mg TiO ₂	$3.0 \cdot 10^{-5}$	12.9	-920		
20 mM Sn(II) + 15 mg Fe(0)	$3.0 \cdot 10^{-5}$	8.1	-617		
20 mM Sn(II) + 15 mg Fe(0)	$3.0 \cdot 10^{-5}$	9.7	-715		
20 mM Sn(II) + 15 mg Fe(0)	$3.0 \cdot 10^{-5}$	10.9	-793		
20 mM Sn(II) + 15 mg Fe(0)	$3.0 \cdot 10^{-5}$	11.8	-851		
20 mM Sn(II) + 15 mg Fe(0)	$3.0 \cdot 10^{-5}$	12.9	-915		
20 mM Sn(II) + 10 mg Fe ₃ O ₄	$3.0 \cdot 10^{-5}$	8.1	-693		
20 mM Sn(II) + 10 mg Fe ₃ O ₄	$3.0 \cdot 10^{-5}$	9.6	-782		
20 mM Sn(II) + 10 mg Fe ₃ O ₄	$3.0 \cdot 10^{-5}$	10.9	-856		
20 mM Sn(II) + 10 mg Fe ₃ O ₄	$3.0 \cdot 10^{-5}$	11.8	-843		
20 mM Sn(II) + 10 mg Fe ₃ O ₄	$3.0 \cdot 10^{-5}$	12.9	-921		

a: ± 0.05 ; **b:** ± 30 mV

2.3 U(IV) solubility experiments

2.3.1 U(IV) solid phase preparation

A 0.1 M U(VI) stock solution was prepared in 1.0 M HCl and transferred to a glass vessel with a magnetic stirrer, a Pt-working electrode and two galvanic cells (filled with 1.0 M HCl) containing the Pt-counter electrode (Metrohm) and the Ag/AgCl reference electrode (Metrohm, filled with 3.0 M KCl). The redox potential was adjusted to -280 mV (with respect to the Ag/AgCl reference electrode) by using a potentiostat (Princeton Applied Research, Model 362). In the first four hours of the electrolysis, the color of the solution converted slowly from yellow to pale green, which evolved to a dark green solution after $t = 4$ hours. The electrolysis process was terminated at $t \approx 10$ hours after ensuring by UV-vis the redox purity of the resulting solution. Figure 2.1 shows the UV-vis data measured before, after 4 hours and after 10 hours of electrolysis. The figure shows that the contribution of U(VI) completely vanished after 10 h of electrolysis, and a U(IV) spectrum in excellent agreement with reference data reported by Cohen and Carnall [125] was collected. This was taken as a conclusive proof of the redox purity of the resulting U(IV) stock solution.

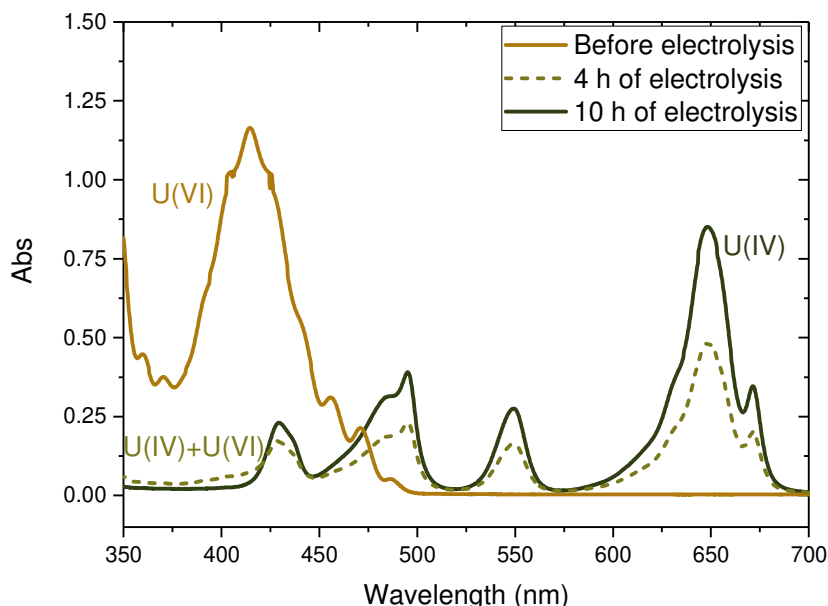


Figure 2.1. UV spectra before (yellow line), after 4 h (light green dash line) and 10 h (dark green line) of electrolysis of a 0.1 M U(VI) stock solution in 1.0 M HCl at a potential of -280 mV (vs. Ag/AgCl).

The pH of the resulting U(IV) solution was shifted to $\text{pH} \approx 3$ with 4 M NaOH. Afterwards, this solution was added drop by drop to a 10 mM $\text{Na}_2\text{S}_2\text{O}_4$ solution at $\text{pH} \approx 12.5$ in a Kautex bottle under gentle agitation. The pH value was monitored during the addition to control / avoid the shift towards less alkaline values, which are known to cause the disproportionation of $\text{Na}_2\text{S}_2\text{O}_4^\ddagger$ [126, 127]. Approximately 250 mg of U(IV) solid phase were precipitated with this approach. The resulting solid was aged during 3 months and characterized as summarized in Section 2.1.6 before its use in the solubility experiments.

2.3.2 Sample preparation

The solubility of U(IV) was investigated from undersaturation conditions in 0.1 M HCl, 0.1-5.0 M NaCl, 0.25-4.5 M MgCl_2 and 0.25-4.5 M CaCl_2 solutions at $1.0 \leq \text{pH}_m \leq 14.5$. Sn(II) solutions or suspensions as $\text{Sn}(\text{OH})_2(\text{s})$ (depending on the pH_m) were prepared in the corresponding background electrolyte solutions (HCl, NaCl, MgCl_2 and CaCl_2), and added to each individual sample to achieve “5 mM” Sn(II). As discussed in Chapter 3 of this PhD thesis, the very reducing conditions set by Sn(II) stabilize uranium in the +IV redox state within the complete pH-range investigated. Before the addition of the U(IV) solid phase, the background electrolyte

[‡] $\text{Na}_2\text{S}_2\text{O}_4$ is known to disproportionate at $\text{pH} \leq 11$ [126-127].

solutions containing Sn(II) were equilibrated during two weeks until attaining stable pH and E_h readings. The main experimental features of the samples prepared in HCl/NaCl, MgCl₂ and CaCl₂ systems are summarized in Table 2.5, Table 2.6 and Table 2.7, respectively. The pH of some of the samples was adjusted using small volumes of HCl and NaOH (of appropriate ionic strength), or otherwise with Mg(OH)₂(s) or Ca(OH)₂(s) (\approx 5 mg). Finally, 3-5 mg of U(IV) precipitate were added to each sample after washing 3 times with the corresponding pre-equilibrated background electrolyte and added to 2-30 ml of matrix solution[§]. Most of the samples were stored in 50 mL screw-cap centrifuge vials (Nalgene™, Thermo Scientific), but 5 mL screw-cap tubes were preferred for samples with small volumes. Uranium concentrations and pH_m values were measured at regular time intervals from 6 to 605 days. After attaining equilibrium conditions, aqueous and solid phases of selected solubility samples were characterized as summarized in Sections 2.1.5 and 2.1.6.

[§] The final volume of the samples was chosen as a function of the expected concentration / solubility. Hence, the volume used in very acidic conditions was limited to 2-5 mL due to high solubility foreseen in these conditions.

Table 2.5. Composition of the solutions used in the preparation of U(IV) solubility samples in HCl and NaCl systems.

Background solution composition	pH_m
750 µL 0.1 M Sn(II) + 14.25 mL 0.1 M HCl	1.0
750 µL 0.1 M Sn(II) + 5.25 mL 0.1 M NaCl + 9 mL 0.1 M HCl	1.2
750 µL 0.1 M Sn(II) + 8.25 mL 0.1 M NaCl + 6 mL 0.1 M HCl	1.4
2.8 mL 0.09 M Sn(II) + 47.2 mL 0.1 M NaCl	2.2
2.8 mL 0.09 M Sn(II) + 47.2 mL 0.1 M NaCl	2.8
2.8 mL 0.09 M Sn(II) + 47.2 mL 0.1 M NaCl	2.9
2.8 mL 0.09 M Sn(II) + 47.2 mL 0.1 M NaCl	4.3
2.8 mL 0.09 M Sn(II) + 46 mL 0.1 M NaCl + 1.2 mL 1.0 M MES	5.8
2.8 mL 0.09 M Sn(II) + 47.0 mL 0.1 M NaCl + 200 µL 1.0 M TRIS	8.4
2.8 mL 0.09 M Sn(II) + 47.2 mL 0.1 M NaCl + 60 µL 1.0 M NaOH	11.4
2.8 mL 0.09 M Sn(II) + 42.7 mL 0.1 M NaCl + 4.5 mL 1.0 M NaOH	12.8
750 µL 0.1 M Sn(II) + 11.25 mL 0.5 M NaCl + 3.0 mL 0.5 M HCl	1.1
750 µL 0.1 M Sn(II) + 11.85 mL 0.5 M NaCl + 2.4 mL 0.5 M HCl	1.2
750 µL 0.1 M Sn(II) + 12.45 mL 0.5 M NaCl + 1.8 µL 0.5 M HCl	1.3
2.5 mL 0.1 M Sn(II) + 47.5 mL 0.5 M NaCl	1.9
2.5 mL 0.1 M Sn(II) + 47.5 mL 0.5 M NaCl	2.7
2.5 mL 0.1 M Sn(II) + 47.5 mL 0.5 M NaCl	2.9
2.5 mL 0.1 M Sn(II) + 47.5 mL 0.5 M NaCl	4.0
2.5 mL 0.1 M Sn(II) + 46.5 mL 0.5 M NaCl + 1.0 mL 1.0 M MES	5.8
2.5 mL 0.1 M Sn(II) + 47.2 mL 0.5 M NaCl + 300 µL 1.0 M TRIS	8.2
2.5 mL 0.1 M Sn(II) + 47.3 mL 0.5 M NaCl + 100 µL 0.5 M NaOH	10.9
2.5 mL 0.1 M Sn(II) + 37.5 mL 0.5 M NaCl + 5 mL 0.5 M NaOH	12.9
750 µL 0.1 M Sn(II) + 14.0 mL 2.0 M NaCl + 250 µL 2.0 M HCl	1.3
750 µL 0.1 M Sn(II) + 14.15 mL 2.0 M NaCl + 150 µL 2.0 M HCl	1.5
2.5 mL 0.1 M Sn(II) + 47.5 mL 2.0 M NaCl	1.9
2.5 mL 0.1 M Sn(II) + 47.5 mL 2.0 M NaCl	2.7
2.5 mL 0.1 M Sn(II) + 47.5 mL 2.0 M NaCl	2.9
2.5 mL 0.1 M Sn(II) + 47.5 mL 2.0 M NaCl	4.0
2.5 mL 0.1 M Sn(II) + 46.3 mL 2.0 M NaCl + 1.2 mL 1.0 M MES	5.8
2.5 mL 0.1 M Sn(II) + 47.2 mL 2.0 M NaCl + 300 µL 1.0 M TRIS	8.2
2.5 mL 0.1 M Sn(II) + 47.3 mL 2.0 M NaCl + 100 µL 1.0 M NaOH	10.9
2.5 mL 0.1 M Sn(II) + 45.3 mL 2.0 M NaCl + 2.2 mL 2.0 M NaOH	12.8
750 µL 0.09 M Sn(II) + 14.22 mL 5.0 M NaCl + 30 µL 1.0 M HCl	1.3
750 µL 0.09 M Sn(II) + 14.25 mL 5.0 M NaCl	1.5
2.8 mL 0.09 M Sn(II) + 47.2 mL 5.0 M NaCl	2.1
2.8 mL 0.09 M Sn(II) + 47.2 mL 5.0 M NaCl	2.7
2.8 mL 0.09 M Sn(II) + 47.2 mL 5.0 M NaCl	3.2
2.8 mL 0.09 M Sn(II) + 47.2 mL 5.0 M NaCl	4.0
2.8 mL 0.09 M Sn(II) + 46.0 mL 5.0 M NaCl + 1.2 mL 1.0 M MES	5.8
2.8 mL 0.09 M Sn(II) + 47.0 mL 5.0 M NaCl + 300 µL 1.0 M TRIS	8.5
2.8 mL 0.09 M Sn(II) + 47.2 mL + 25 µL 1.0 M NaOH	11.2
2.8 mL 0.09 M Sn(II) + 47.0 mL 5.0 M NaCl + 200 µL 5.0 M NaOH	12.9
2.8 mL 0.09 M Sn(II) + 47.2 mL 4.0 M NaCl/ 1.0 M NaOH	14.5

Table 2.6. Composition of the solutions used in the preparation of U(IV) solubility samples in MgCl₂ systems.

Background solution composition	pH _m
0.5 mL 0.1 M Sn(II) + 9 mL 0.25 M MgCl ₂ + 500 μL 1.0 M HCl	1.2
0.5 mL 0.1 M Sn(II) + 9.25 mL 0.25 M MgCl ₂ + 250 μL 1.0 M HCl	1.5
1 mL 0.1 M Sn(II) + 18.74 mL 0.25 M MgCl ₂ + 260 μL 1.0 M HCl	1.8
1 mL 0.1 M Sn(II) + 18.84 mL 0.25 M MgCl ₂ + 160 μL 1.0 M HCl	2.0
1 mL 0.1 M Sn(II) + 18.9 mL 0.25 M MgCl ₂ + 100 μL 1.0 M HCl	2.2
1 mL 0.1 M Sn(II) + 18.95 mL 0.25 M MgCl ₂ + 50 μL 1.0 M HCl	2.5
1 mL 0.1 M Sn(II) + 18.98 mL 0.25 M MgCl ₂ + 20 μL 1.0 M HCl	3.0
1 mL 0.1 M Sn(II) + 19.0 mL 0.25 M MgCl ₂	3.7
1 mL 0.1 M Sn(II) + 19.0 mL 0.25 M MgCl ₂ + Mg(OH) ₂ (s)	5.9
1 mL 0.1 M Sn(II) + 19.0 mL 0.25 M MgCl ₂ /Mg(OH) ₂ (s)	8.9
0.5 mL 0.1 M Sn(II) + 9.4 mL 2.0 M MgCl ₂ + 100 μL 1.0 M HCl	1.3
0.5 mL 0.1 M Sn(II) + 9.45 mL 2.0 M MgCl ₂ + 50 μL 1.0 M HCl	1.5
1 mL 0.1 M Sn(II) + 18.95 mL 2.0 M MgCl ₂ + 50 μL 1.0 M HCl	1.8
1 mL 0.1 M Sn(II) + 18.97 mL 2.0 M MgCl ₂ + 30 μL 1.0 M HCl	2.0
1 mL 0.1 M Sn(II) + 18.98 mL 2.0 M MgCl ₂ + 20 μL 1.0 M HCl	2.3
1 mL 0.1 M Sn(II) + 19.0 mL 2.0 M MgCl ₂	2.5
1 mL 0.1 M Sn(II) + 19.0 mL 2.0 M MgCl ₂	3.0
1 mL 0.1 M Sn(II) + 19.0 mL 2.0 M MgCl ₂	4.2
1 mL 0.1 M Sn(II) + 19.0 mL 2.0 M MgCl ₂ + Mg(OH) ₂ (s)	7.7
1 mL 0.1 M Sn(II) + 19.0 mL 2.0 M MgCl ₂ /Mg(OH) ₂ (s)	8.9
1 mL 0.1 M Sn(II) + 18.98 mL 4.5 M MgCl ₂ + 20 μL 1.0 M HCl	1.9
1 mL 0.1 M Sn(II) + 19.0 mL 4.5 M MgCl ₂	2.1
1 mL 0.1 M Sn(II) + 19.0 mL 4.5 M MgCl ₂	2.3
1 mL 0.1 M Sn(II) + 19.0 mL 4.5 M MgCl ₂	2.4
1 mL 0.1 M Sn(II) + 19.0 mL 4.5 M MgCl ₂	2.7
1 mL 0.1 M Sn(II) + 19.0 mL 4.5 M MgCl ₂	3.2
1 mL 0.1 M Sn(II) + 19.0 mL 4.5 M MgCl ₂ + Mg(OH) ₂ (s)	7.1
1 mL 0.1 M Sn(II) + 19.0 mL 4.5 M MgCl ₂ /Mg(OH) ₂ (s)	8.9

Table 2.7. Composition of the solutions used in the preparation of U(IV) solubility samples in CaCl₂ systems.

Background solution composition	pH _m
2.5 mL 0.1 M Sn(II) + 47.5 mL 0.25 M CaCl ₂ + Ca(OH) ₂ (s)	9.0
2.5 mL 0.1 M Sn(II) + 47.5 mL 0.25 M CaCl ₂ + Ca(OH) ₂ (s)	11.2
2.5 mL 0.1 M Sn(II) + 47.5 mL 0.25 M CaCl ₂ + Ca(OH) ₂ (s)	11.0
2.5 mL 0.1 M Sn(II) + 47.5 mL 0.25 M CaCl ₂ /Ca(OH) ₂ (s)	12.0
2.5 mL 0.1 M Sn(II) + 47.5 mL 2.0 M CaCl ₂ + Ca(OH) ₂ (s)	8.6
2.5 mL 0.1 M Sn(II) + 47.5 mL 2.0 M CaCl ₂ + Ca(OH) ₂ (s)	11.1
2.5 mL 0.1 M Sn(II) + 47.5 mL 2.0 M CaCl ₂ + Ca(OH) ₂ (s)	11.4
2.5 mL 0.1 M Sn(II) + 47.5 mL 2.0 M CaCl ₂ /Ca(OH) ₂ (s)	11.9
2.5 mL 0.1 M Sn(II) + 47.5 mL 4.5 M CaCl ₂ + Ca(OH) ₂ (s)	9.1
2.5 mL 0.1 M Sn(II) + 47.5 mL 4.5 M CaCl ₂ + Ca(OH) ₂ (s)	10.8
2.5 mL 0.1 M Sn(II) + 47.5 mL 4.5 M CaCl ₂ + Ca(OH) ₂ (s)	11.5
2.5 mL 0.1 M Sn(II) + 47.5 mL 4.5 M CaCl ₂ /Ca(OH) ₂ (s)	11.9

2.4 U(VI) solubility experiments in KCl solutions

2.4.1 U(VI) solid phase preparation

The potassium uranate solid phase used in the solubility experiments was prepared by the slow addition of a nitrate-free 0.48 M UO₂Cl₂(aq) stock solution to a 2.43 M KCl + 0.07 M KOH solution under continuous agitation and pH monitoring. The precipitation and storage of the resulting solid was performed under Ar atmosphere. Approximately 300 mg of solid phase were obtained in this process. The resulting solid phase was aged for 2 months and then characterized using XRD, quantitative chemical analysis using ICP-MS, SEM-EDS and TG-DTA as described in Section 2.1.6.

2.4.2 Sample preparation

The solubility of potassium uranate was investigated from undersaturation conditions. Experiments were performed in 0.1, 0.5, 1.0, 3.0 and 4.0 M KCl solutions at $7.5 \leq \text{pH}_m \leq 14.6$. HCl-KCl and KCl-KOH solutions of appropriate ionic strength were used for pH_m adjustments. Before the addition of the U(VI) solid phase, the background electrolyte solutions were equilibrated 2-3 weeks until attaining stable pH_m readings. For each independent batch solubility sample, approximately 5 mg of U(VI) solid phase were washed 3-5 times with the

corresponding background solution and added to 20 mL of matrix solution in 50 mL screw-cap centrifuge vials (Nalgene™, Thermo Scientific). The pH_m and uranium concentration were measured at regular time intervals from 6 to 250 days. After attaining equilibrium conditions, the solid phases of selected solubility samples were characterized as summarized in Section 2.1.6. Table 2.8 shows the composition of the background solution and corresponding pH_m values before the addition of potassium uranate.

Table 2.8. Composition of the background solutions used in the solubility experiments with potassium urinate in alkaline KCl systems.

Background solution composition	pH_m
50 mL 0.1 M KCl	8.2
50 mL 0.1 M KCl	10.1
50 mL 0.1 M KCl	10.9
50 ml 0.9 M KCl / 0.01 M KOH	11.8
50 mL 0.1 M KOH	12.8
50 mL 0.5 M KCl	7.9
50 mL 0.5 M KCl	8.7
50 mL 0.5 M KCl	10.1
50 mL 0.5 M KCl	11.3
50 mL 0.48 M KCl / 0.02 M KOH	11.9
50 mL 0.35 M KCl / 0.15 M KOH	12.9
50 mL 1.0 M KCl	7.9
50 mL 1.0 M KCl	8.4
50 mL 1.0 M KCl	10.2
50 mL 1.0 M KCl	11.2
50 mL 0.985 M KCl / 0.015 M KOH	11.9
50 mL 0.975 M KCl / 0.025 M KOH	12.2
50 mL 0.95 M KCl / 0.05 M KOH	12.6
50 mL 0.7 M KCl / 0.3 M KOH	13.3
50 mL 3.0 M KCl	7.5
50 mL 3.0 M KCl	7.9
50 mL 3.0 M KCl	9.9
50 mL 3.0 M KCl	10.9
50 mL 2.995 M KCl / 0.005 M KOH	12.0
50 mL 2.9 M KCl / 0.1 M KOH	13.3
50 mL 2.0 M KCl / 1.0 M KOH	14.3
50 mL 4.0 M KCl	7.6
50 mL 4.0 M KCl	7.9
50 mL 4.0 M KCl	9.6
50 mL 4.0 M KCl	10.5
50 mL 3.997 M KCl / 0.003 M KOH	11.9
50 mL 3.975 M KCl / 0.025 M KOH	12.9
50 mL 3.93 M KCl / 0.4 M KOH	13.3
50 mL 3.6 M KCl / 0.1 M KOH	14.1
50 mL 3.0 M KCl / 1.0 M KOH	14.6

3 Redox chemistry of uranium in reducing systems

The redox chemistry of uranium was investigated in 0.1 and 5.0 M NaCl solutions with $2 \leq \text{pH}_m \leq 14.5$. Individual (Sn(II), Na₂S₂O₄) and mixed (Sn(II) + TiO₂, Sn(II) + Fe(0) and Sn(II) + Fe₃O₄(cr)) reducing systems were used in order to follow the reduction kinetics and to evaluate the effect of surfaces on the reduction process. Data were evaluated by systematizing the experimentally measured E_h and pH_m in *Pourbaix* diagrams and comparing the measured uranium concentration of each sample with the calculated U(IV) and U(VI) solubility for the investigated pH_m and [NaCl] conditions. All the measurements were performed at regular time intervals from 9 to 635 days. Thermodynamic data selection summarized in Tables 1.2 and 1.3 were used for the calculation of *Pourbaix* diagrams and solubility curves in Figures 3.1–3.7. *Pourbaix* diagrams are prepared with the code Medusa / Spana developed by Ignasi Puigdomènech [128]. The expected difference in solubility between U(IV) and U(VI) within the complete pH_m -range investigated is taken as main criteria for the evaluation of U(VI) reduction. For selected samples, the oxidation state of uranium in the aqueous and solid phases was additionally investigated by solvent extraction and XANES techniques.

3.1 Reduction of U(VI) in 0.1 and 5.0 M NaCl solutions using a Sn(II) redox buffer

The redox behavior of U(VI/IV) was investigated at three Sn(II) concentrations (2, 10 and 20 mM) starting with two different initial uranium concentrations ($4.2 \cdot 10^{-4}$ M and $3.0 \cdot 10^{-5}$ M). Figure 3.1a shows the monitored E_h - pH_m values in this system during the equilibration time (238 days). All experimental values are below the calculated U(VI/IV) redox borderline and confirm the strong reducing capacity of Sn(II) regardless of its concentration. Thus, the combination of E_h - pH_m measurements and thermodynamic calculations in *Pourbaix* diagrams indicates that the reduction of U(VI) to U(IV) in Sn(II) systems is thermodynamically favored. Figure 3.1b shows the measured uranium concentration (after 10 kD ultrafiltration) in this system together with the solubility of U(VI) (UO₃·2H₂O(cr) and Na₂U₂O₇·H₂O(cr)) and U(IV) (UO₂(am, hyd)) solid phases calculated for 0.1 M NaCl systems based on the selected thermodynamic data (Table 1.2 and 1.3). Measured uranium concentration in the samples with $[\text{U(VI)}]_0 = 3.0 \cdot 10^{-5}$ M and $[\text{Sn(II)}] = 20$ mM showed the decrease of uranium concentration to 10^{-8} - 10^{-9} M within 59 days of contact time. This concentration range is in excellent agreement

with the solubility expected for $\text{UO}_2(\text{am, hyd})$, and clearly below (1 to 3 orders of magnitude, depending upon pH_m) the solubility of $\text{Na}_2\text{U}_2\text{O}_7 \cdot \text{H}_2\text{O}(\text{cr})$. These observations strongly support the complete reduction of the initial U(VI) to U(IV). For the samples with $[\text{U}(\text{VI})]_0 = 4.2 \cdot 10^{-4}$ M and $[\text{Sn}(\text{II})] = 10$ mM, reduction started to occur after 59 days, and it is only complete after 238 days. Very slow reduction was observed in the sample containing $[\text{U}(\text{VI})]_0 = 4.2 \cdot 10^{-4}$ M, $[\text{Sn}(\text{II})] = 2$ mM and $\text{pH}_m = 12.8$. In this case, the solubility control by $\text{Na}_2\text{U}_2\text{O}_7 \cdot \text{H}_2\text{O}(\text{cr})$ was clearly observed with the first drop in uranium concentration to $[\text{U}] \approx 10^{-5}$ M within 19 days. This concentration of uranium was retained even at $t = 238$ days, and only after 635 days uranium concentration decreased down to $10^{-8} - 10^{-9}$ M, corresponding to the complete reduction of U(VI) to U(IV). These results most probably indicate that $\text{Na}_2\text{U}_2\text{O}_7 \cdot \text{H}_2\text{O}(\text{cr})$ and $\text{UO}_2(\text{am, hyd})$ solid phases co-exist for a long time until the solid phase transformation is completed. However, the solubility was controlled by the more soluble solid phase in such cases.

Solubility data support that the complete reduction of U(VI) to U(IV) was achieved in all investigated systems, in good agreement with thermodynamic calculations and E_h - pH_m measurements. It must be noted that reduction kinetics are strongly affected by $[\text{U}(\text{VI})]_0$, $[\text{Sn}(\text{II})]$ and pH_m . The slowest reduction ($t = 635$ days) was observed in the sample containing the lowest $[\text{Sn}(\text{II})]$ (2 mM) and highest $[\text{U}(\text{VI})]_0$ ($4.2 \cdot 10^{-4}$ M) at $\text{pH}_m = 12.8$, whereas the fastest reduction ($t \approx 59$ days) was obtained for those samples with highest $[\text{Sn}(\text{II})]$ (20 mM) and lowest $[\text{U}(\text{VI})]_0$ ($3.0 \cdot 10^{-5}$ M) at $10 \leq \text{pH}_m \leq 12$. The slower kinetics especially under alkaline conditions can be explained with the decreasing stability field of U(IV), accordingly resulting in smaller Δp_e (as $|\text{pe}_{\text{exp}} - \text{pe}_{\text{borderline}}|$) with increasing pH_m (see Figure 3.1b) [117, 129].

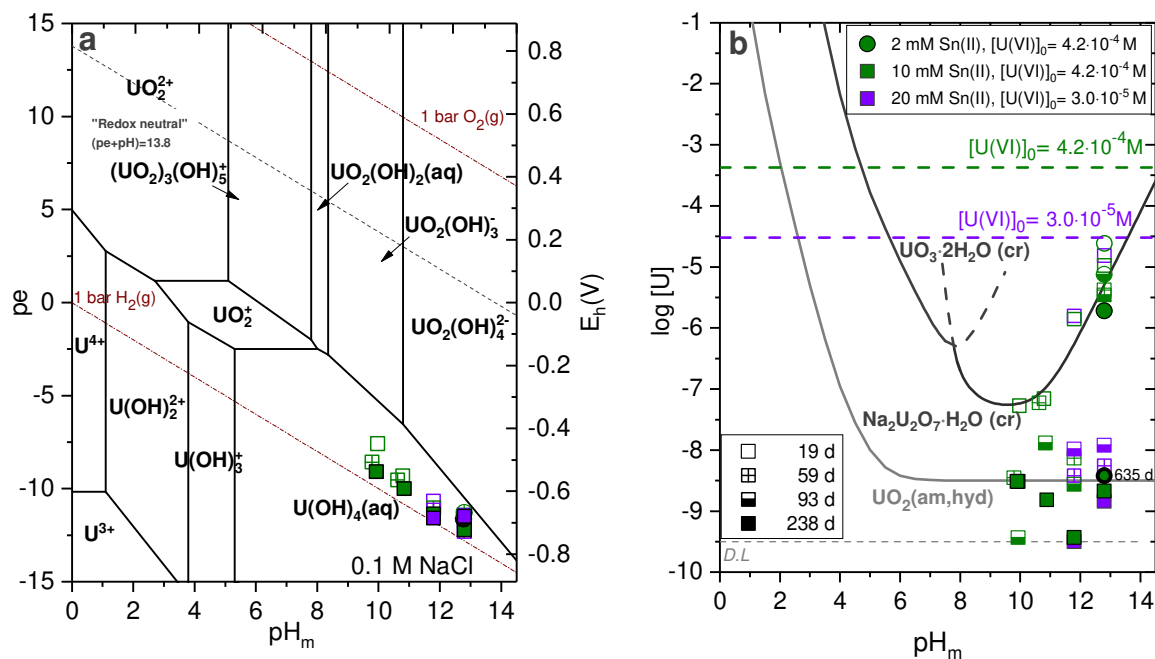


Figure 3.1. a. Pourbaix diagram of uranium calculated for $[U] = 3.0 \cdot 10^{-5} M$ and $0.1 M NaCl$ (minor differences observed for calculations using $4.2 \cdot 10^{-4} M$). b. concentrations of uranium measured after 10 kD ultrafiltration for $0.1 M NaCl$ systems with $[Sn(II)] = 2, 10$ and $20 mM$, and $[U(VI)]_0 = 4.2 \cdot 10^{-4}$ and $3.0 \cdot 10^{-5} M$. Solid lines correspond to solubility curves of $UO_3 \cdot 2H_2O(cr)$, $Na_2U_2O_7 \cdot H_2O(cr)$ and $UO_2(am, hyd)$. Dashed horizontal lines show the initial $U(VI)$ concentrations in the experiments. Different shapes and colors of data points correspond to different concentrations of $Sn(II)$ and uranium. The different filling of the data points refers to the different equilibration time. Precipitation of $UO_3 \cdot 2H_2O(cr)$, $Na_2U_2O_7 \cdot H_2O(cr)$ and $UO_2(am, hyd)$ is allowed in calculations in Figure a, accordingly resulting in the variation of $[U]_{aq}$ as a function of $(pe + pH_m)$.

Considering the results above, a set of samples were prepared in the presence of $20 mM Sn(II)$ with $3 \cdot 10^{-5} M$ initial uranium concentration in $0.1 M NaCl$ solutions, but extending the pH_m range to 2–13. $Sn(II)$ provides strong reducing conditions ($pe + pH_m = 2 \pm 1$) within the complete pH_m range as shown in Figure 3.2a, in excellent agreement with previous redox studies involving the use of this reducing system [129, 130]. In all cases, experimental ($pe + pH_m$) values are in the predominance area of $U(IV)$ in the complete pH_m -range investigated. Figure 3.2b shows uranium concentrations measured from 9 days up to 177 days. A very significant decrease of $[U]$ in agreement with the reduction of $U(VI)$ to $U(IV)$ was observed within $t \leq 177$ days for those samples at $pH_m \geq 4$. A longer contact time ($t = 574$ days) was required to observe complete reduction in the sample at $pH_m = 5.9$, possibly due to the closeness of its ($pe + pH_m$) to the stability field of $U(V)$ at this pH_m . The reduction behaviour of the sample at $pH_m = 2.2$ could not be interpreted by the solubility difference of $U(VI)$ and $U(IV)$ solid

phases since both solids are completely dissolved at this pH and [U]. Therefore, solvent extraction and XANES analysis are performed for this sample (see Section 3.5). The solubility behaviour of the data obtained within $2 \leq \text{pH}_m \leq 12.8$ is in excellent agreement with thermodynamic calculations performed for U(IV) based on the selected data (Table 1.2 and 1.3). This observation is not only a strong evidence of the complete reduction of U(VI) to U(IV), but also hints towards the expected role of $\text{UO}_2(\text{am, hyd})$ as solubility controlling solid phase in equilibrium with the hydrolysis species proposed by Neck and Kim [42].

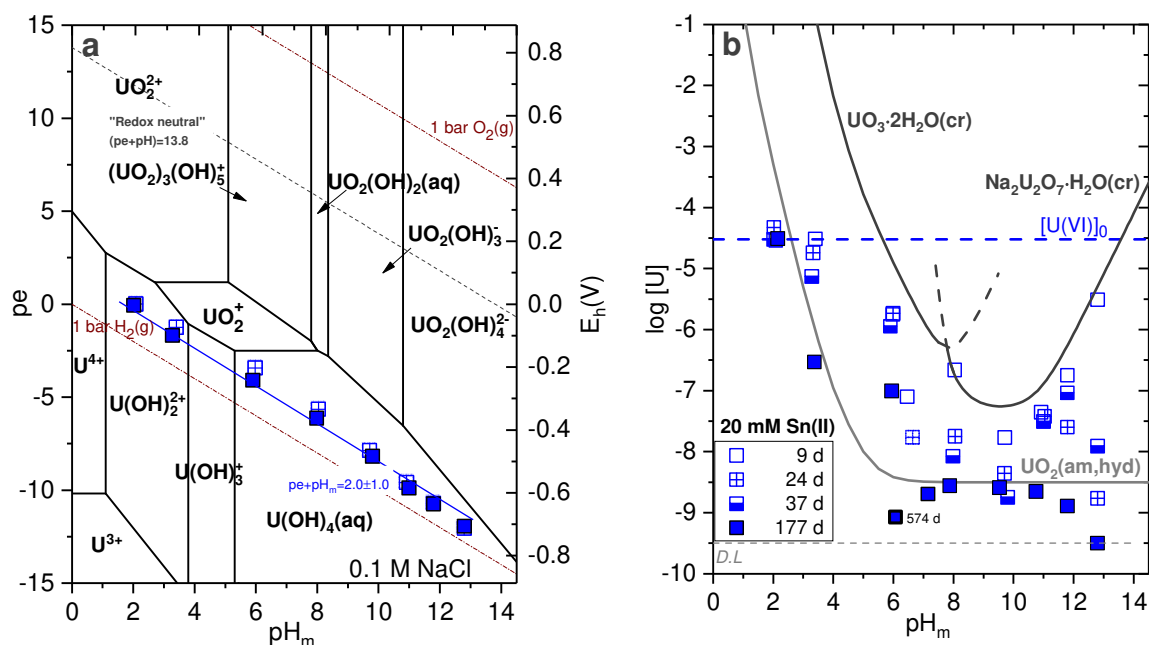


Figure 3.2. a. Pourbaix diagram of uranium calculated for $[\text{U}] = 3.0 \cdot 10^{-5} \text{ M}$ and 0.1 M NaCl . b. concentrations of uranium measured after 10 kD ultrafiltration for 0.1 M NaCl systems with $[\text{Sn(II)}] = 20 \text{ mM}$, and $[\text{U(VI)}]_0 = 3.0 \cdot 10^{-5} \text{ M}$. Solid lines correspond to solubility curves of $\text{UO}_3 \cdot 2\text{H}_2\text{O}(\text{cr})$, $\text{Na}_2\text{U}_2\text{O}_7 \cdot \text{H}_2\text{O}(\text{cr})$ and $\text{UO}_2(\text{am, hyd})$. Dashed horizontal line shows the initial U(VI) concentrations in the experiments. The different filling of the data points refers to the different equilibration time. Precipitation of $\text{UO}_3 \cdot 2\text{H}_2\text{O}(\text{cr})$, $\text{Na}_2\text{U}_2\text{O}_7 \cdot \text{H}_2\text{O}(\text{cr})$ and $\text{UO}_2(\text{am, hyd})$ is allowed in calculations in Figure a, accordingly resulting in the variation of $[\text{U}]_{\text{aq}}$ as a function of $(\text{pe} + \text{pH}_m)$.

The redox behavior of U(VI/IV) was also investigated in 5.0 M NaCl in the presence of 20 mM Sn(II) with $3 \cdot 10^{-5} \text{ M}$ initial uranium concentration. Figures 3.3a and 3.3b show the Pourbaix and solubility diagrams calculated for $I = 5.0 \text{ M NaCl}$. The Sn(II/IV) redox couple was impacted by ionic strength, showing slightly less reducing conditions ($\text{pe} + \text{pH}_m = 4 \pm 1$) in this system. A similar behaviour was reported for Sn(II) solutions in 5.0 M NaCl by Yalcintas *et al.* (2015)

[130]. In all samples, measured E_h values after 178 days were well within the predominance area of U(IV) species. Measured uranium concentrations after 178 days of contact time showed that all the samples in neutral to hyper-alkaline pH region are at the detection limit of ICP-MS (for this NaCl concentration). The slight decrease in uranium concentration observed at $\text{pH}_m \approx 4$ is consistent with the reduction of U(VI) to U(IV) and a solubility-control by $\text{UO}_2(\text{am, hyd})$. Solvent extraction performed to determine the oxidation state of U in this sample confirmed the predominance of U(IV) (see Table 4). The redox behaviour of uranium could not be conclusively evaluated in the samples at $\text{pH}_m = 7.6$ and 11.9 . The higher detection limit imposed by the concentrated salt system is indeed consistent (for this pH_m -region) with a solubility control of either $\text{Na}_2\text{U}_2\text{O}_7 \cdot \text{H}_2\text{O}(\text{cr})$ or $\text{UO}_2(\text{am, hyd})$. Although the reduction of U(VI) is expected considering that E_h values of both samples are within the stability field of U(IV), it cannot be concluded without further experimental evidences that 178 days are sufficient for the complete reduction to U(IV). Note for instance that up to 574 and 635 days were required in specific systems (see discussion above) to attain the complete reduction of U(VI) into U(IV). Additional insights on the sample at $\text{pH}_m = 11.9$ are gained by XANES analysis as discussed in Section 3.5.2. The clear decrease of [U] observed at $\text{pH}_m = 13.2$ and 14.5 is well below the solubility of $\text{Na}_2\text{U}_2\text{O}_7 \cdot \text{H}_2\text{O}(\text{cr})$, thus strongly supporting the complete reduction to U(IV). No evidence was found indicating the formation of anionic hydrolysis species ($\text{U}(\text{OH})_5^-$ and $\text{U}(\text{OH})_6^{2-}$) reported previously, even at $\text{pH}_m = 14.5$.

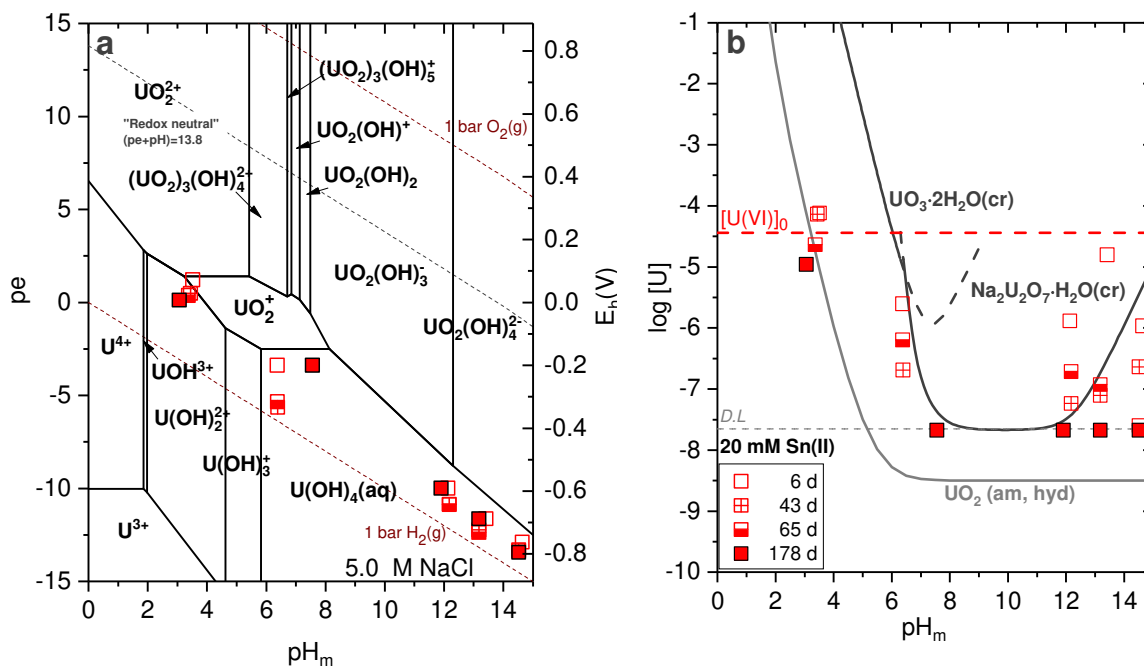


Figure 3.3. a. Pourbaix diagram of uranium calculated for $[U] = 3.0 \cdot 10^{-5} \text{ M}$ and 5.0 M NaCl . b. concentrations of uranium measured after 10 kD ultrafiltration for 5.0 M NaCl systems with $[\text{Sn(II)}] = 20 \text{ mM}$, and $[\text{U(VI)}]_0 = 3.0 \cdot 10^{-5} \text{ M}$. Solid lines correspond to solubility curves of $\text{UO}_3 \cdot 2\text{H}_2\text{O}(\text{cr})$, $\text{Na}_2\text{U}_2\text{O}_7 \cdot \text{H}_2\text{O}(\text{cr})$ and $\text{UO}_2(\text{am, hyd})$. Dashed horizontal line shows the initial U(VI) concentrations in the experiments. The different filling of the data points refers to the different equilibration time. Precipitation of $\text{UO}_3 \cdot 2\text{H}_2\text{O}(\text{cr})$, $\text{Na}_2\text{U}_2\text{O}_7 \cdot \text{H}_2\text{O}(\text{cr})$ and $\text{UO}_2(\text{am, hyd})$ is allowed in calculations in Figure a, accordingly resulting in the variation of $[U]_{\text{aq}}$ as a function of $(pe + \text{pH}_m)$.

3.2 Reduction of U(VI) in 0.1 M NaCl solutions using a $\text{Na}_2\text{S}_2\text{O}_4$ redox buffer

The redox behavior of U(VI/IV) was investigated in the presence of $20 \text{ mM Na}_2\text{S}_2\text{O}_4$ in 0.1 M NaCl solutions at $\text{pH}_m \geq 12$. $\text{Na}_2\text{S}_2\text{O}_4$ (slowly) degrades at lower pH_m -values, and accordingly this system was investigated only in hyperalkaline conditions [126, 127, 130]. Figure 3.4a shows that $\text{Na}_2\text{S}_2\text{O}_4$ is a strong reducing system with pe values at the border of water reduction ($pe + \text{pH}_m \approx 0$), thus in the stability field of U(IV). A fast decrease of uranium concentration to the solubility limit of U(IV) ($\approx 10^{-9} \text{ M}$) was observed within 9 days, indicating the complete reduction of U(VI). Fujiwara *et al.* (2005) [52] conducted similar U redox experiments in the presence of $\text{Na}_2\text{S}_2\text{O}_4$, but using higher initial uranium concentration than the present work ($[\text{U(VI)}]_0 = 1 \cdot 10^{-3} \text{ M}$). The authors observed relatively higher uranium concentration after 56 days of equilibration time (see Figure 3.4b), with an increasing trend of the solubility with

increasing pH. This observation was explained by the authors with the formation of $\text{U}(\text{OH})_5^-$ and $\text{U}(\text{OH})_6^{2-}$ species. Note that a very similar increase in uranium concentration under similar reducing conditions was interpreted by Ryan *et al.* (1983) [47] as the partial oxidation of U(IV) to U(VI). The concentrations of uranium measured in the present study under hyperalkaline conditions ($\approx 10^{-9}$ M) agree very well with thermodynamic calculations for the solubility of $\text{UO}_2(\text{am, hyd})$ in equilibrium with $\text{U}(\text{OH})_4(\text{aq})$ species, thus contradicting the formation of anionic U(IV) species within the investigated pH_m -range.

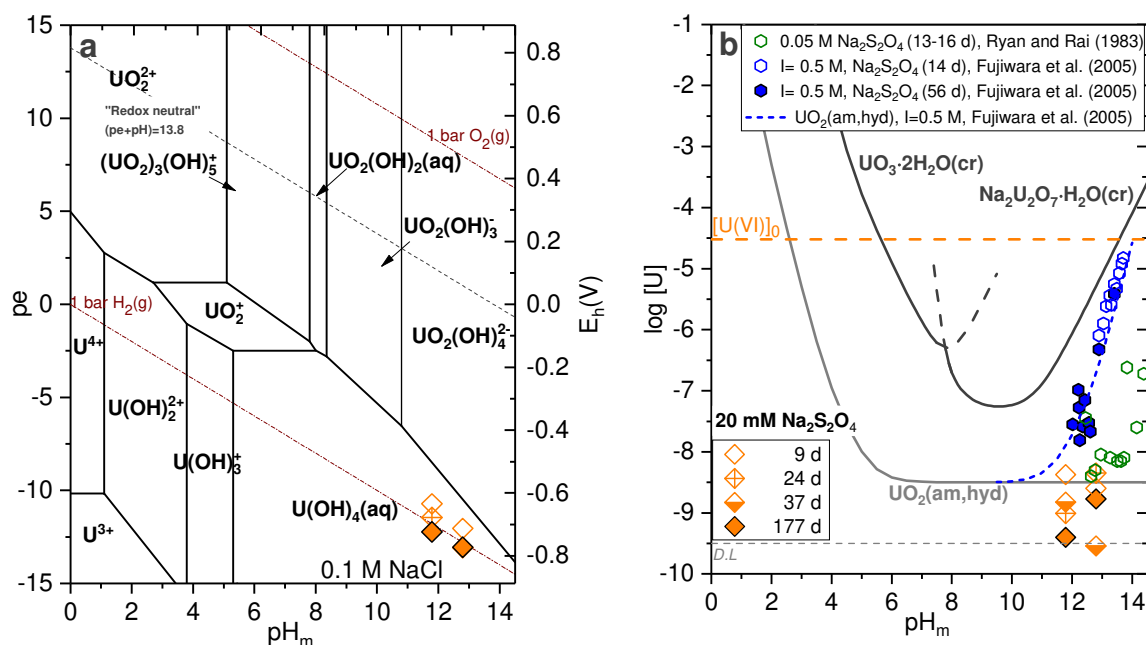


Figure 3.4. a. Pourbaix diagram of uranium calculated for $[\text{U}] = 3.0 \cdot 10^{-5}$ M and 0.1 M NaCl. Symbols represent experimentally measured E_h and pH_m values in 0.1 M NaCl systems containing 20 mM $\text{Na}_2\text{S}_2\text{O}_4$; b. red diamonds: concentrations of uranium measured in this work after 10 kD ultrafiltration for 0.1 M NaCl systems with $[\text{Na}_2\text{S}_2\text{O}_4] = 20$ mM and $[\text{U}(\text{VI})]_0 = 3.0 \cdot 10^{-5}$ M; blue / green hexagon: solubility data reported in Fujiwara *et al.* [52] and Ryan *et al.* [47], respectively. Solid lines correspond to solubility curves of $\text{UO}_3 \cdot 2\text{H}_2\text{O}(\text{cr})$, $\text{Na}_2\text{U}_2\text{O}_7 \cdot \text{H}_2\text{O}(\text{cr})$ and $\text{UO}_2(\text{am, hyd})$. Dashed blue line corresponds to the solubility of $\text{UO}_2(\text{am, hyd})$ at $I = 0.5$ M calculated including the formation of $\text{U}^{\text{IV}}(\text{OH})_5^-$ and $\text{U}^{\text{IV}}(\text{OH})_6^{2-}$ as reported by Fujiwara *et al.* [52]. Dashed horizontal line shows the initial U(VI) concentration in the experiments. The different filling of the data points refers to the different equilibration times. Precipitation of $\text{UO}_3 \cdot 2\text{H}_2\text{O}(\text{cr})$, $\text{Na}_2\text{U}_2\text{O}_7 \cdot \text{H}_2\text{O}(\text{cr})$ and $\text{UO}_2(\text{am, hyd})$ is allowed in calculations in Figure a, accordingly resulting in the variation of $[\text{U}]_{\text{aq}}$ as a function of $(pe + \text{pH}_m)$.

3.3 Reduction of U(VI) in 0.1 M NaCl solutions using a Sn(II) + TiO₂ redox buffer

Figure 3.5 shows the U(VI/IV) redox behavior in the presence of 20 mM Sn(II) and 10 mg TiO₂ in 0.1 M NaCl solutions with $2 \leq \text{pH}_m \leq 12.8$. The measured E_h values are in line with the values obtained in pure Sn(II) system, and are clearly situated in the stability field of U(IV). Figure 3.5b indicates that the complete reduction takes place within 37 days in most of the investigated samples at $\text{pH}_m \geq 4$. This observation confirms significantly faster reduction kinetics than in pure Sn(II) system (Figure 3.3b). As in the case of pure Sn(II) system, slower reduction kinetics are observed at $\text{pH}_m \approx 6$.

The discussion above highlights that despite the analogous ($pe + \text{pH}_m$) values measured in Sn(II) and Sn(II) + TiO₂ systems, the presence of TiO₂ accelerates the reduction of U(VI) to U(IV). This behavior is consistent with the role of TiO₂ in catalysing redox processes [131-133]. The formation of U(VI) surface complexes on TiO₂, which facilitate the thermodynamically favored reduction to U(IV) is very well-known and supported by different spectroscopic methods in a number of studies [134-138].

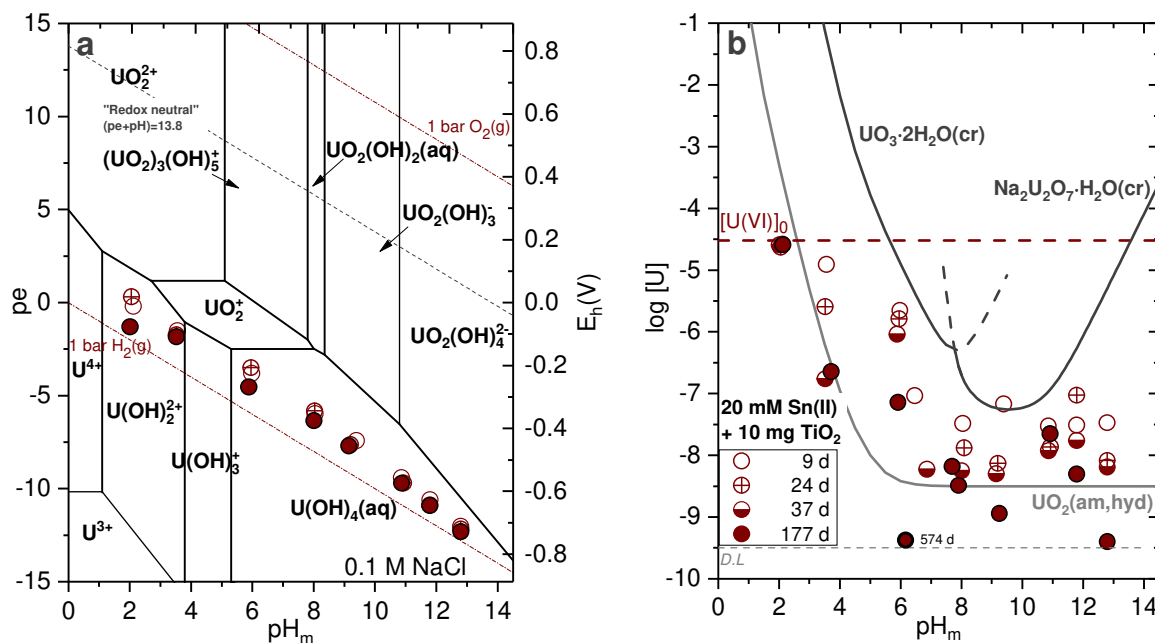


Figure 3.5. a. Pourbaix diagram of uranium calculated for $[U] = 3.0 \cdot 10^{-5} M$ and $0.1 M NaCl$. Symbols represent experimentally measured E_h and pH_m values in $0.1 M NaCl$ systems containing $20 mM Sn(II) + 10 mg TiO_2$; b. concentrations of uranium measured after $10 kD$ ultrafiltration for $0.1 M NaCl$ systems with $[Sn(II)] = 20 mM + 10 mg TiO_2$ and $[U(VI)]_0 = 3.0 \cdot 10^{-5} M$. Solid lines correspond to solubility curves of $UO_3 \cdot 2H_2O(cr)$, $Na_2U_2O_7 \cdot H_2O(cr)$ and $UO_2(am, hyd)$. Dashed horizontal line indicates the initial $U(VI)$ concentration in the experiments. The different filling of the data points refers to the different equilibration times. Precipitation of $UO_3 \cdot 2H_2O(cr)$, $Na_2U_2O_7 \cdot H_2O(cr)$ and $UO_2(am, hyd)$ is allowed in calculations in Figure a, accordingly resulting in the variation of $[U]_{aq}$ as a function of $(pe + pH_m)$.

3.4 Reduction of U(VI) in 0.1 M NaCl solutions using Sn(II) + Fe(0) and Sn(II) + Fe₃O₄(cr) redox buffers

The Pourbaix diagrams of uranium in the presence of Sn(II) + Fe(0) and Sn(II) + Fe₃O₄ are shown in Figure 3.6a and Figure 3.7a, respectively. Fe(0) provides very reducing conditions ($pe + pH_m = 2 \pm 1$) at $pH_m \leq 10$ [79, 130, 139], whereas passivation/corrosion of the surface occurs in alkaline pH region due to the oxidation to higher redox states and precipitation of Fe-hydroxides leading to the increase of the redox potential [129, 130, 140]. Magnetite (in the absence of other reducing chemicals) can buffer a range of redox potentials depending on the synthetic method and resulting material properties (e.g. particle size) [129, 130]. Both in Sn(II) + Fe(0) and Sn(II) + Fe₃O₄ systems, the measured E_h values ($pe + pH_m = 2 \pm 1$) are the same as

observed in Sn(II) systems, thus indicating that the redox potential is mostly controlled by Sn(II) rather than Fe(0) or Fe₃O₄.

Total uranium concentrations measured at different equilibration times are shown in Figure 3.6b and Figure 3.7b for Sn(II) + Fe(0) and Sn(II) + Fe₃O₄ systems, respectively. Uranium concentration in the samples at pH_m ≤ 10 decreased to the U(IV) solubility limit within 37 days, whereas slow kinetics (up to 574 days) were observed at pH_m ≥ 11 in both Fe systems. Slower kinetics in the hyperalkaline pH region are possibly related with changes in the solid phase properties, solubility and aqueous speciation of Fe within the investigated conditions. Similar U(VI) redox experiments were performed by Rai *et al.* (1990) [50] in the presence of Fe(0) and are shown in Figure 3.6b. The data collected by the authors after 6 days of equilibration time are in a very good agreement with the data in the present study after 9 days. The authors reported the presence of U(VI) due to the incomplete reduction in the data at pH = 11.7, which is also consistent with the slow reduction kinetics observed in this study for these pH_m conditions. González-Siso *et al.* (2015) [140] investigated the redox behavior of U(VI/IV) at pH_m = 12.8 with 3.0 · 10⁻⁵ M as initial uranium concentration and Sn(II) + Fe₃O₄ as reducing system. Data reported by the authors shows a slow decrease of the original uranium concentration agreeing well with the behaviour observed in the present work. The oxidation state of U in the solid phase was determined as +4 by XPS analysis, as it is expected in the present study based on measured redox potentials.

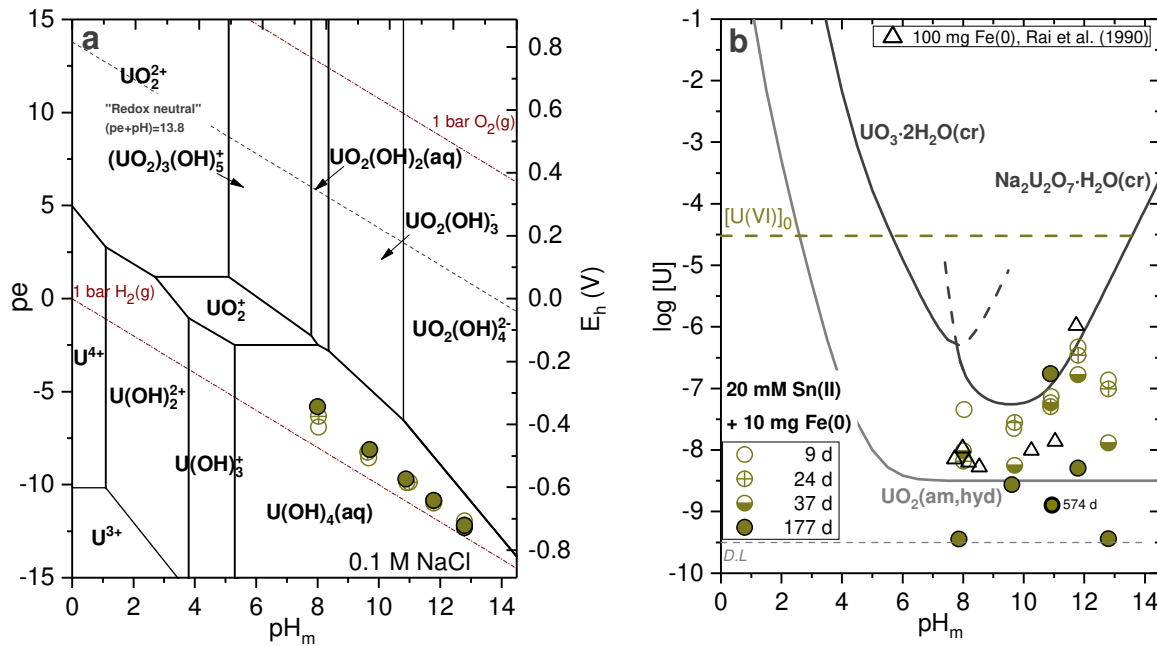


Figure 3.6. a. Pourbaix diagram of uranium calculated for $[U] = 3.0 \cdot 10^{-5} M$ and 0.1 M NaCl systems containing 20 mM Sn(II) + 15 mg Fe(0); b. concentrations of uranium measured after 10 kD ultrafiltration for 0.1 M NaCl systems with $[Sn(II)] = 20$ mM + 15 mg Fe(0) and $[U(VI)]_0 = 3.0 \cdot 10^{-5} M$; black triangles: solubility of $UO_2(am, hyd)$ in Fe(0) systems as reported in Rai et al. (1990). Solid lines correspond to solubility curves of $UO_3 \cdot 2H_2O(cr)$, $Na_2U_2O_7 \cdot H_2O(cr)$ and $UO_2(am, hyd)$. Dashed horizontal line shows the initial U(VI) concentration in the experiments. The different filling of the data points refers to the different equilibration times. Precipitation of $UO_3 \cdot 2H_2O(cr)$, $Na_2U_2O_7 \cdot H_2O(cr)$ and $UO_2(am, hyd)$ is allowed in calculations in Figure a, accordingly resulting in the variation of $[U]_{aq}$ as a function of $(pe + pH_m)$.

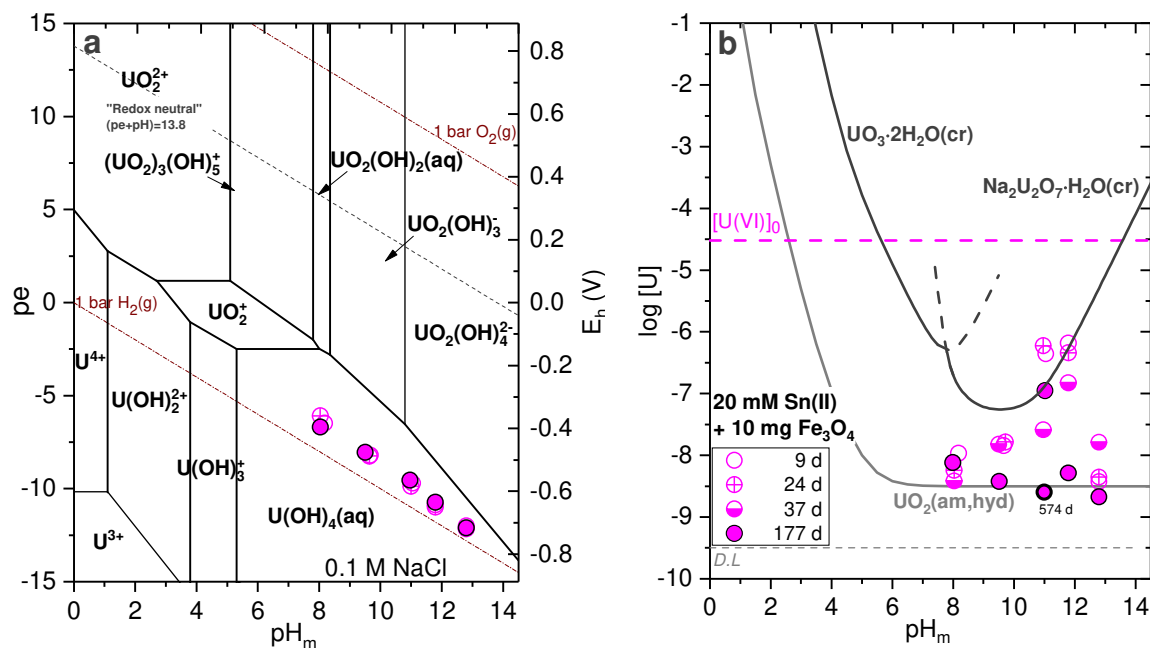


Figure 3.7. a. Pourbaix diagram of uranium calculated for $[U] = 3.0 \cdot 10^{-5} \text{ M}$ and 0.1 M NaCl in 0.1 M NaCl systems containing $20 \text{ mM Sn(II)} + 10 \text{ mg Fe}_3\text{O}_4(\text{cr})$; b. concentrations of uranium measured after 10 kD ultrafiltration for 0.1 M NaCl systems with $[\text{Sn(II)}] = 20 \text{ mM} + 10 \text{ mg Fe}_3\text{O}_4(\text{cr})$ and $[\text{U(VI)}]_0 = 3.0 \cdot 10^{-5} \text{ M}$. Solid lines correspond to solubility curves of $\text{UO}_3 \cdot 2\text{H}_2\text{O}(\text{cr})$, $\text{Na}_2\text{U}_2\text{O}_7 \cdot \text{H}_2\text{O}(\text{cr})$ and $\text{UO}_2(\text{am, hyd})$. Dashed horizontal line indicates the initial U(VI) concentration in the experiments. The different filling of the data points refers to the different equilibration times. Precipitation of $\text{UO}_3 \cdot 2\text{H}_2\text{O}(\text{cr})$, $\text{Na}_2\text{U}_2\text{O}_7 \cdot \text{H}_2\text{O}(\text{cr})$ and $\text{UO}_2(\text{am, hyd})$ is allowed in calculations in Figure a, accordingly resulting in the variation of $[\text{U}]_{\text{aq}}$ as a function of $(pe + \text{pH}_m)$.

3.5 Redox speciation of uranium in the aqueous and solid phases

3.5.1 Solvent extraction

Solvent extraction was used to determine the oxidation state of uranium in samples containing $[\text{U}] \geq 10^{-5} \text{ M}$. Due to the low solubility of U(IV) , the application of the extraction method was limited to samples within $2 \leq \text{pH}_m \leq 3.1$. Table 3.1 summarizes the results obtained for selected acidic samples. Since the solid phases at this pH range are mostly dissolved, no conclusions could be drawn from the solubility behavior (see discussion in Sections 3.1 to 3.3). As expected from the experimental $(pe + \text{pH}_m)$ values and corresponding thermodynamic calculations (*e.g.*

Pourbaix diagrams), the presence of U(IV) in solution ($\geq 97\%$) after attaining equilibrium conditions was confirmed by solvent extraction in the three investigated samples.

Table 3.1 Fraction of U(IV) in the aqueous phase of selected solubility samples in acidic, dilute to concentrated NaCl solutions, as quantified by solvent extraction after 10 kD ultrafiltration.

Sample	pH _m ^a	E _h [mV] ^b	U(IV) [%] ^c
0.1 M NaCl, 20 mM Sn(II)	2.2	-284	98 %
0.1 M NaCl, 20 mM Sn(II) + 10 mg TiO ₂	2.1	-357	97 %
5.0 M NaCl, 20 mM Sn(II)	3.1	-288	99 %

a. ± 0.05 ; b. ± 20 mV; c. $\pm 10\%$

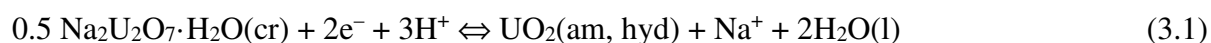
3.5.2 XANES analysis

U-L_{III}-edge XANES spectra of selected aqueous (measured at CAT-ACT beamline) and solid samples (measured at INE-beamline) are shown in Figure 3.8a and Figure 3.8b. Table 3.2 summarizes the edge positions of spectra together with the experimental conditions. Some significant differences were observed in the edge position (white line, WL) of solid and aqueous references for U(IV) and U(VI), arising from the use of different beamlines and impact of the difference between aqueous and solid moieties as previously discussed in the literature [141]. Accordingly, spectra collected of unknown aqueous / solid samples were compared to reference spectra of aqueous species/ solid compounds obtained at the same beamline.

The XANES spectrum of the aqueous sample containing 20 mM Sn(II) in 0.1 M NaCl at pH_m ≈ 2 agrees very well with the reference spectrum of U(IV). The combination of this observation with E_h measurements, solubility behaviour and solvent extraction unequivocally confirms the complete reduction of U(VI) to U(IV) in this sample, in agreement with thermodynamic calculations.

Solid phases of two solubility samples were investigated by XANES: (i) 0.1 M NaCl at pH_m = 10.9, with 20 mM Sn(II) + 15mg Fe(0), and (ii) 5.0 M NaCl at pH_m = 11.9, with 20 mM Sn(II). Figure 3.7b shows that the edge position of the solid phase equilibrated in 0.1 M NaCl matches very well with the edge position of UO₂(am, hyd) reference. However, a shift to higher energies ($\approx +1.5$ eV) compared to the U(IV) solid reference was observed in the solid phase equilibrated in 5.0 M NaCl. Although the predominance of U(IV) can be safely proposed based on the

absence of the typical shoulder of uranyl/uranate moieties, the shift in energy with respect to the U(IV) reference supports that a mixture of U(IV) and higher uranium oxidation states (U(V) and/or U(VI)) solid phases is present in the investigated sample. It is likely that the respective solid phase consists of a non-stoichiometric UO_{2+x} (am, hyd) phase. This observation is consistent with the expected slow solid phase transformation of a rapidly precipitated $\text{Na}_2\text{U}_2\text{O}_7 \cdot \text{H}_2\text{O}(\text{cr})$ to $\text{UO}_2(\text{am, hyd})$ (see further discussion in Section 3:1). XANES data under discussion were collected after 330 days of equilibration time, thus indicating that longer equilibration times are needed to achieve a complete reduction at this pH_m in 5.0 M NaCl. Note however that the same equilibration time was sufficient to achieve a complete reduction of U(VI) to U(IV) in a 0.1 M NaCl solution at $\text{pH}_m = 10.9$. This observation can be rationalized by considering the equilibrium reaction defining the transformation of $\text{Na}_2\text{U}_2\text{O}_7 \cdot \text{H}_2\text{O}(\text{cr})$ (first, fast precipitated U(VI) solid phase) to $\text{UO}_2(\text{am, hyd})$ (end-member, U(IV) solid phase thermodynamically expected):



Reaction (3.1) shows that the transformation of $\text{Na}_2\text{U}_2\text{O}_7 \cdot \text{H}_2\text{O}(\text{cr})$ into $\text{UO}_2(\text{am, hyd})$ is favoured at lower pH_m , p_e and $[\text{NaCl}]$, thus providing a consistent picture with XANES data collected for samples in 0.1 M NaCl at $\text{pH}_m = 10.9$ (complete reduction after $t = 330$ days) and 5.0 M NaCl at $\text{pH}_m = 11.9$ (incomplete reduction after $t = 330$ days). This observation supports again that redox transformations of U(VI) to U(IV) are strongly affected by kinetics.

Table 3.2 XANES results of selected aqueous and solid samples. Solid and aqueous, U(IV) and U(VI) references measured at INE- and ACT- Beamline, respectively.

Sample	pH _m ^a	E ₁ ^b [mV]	Contact time [days]	Edge position (eV)	Beamline
Solid phase					
Reference Na ₂ U ₂ O ₇ ·H ₂ O(cr)	≈ 12	n. m.		17180.0	INE
Reference UO ₂ (am, hyd)	≈ 12	n. m.		17177.0	INE
0.1 M NaCl, 20mM Sn(II) + Fe(0)	10.9	-798	330	17177.0	INE
5.0 M NaCl, 20mM Sn(II)	11.9	-799	330	17178.5	INE
Aqueous phase					
Reference U(VI), 1.0 M HCl	≈ 0	n. m.		17176.5	ACT
Reference U(IV), 1.0 M HCl, 20 mM Sn(II)	≈ 0	n. m.		17175.2	ACT
0.1 M NaCl, 20 mM Sn(II)	2.2	-284	330	17175.2	ACT

a. ± 0.05; b. ± 20 mV; n.m: not measured.

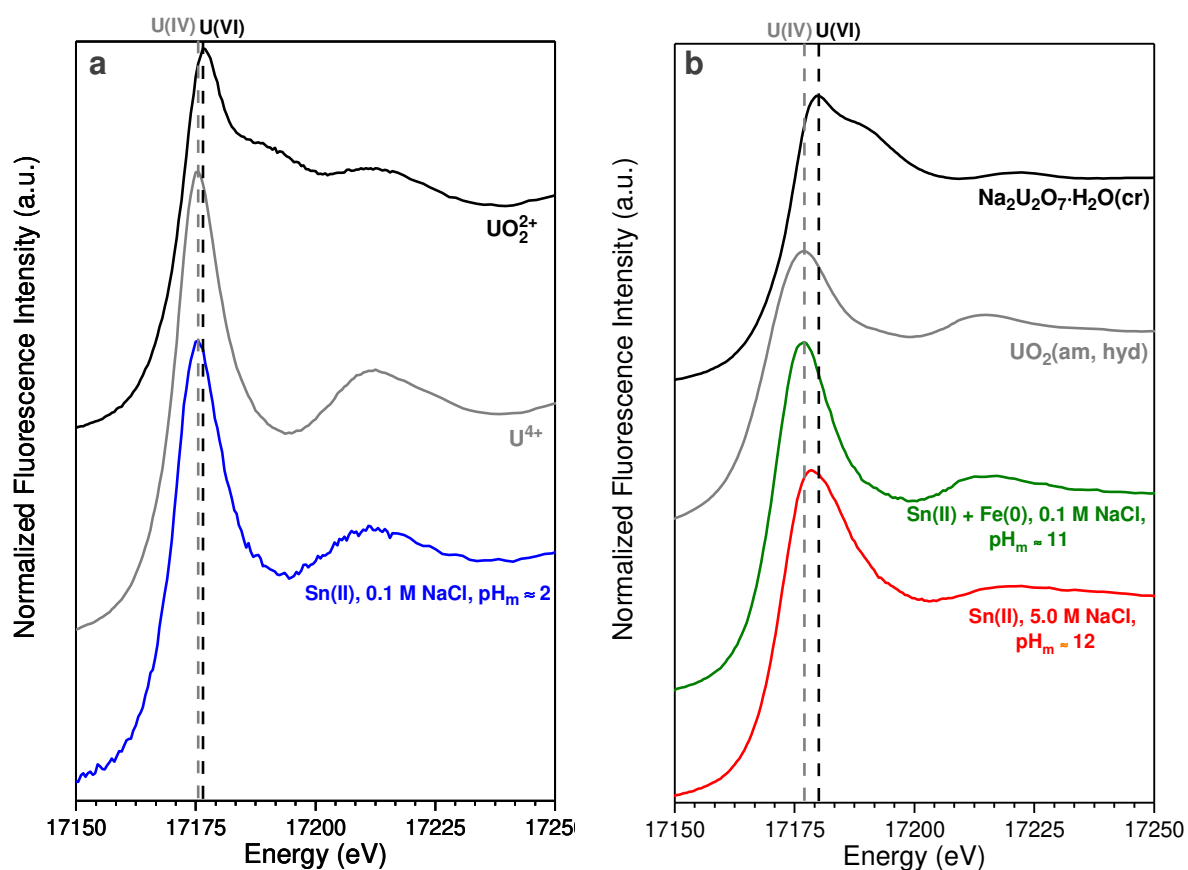


Figure 3.8. U L_{III} XANES spectra collected for (a) aqueous sample in 0.1 M NaCl, 20 mM Sn(II) at pH_m ≈ 2; (b) uranium solid phases collected from solubility experiments in 0.1 M NaCl, 20 mM Sn(II) + 15 mg Fe(0) at pH_m ≈ 11 (green line), and in 5.0 M NaCl, 20 mM Sn(II) at pH_m ≈ 12 (red line). Black and grey spectra in (a) and (b) correspond to U(VI) and U(IV) references, respectively.

3.6 Discussion of kinetic aspects of U(VI) reduction to U(IV) and comparison with literature data

Figure 3.9a shows the time evolution of $\log [U]$ in Sn(II) systems with different Sn(II) concentrations (2, 10 and 20 mM) and $[U(VI)]_0$ ($4.2 \cdot 10^{-5}$ M and $3 \cdot 10^{-5}$ M) at $pH_m \approx 13$. The fastest complete reduction of U(VI) to U(IV) (≈ 50 days) was obtained in the system containing the lowest $[U(VI)]_0$ ($3 \cdot 10^{-5}$ M) and highest $[Sn(II)]$. In the system with the highest $[U(VI)]_0$ ($4.2 \cdot 10^{-4}$ M) and lowest $[Sn(II)]$ (2 mM), the complete reduction was achieved only after an equilibration time of ≈ 600 days. In all systems, a clear and fast decrease down to the solubility level controlled by the $Na_2U_2O_7 \cdot H_2O(cr)$ was observed after ≈ 20 days and ≈ 50 days in 20 mM and 2-10 mM Sn(II) systems, respectively. This confirms that the reduction of U(VI) to U(IV) from oversaturation conditions occurs in two steps: first, a fast precipitation of U(VI) solid phases and subsequently a slow transformation of this solid phase into $UO_2(am, hyd)$.

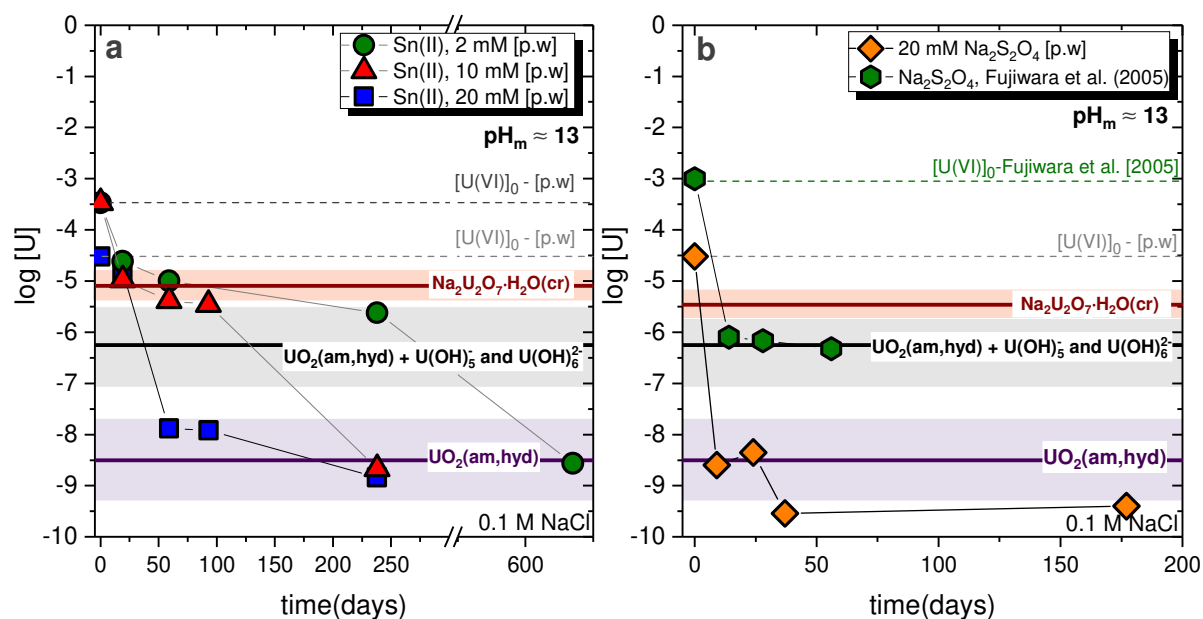


Figure 3.9. Evolution of $[U]$ with time in reducing a. Sn(II) systems with $[U(VI)]_0 = 4.2 \cdot 10^{-4} - 3 \cdot 10^{-5}$ M and $[Sn(II)] = 2 - 20$ mM at $pH_m \approx 13$ b. $Na_2S_2O_4$ systems at $pH_m \approx 13$, as determined in the present work (0.1 M NaCl) and reported by Fujiwara *et al.* [52] (0.5 M NaClO₄–NaOH). Solid horizontal lines in the figure correspond to the solubility of $Na_2U_2O_7 \cdot H_2O(cr)$ (dark red) for 0.5 M NaCl–NaOH and $UO_2(am, hyd)$ (purple) calculated at $pH_m = 13$. Black line corresponds to the solubility of $UO_2(am, hyd)$ calculated including the formation of $U(OH)_5^-$ and $U(OH)_6^{2-}$ as reported in Fujiwara *et al.* (2005). Coloured area (in red / grey / purple) gives an indication of the uncertainty in the given solubility equilibria. Dashed horizontal lines indicate the initial U(VI) concentration in the experiments.

Figure 3.9b shows the reduction of U(VI) in $Na_2S_2O_4$ systems at $pH_m \approx 13$, as determined in the present work and reported in Fujiwara *et al.* [52]. The figure shows that a very fast decrease of $[U]_{aq}$ to $\approx 10^{-8.5}$ M was observed in the present work after 9 days, supporting a solubility control by $UO_2(am, hyd)$ in equilibrium with $U(OH)_4(aq)$. However, a significantly higher uranium concentration ($\approx 10^{-6}$ M) was reported by Fujiwara and co-authors [52] after ≈ 50 days contact time. The authors interpreted this behaviour with the formation of $U(OH)_5^-$ and $U(OH)_6^{2-}$ species in equilibrium with $UO_2(am, hyd)$. Differences in some key parameters between both studies have probably lead to such different observations and conclusions. First of all, a significantly higher $[U(VI)]_0$ was used in Fujiwara *et al.* [52] compared to the present work ($1 \cdot 10^{-3}$ M vs. $3 \cdot 10^{-5}$ M). As it is shown in Figure 3.9a, a longer equilibration time of up to 635 days was needed for a complete reduction to U(IV) in the samples with higher initial U(VI) concentration ($4.2 \cdot 10^{-4}$ M). The concentration of $Na_2S_2O_4$ is another parameter that needs to be considered, but unfortunately the concentration used by the Fujiwara and co-authors was

not reported. Last but not least, the concentration of Na (as 0.5 M NaClO₄–NaOH) was larger in Fujiwara *et al.* [52] than in the present work (0.1 M NaCl–NaOH). As elaborated above, all these differences are in line with slower reduction kinetics in the study by Fujiwara *et al.* [52], compared to the present work. Together with the shorter monitoring time (\approx 50 days, compared to 176 days in the present study), such differences strongly suggest that insufficient equilibration time was applied by Fujiwara and co-workers. Accordingly, the authors only observed the first step in the reduction process (*e.g.* fast precipitation of Na₂U₂O₇·H₂O(cr)) and missed the second, slower step involving the complete transformation of this U(VI) phase into UO₂(am, hyd). The solubility data obtained in their system are most likely controlled by Na₂U₂O₇·H₂O(cr) considering the agreement of the measured [U] with the solubility calculated using $\log^* K'_{s,(1,4)} = -(19.05 \pm 0.1)$ as reported by Altmaier *et al.* [52]. Furthermore, it must be noted that the data collected in the present work are in excellent agreement with the solubility data reported by Ryan and Rai (1983) (data not shown) with UO₂(am, hyd) precipitated from a U(IV) stock solution treated in Na₂S₂O₄ reducing system.

The evolution of uranium concentration with time at pH_m = 8 – 13 is shown in Figure 3.10 for all investigated reducing systems containing Sn(II): 20 mM Sn(II), 20 mM Sn(II) + 10 mg Fe(0), 20 mM Sn(II) + 10 mg Fe₃O₄(cr) and Sn(II) + 10 mg TiO₂. In the figures, solubility of U(VI) (as Na₂U₂O₇·H₂O(cr)) and U(IV) (as UO₂(am, hyd)) are also included as calculated using thermodynamic data summarized in Tables 1.2 and 1.3. Besides the relatively faster reduction kinetics observed in TiO₂ containing systems at pH_m \geq 12, no significant differences were observed for these systems. The two-step reduction in oversaturated solutions of U(VI) was clearly observed in almost all investigated systems, indicating a fast decrease of [U] to a concentration level defined by Na₂U₂O₇·H₂O(cr), followed by a slower decrease of concentration to [U] \approx 10⁻⁸ – 10^{-9.5} M as solubility-limit of UO₂(am, hyd). Such behaviour was more evident in the pH_m-range 12–13 because of the larger differences in the solubility of U(IV) and U(VI), compared to lower pH_m values.

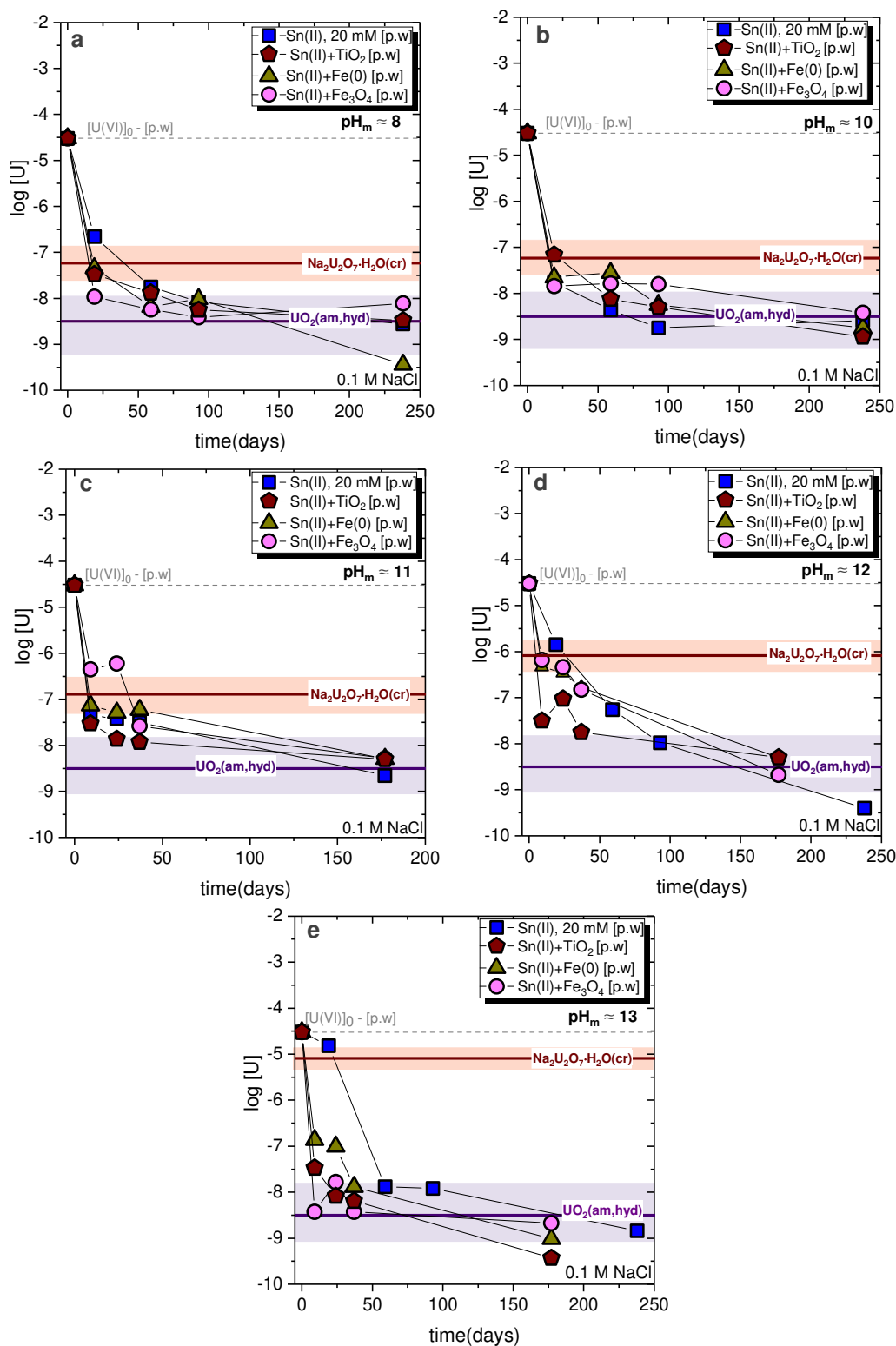


Figure 3.10. Evolution of $[U]$ with time in reducing systems in the presence of Sn(II), Sn(II) + TiO₂, Sn(II) + Fe(0) and Sn(II) + Fe₃O₄(cr) at: a. $pH_m \approx 8$; b. $pH_m \approx 10$; c. $pH_m \approx 11$, d. $pH_m \approx 12$ and e. $pH_m \approx 13$. Solid horizontal lines in the figures indicate the solubility of $Na_2U_2O_7 \cdot H_2O(cr)$ (red) and $UO_2(am,hyd)$ (blue) at the related pH_m . Coloured areas (in red / blue) correspond to the uncertainty of the calculated solubility. Dashed horizontal line indicate the initial U(VI) concentration in the experiments.

The results obtained in the present work clearly disagree with a predominant role of anionic hydrolysis species in the solution chemistry of U(IV) under alkaline to hyperalkaline conditions, whilst highlighting the relevance of kinetics in the correct interpretation of redox processes in such systems. Furthermore, experimental evidences gained in this study support that $\text{UO}_2(\text{am, hyd})$ is the solid phase controlling the solubility of U(IV) when approached from oversaturation conditions.

4 Solubility and hydrolysis of U(IV) in reducing, dilute to concentrated NaCl, MgCl₂ and CaCl₂ solutions

U(IV) solubility and hydrolysis were investigated in 0.1, 0.5, 2.0 and 5.0 M NaCl-NaOH solutions at $1 \leq \text{pH}_m \leq 14.5$, in 0.25, 2.0 and 4.5 M MgCl₂ solutions at $1 \leq \text{pH}_m \leq 9$, and in 0.25, 2.0 and 4.5 M CaCl₂ solutions at $9 \leq \text{pH}_m \leq 12$. Solubility was studied from undersaturation conditions using a well-characterized solid phase, UO₂(s, hyd). Based on the knowledge gained in Chapter 3, reducing conditions were chemically controlled with Sn(II) ($\text{pe} + \text{pH}_m \approx 2$). Concentration of uranium and pH_m values were monitored at regular time intervals for up to 605 days. The UO₂(s, hyd) “starting material” and solid phases recovered from selected solubility samples after attaining equilibrium conditions were characterized by XRD, SEM-EDS, TG-DTA, quantitative chemical analysis and XANES/EXAFS analysis. Chemical, thermodynamic and (SIT) activity models were derived for the system U⁴⁺-Na⁺-Mg²⁺-Ca²⁺-H⁺-Cl⁻-OH⁻-H₂O(l) based on the newly generated experimental data, but taking also advantage of the previous thermodynamic data selection in the NEA-TDB and the comprehensive review and estimation work by Neck and Kim (2001).

4.1 Solubility data of U(IV) in reducing, dilute to concentrated NaCl, MgCl₂ and CaCl₂ solutions

4.1.1 Solubility data of U(IV) in reducing, dilute to concentrated NaCl solutions

Figure 4.1 shows the concentration of U(IV) in equilibrium with UO₂(s, hyd) as determined in 0.1, 0.5, 2.0 and 5.0 M NaCl solutions. Under acidic conditions ($\text{pH}_m \leq 5$), a steep decrease in the solubility is observed with increasing pH_m . Furthermore, a slight increase of the solubility takes place with increasing ionic strength. Figure 4.1 shows also experimental solubility data with UO₂(am, hyd) as reported by Rai *et al.* (1997) [84], as well as the solubility curve of UO₂(am, hyd) calculated using the thermodynamic model reported by Neck and Kim (2001) [42]. The trend in the solubility data determined in this work is in good agreement with solubility data reported by Rai *et al.* [84] and model calculations using thermodynamic data in Neck and Kim. (2001) [42], although uranium concentrations measured in the present work are approximately 2 orders of magnitude lower. Such discrepancies could be attributed to the

particle size of the solid phase used in different studies. The method used by Rai and co-workers and in the present work for the synthesis of $\text{UO}_2(\text{s, hyd})$ is very similar. However, most of the data reported by the former authors were collected after equilibration times of 50 – 100 days. Only for a limited number of samples / systems, an additional, long-term sampling step was performed after 300 – 400 days. Indeed, a clear trend to decrease [U] with time can be observed in most of their NaCl systems. In this study, the freshly prepared $\text{UO}_2(\text{s, hyd})$ was aged for 3 months before starting the undersaturation solubility experiments. After preparation of the individual samples, these were equilibrated for up to 605 days in the corresponding matrix solutions. Such differences in the equilibration time may have resulted in differences in the particle size and, accordingly, in the solubility. A thorough discussion on the $\text{UO}_2(\text{s, hyd})$ solid phase used in the present study and in Rai *et al.* (1997) [84] is provided in Section 4.2.1.

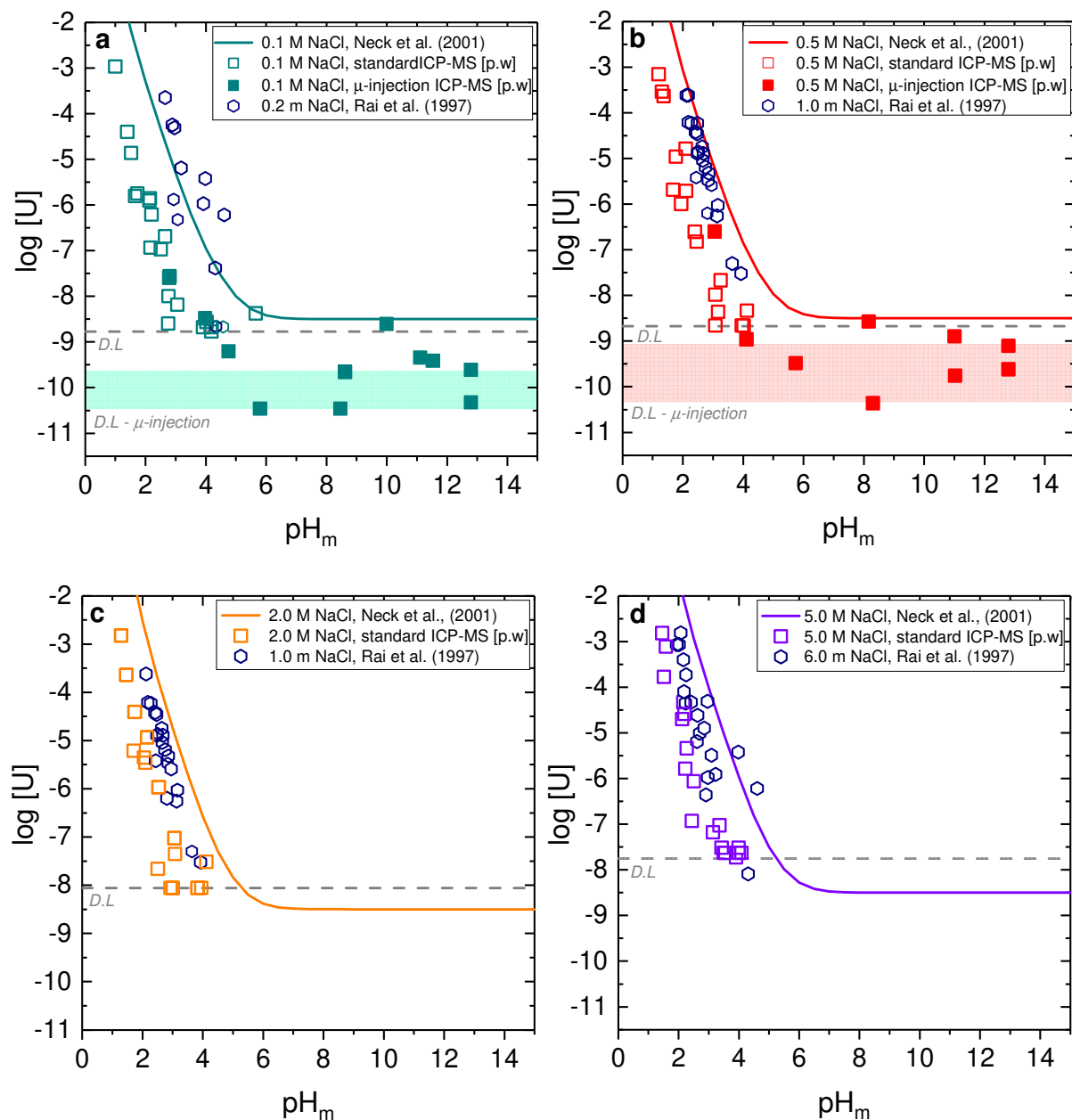


Figure 4.1. Experimental solubility data obtained in this work in a. 0.1 M, b. 0.5 M, c. 2.0 M and d. 5.0 M NaCl systems, in comparison with previously reported data by Rai et al. [84]. Solid lines corresponding to the solubility of $UO_2(am, hyd)$ solid phase calculated for each ionic strength by using the data reported by Neck and Kim (2001). Detection limits for μ -injection ICP-MS measurements in 0.1 and 0.5 M NaCl systems are shown as shadowed areas in light cyan and light red and correspond to detection limits from different measurements (calculated as 3σ of the blank).

The detection of [U] at $\text{pH}_m \geq 4 / 5$ (depending upon ionic strength) is challenging due to the very low solubility and the strong dilution steps (100 to 5000 times) needed in the most concentrated NaCl systems. For this reason, μ -injection ICP-MS was used to achieve lower detection limits in 0.1 and 0.5 M NaCl solutions ($\approx 10^{-9} - 10^{-11}$ M, see Chapter 2). This technique could not be applied to 2.0 and 5.0 M NaCl as respective detection limits after appropriate dilution of the samples were too low.

Figure 4.2 shows the experimental solubility data in dilute to concentrated NaCl solutions at $\text{pH}_m \geq 5$ after 10 kD ultrafiltration (colored symbols) and without phase separation (clear supernatant, gray diamonds). Solubility data after 10 kD ultrafiltration could only be gained for 0.1 and 0.5 M NaCl systems, for which μ -injection ICP-MS was used. The largely scattered solubility data observed in this pH_m -region is most likely caused by the formation / presence of U(IV) intrinsic colloids [39, 142], the very low U(IV) solubility and / or the sorption of neutral $\text{U}(\text{OH})_4(\text{aq})$ species in the filter. All uranium concentrations measured after 10 kD ultrafiltration in 2.0 and 5.0 M NaCl systems were below the detection limit of the standard ICP-MS. In 0.1 and 0.5 M NaCl systems, the experimentally measured $[\text{U}]_{\text{aq}}$ falls clearly below the solubility of $\text{UO}_2(\text{am, hyd})$ calculated using the thermodynamic and activity models summarized in Table 1.2 and 1.3 of the Introduction. This finding is consistent with the observations obtained under acidic conditions, thus further supporting a solubility-control by a more crystalline solid phase. A pH_m -independent behaviour of the solubility was observed at $5 \leq \text{pH}_m \leq 13$ (Figures 4.2 a and b). Assuming a solubility-control by $\text{UO}_2(\text{s, hyd})$, this behaviour implies that the neutral species $\text{U}(\text{OH})_4(\text{aq})$ prevails in the aqueous phase in this pH region as described by equation (4.1).



Although the predominance of the anionic hydrolysis species $\text{U}(\text{OH})_5^-$ and $\text{U}(\text{OH})_6^{2-}$ was reported by some authors [44, 45, 52], the undersaturation solubility data obtained in this study allows precluding the formation of such species within the investigated pH_m -range. This observation is in excellent agreement with the main conclusions derived in Chapter 3 from oversaturation experiments.

Figure 4.2 shows also the concentration of uranium measured without phase separation. This dataset is 2–3 orders of magnitude higher in concentration than the solubility determined after 10 kD ultrafiltration. Such discrepancy is likely due to the presence of U(IV) intrinsic colloids in the

investigated systems in alkaline pH conditions. Similar observations were reported for Th(IV) and Pu(IV) by Altmaier *et al.*, (2004) [142] and Neck *et al.*, (2007) [39], respectively. Note however that $[U]_{\text{aq}}$ measured in the supernatant solutions shows a moderate tendency to decrease with time (see Figure 4.3), at least for the systems 0.1, 0.5 and 2.0 M NaCl. At this point, it remains unclear whether such colloidal species become instable (*i.e.* aggregate) with time.

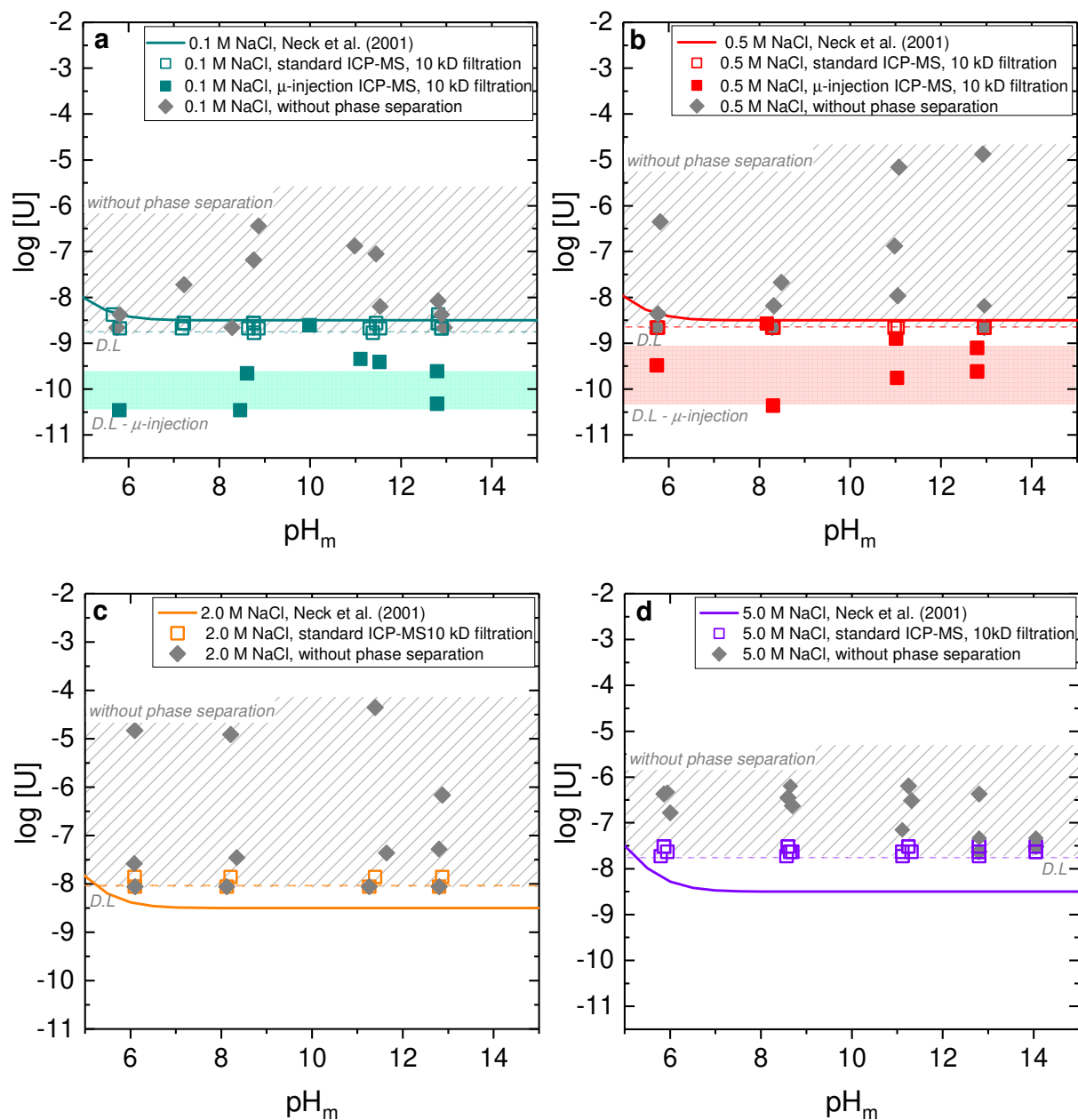


Figure 4.2. Experimental solubility data after 10 kD ultrafiltration and without phase separation obtained in this work for U(IV) in a. 0.1 M, b. 0.5 M, c. 2.0 M and d. 5.0 M NaCl systems. Detection limits for μ -injection ICP-MS measurements are shown as shadowed areas in light cyan and light red in 0.1 and 0.5 M NaCl systems involving detection limits from different measurements (calculated as 3σ of the blank).

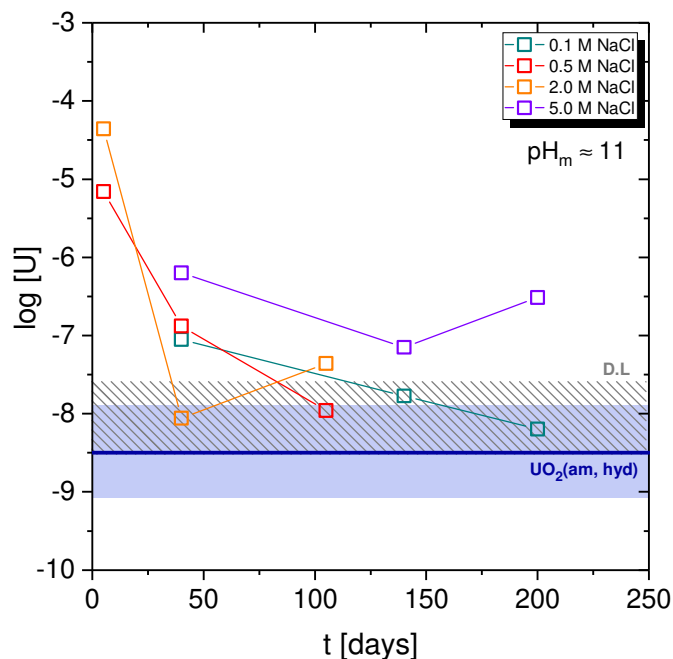


Figure 4.3. Temporal evolution of the measured U concentration without phase separation in 0.1-5.0 M NaCl. Grey area shows the detection limits from different measurements in 0.1-5.0 M NaCl. Light blue area shows the uncertainty of the solubility of $UO_2(am, hyd)$.

4.1.2 Solubility data of U(IV) in reducing, dilute to concentrated $MgCl_2$ solutions

Solubility data of U(IV) determined in 0.25, 2.0 and 4.5 M $MgCl_2$ are shown in Figure 4.4, together with experimental solubility data reported by Rai *et al.* (1997) [84] in analogous $MgCl_2$ solutions and with solubility curves calculated using thermodynamic and SIT activity models reported by Neck and Kim (2001) [106]. Note that ionic strength in 4.5 M $MgCl_2$ systems ($I = 13.5$ M) is well beyond the generally accepted range of SIT, and thus calculations performed for this system must be considered as orientative.

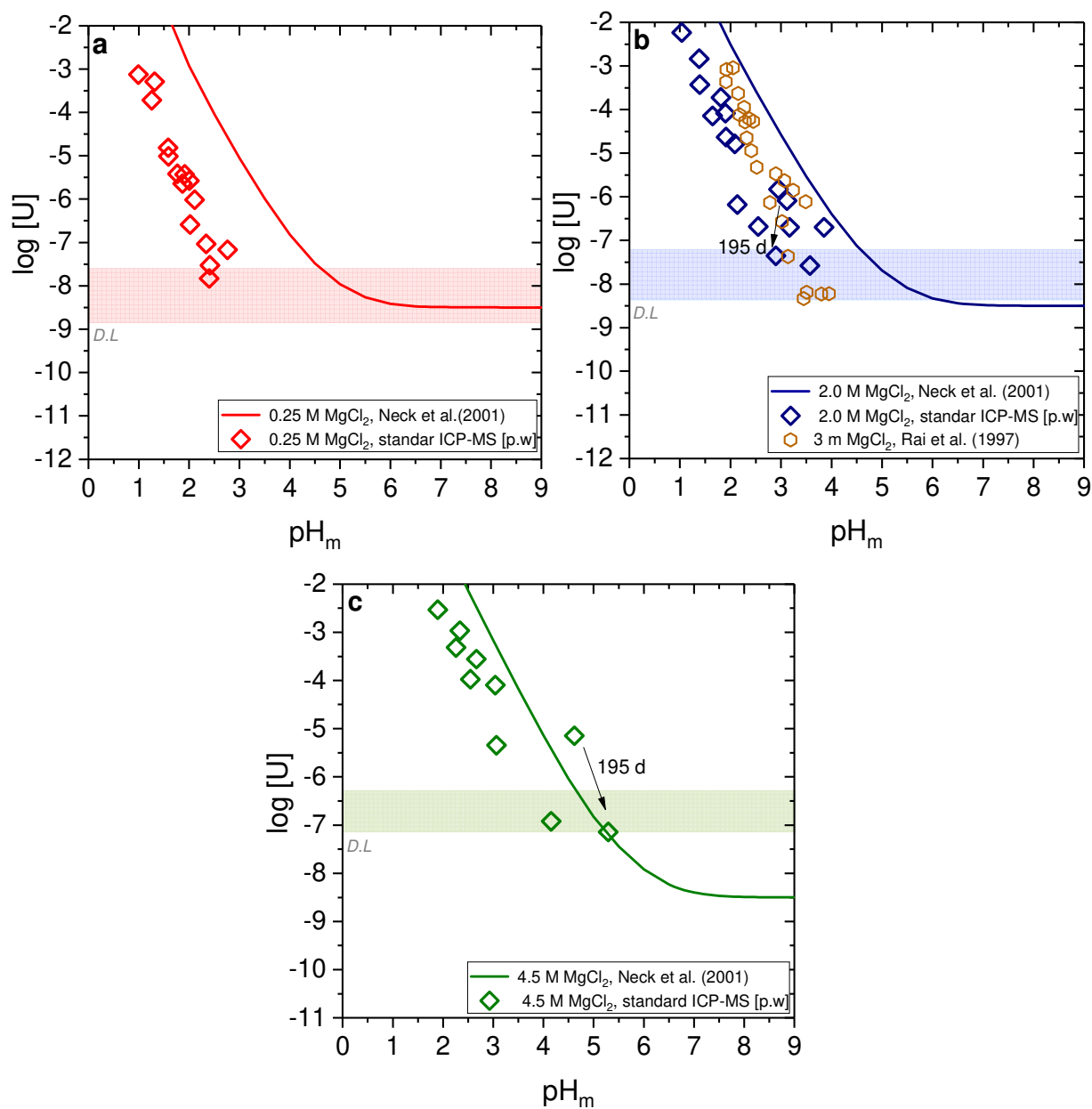


Figure 4.4. Experimental solubility data obtained in this work for U(IV) in a. 0.25 M, b. 2.0 M and c. 4.5 M MgCl_2 systems, in comparison with solubility data reported by Rai et al. for analogous MgCl_2 systems [84]. Solid lines corresponding to the solubility curve of $\text{UO}_2(\text{am, hyd})$ calculated for each ionic strength using thermodynamic data reported by Neck and Kim (2001). Detection limits are shown as shadowed areas in light red, blue and green for 0.25 M, 2.0 and 4.5 M MgCl_2 systems, respectively, involving different detection limits from different measurements (calculated as 3σ of the blank).

Under acidic conditions ($\text{pH}_m \leq 4$) and analogously to NaCl systems, a steep decrease in the solubility of U(IV) is observed with increasing pH_m in all MgCl₂ systems. The increase in MgCl₂ concentration results in a significant increase in the solubility (*ca.* 3 orders of magnitude from 0.25 to 4.5 M MgCl₂). Such a relevant increase in the solubility expectedly results from strong ion interaction processes. In contrast to NaCl systems, the solubility experiments of U(IV) in MgCl₂ systems show slow equilibration kinetics, especially in 2.0 and 4.5 M systems. For these two systems, thermodynamic equilibrium is very likely not attained even after $t = 351$ days. Solubility data in 0.25 M MgCl₂ (Figure 4.4a) are virtually the same as in 0.5 M NaCl (Figure 4.1b), with the same chloride concentration but slightly lower ionic strength. This observation supports that the same solid phase is responsible for the control of U(IV) solubility in both salt systems, at least in dilute solutions. At $\text{pH}_m \geq 3-4$ (depending upon MgCl₂ concentration), the concentration of uranium in equilibrium with UO₂(s, hyd) drops below the detection limit of ICP-MS, and thus no information could be gained for this salt system and pH_m -range. However, based on the results obtained in NaCl systems and data reported for the solubility of Th(IV) in MgCl₂ systems [142], a solubility control by the pH_m -independent solubility reaction $\text{UO}_2(\text{s, hyd}) \Leftrightarrow \text{U}(\text{OH})_4(\text{aq}) + x\text{H}_2\text{O}(\text{l})$ is expected.

The solubility of UO₂(am, hyd) calculated using thermodynamic and activity models reported by Neck and Kim (2001) [42] clearly overestimates (approximately by 2 orders of magnitude) the experimental solubility data determined in the present work. The differences between the current data and solubility data reported by Rai *et al.* in both NaCl and MgCl₂ systems indicates the higher crystallinity degree (smaller particle size) of the solid phase used in the present study.

4.1.3 Solubility data of U(IV) in reducing, dilute to concentrated CaCl₂ solutions

The solubility of U(IV) was additionally investigated in 0.25, 2.0 and 4.5 M CaCl₂ solutions under alkaline conditions $9.5 \leq \text{pH}_m \leq 12$. Based on previous solubility studies with Th(IV), Pu(IV) and Np(IV) in alkaline CaCl₂ solutions [79, 85], a solubility increase above $\text{pH}_m \approx 11$ for $[\text{CaCl}_2] \geq 2.0$ M is expected as a result of the formation of ternary Ca-An(IV)-OH complexes. The solubility and hydrolysis constants $\log^* K_{\text{s},(4,1,8)}^\circ = -(57.2 \pm 1.4)$ and $\log^* \beta_{(4,1,8)}^\circ = -(57.2 \pm 1.4)$ were estimated for Ca₄[U(OH)₈]⁴⁺ by Fellhauer *et al.* [79] using linear free energy relationships (LFER).

Figure 4.5 shows experimental solubility data determined in this work together with the solubility curves calculated for each ionic strength using the thermodynamic and SIT activity models reported by Neck and Kim [42], including also the formation of the complex $\text{Ca}_4[\text{U}(\text{OH})_8]^{4+}$ as estimated by Fellhauer *et al.* [79]. Uranium concentrations below the detection limit are observed in all investigated CaCl_2 systems under alkaline conditions. Based on the solubility curves calculated for $\text{UO}_2(\text{am, hyd})$ and including the formation of the ternary complex $\text{Ca}_4[\text{U}(\text{OH})_8]^{4+}$, however, U(IV) solubility should be well above the current detection limit for $[\text{CaCl}_2] \geq 2.0 \text{ M}$ and $\text{pH}_m \geq 11.5$. On the other hand, this result is consistent with the systematically lower U(IV) solubility observed in the present study for NaCl and MgCl_2 systems. Accordingly, these findings can neither confirm nor exclude the formation of ternary complexes Ca-U(IV)-OH . An extended discussion on this dataset is provided in Section 4.3.1.

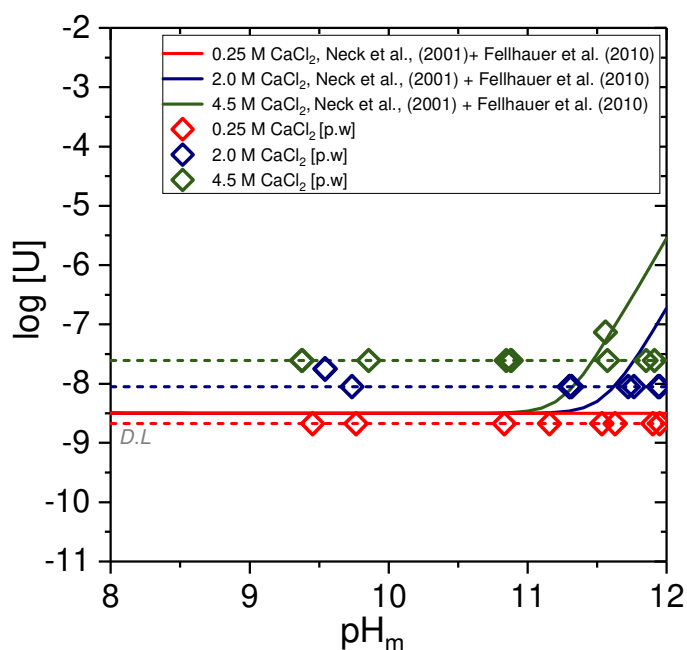


Figure 4.5. Experimental solubility data obtained in this work for U(IV) in CaCl_2 systems. Solid lines corresponding to the solubility curve of $\text{UO}_2(\text{am, hyd})$ calculated for each ionic strength using thermodynamic data reported by Neck and Kim (2001) [42] and Fellhauer *et al.* (2010) [79]. Dashed lines correspond to the detection limits of ICP-MS determined (as 3σ of the blank) for each CaCl_2 concentration.

4.2 U(IV) solid phase characterization

4.2.1 XRD, SEM-EDS, quantitative chemical analysis and TG-DTA

The starting material and solid phases of selected solubility samples were investigated by XRD, SEM-EDS, quantitative chemical analysis and TG-DTA. The main outcome of this characterization is summarized in Table 4.1, together with the experimental conditions of the investigated samples. Additional characterization of selected samples using EXAFS is separately described in Section 4.2.2.

Table 4.1. Experimental conditions of investigated samples and XRD, SEM-EDS, quantitative chemical analysis and TG-DTA results.

Background electrolyte	pH _m	XRD (2 Θ)	Na:U ratio SEM-EDS	Na:U ratio Quantitative chem. analysis	TG-DTA (number of H ₂ O)
“starting material”	12.1	28.4	0.30	0.17	1.0
0.1 M NaCl	2.8	28.6	0.08	0.04	n.m.
0.1 M NaCl	11.4	28.4	0.0	0.02	n.m.
0.5 M NaCl	3.3	28.4	n.m.	0.0	n.m.
0.5 M NaCl	11.1	28.4	n.m.	0.0	n.m.
2.0 M NaCl	3.1	28.5	n.m.	0.0	n.m.
2.0 M NaCl	11.3	28.6	n.m.	0.06	n.m.
5.0 M NaCl	3.1	28.6	0.0	0.07	n.m.
5.0 M NaCl	11.3	28.6	0.06	0.02	n.m.
uncertainty	± 0.05		± 0.1	± 0.03	± 0.5

Figures 4.6a – 4.6c show the XRD diffractograms of the “starting material” and solid phases of selected solubility samples. In all cases, well-defined but broad XRD patterns are observed. This indicates that the solid phases investigated in this study are not amorphous, but rather hold a (nano-)crystalline character. XRD pattern of the “starting material” (Figure 4.6a) are in excellent agreement with those reported for UO₂(cr) [120]. The first and most intense peak in the XRD of the “starting material” is found at $2\Theta = 28.4$, which agrees very well with $2\Theta = 28.2$ (JCPDS file Nr. 73–2293) and 28.3 (JCPDS file Nr. 41-1422) reported for UO₂(cr) [120]. No reflections are observed in the region $10^\circ \leq 2\Theta \leq 20^\circ$, where the first and most intense peak of relevant (layered)

U(VI) solid phases is observed, *i.e.* $\text{UO}_3 \cdot 2\text{H}_2\text{O}(\text{cr})$ ($2\Theta = 12.0$) or $\text{Na}_2\text{U}_2\text{O}_7 \cdot \text{H}_2\text{O}(\text{cr})$ ($2\Theta = 14.9$) [143]. These results confirm the absence of any crystalline U(VI) phase in the “starting material”. Furthermore, Rietveld analysis of the XRD data indicates the average crystal size of (3 ± 1) nm.

XRD of the solid phases equilibrated in 0.1, 0.5, 2.0 and 5.0 M NaCl solutions under acidic and alkaline conditions are shown in Figure 4.6b and 4.6c, respectively. Solid phases in both acidic and alkaline systems retain the same XRD patterns of the “starting material”, indicating that no phase transformation occurred in the course of the solubility experiment. On the other hand, some additional sharp features are observed in 0.1, 0.5 and 2.0 M NaCl solutions at $\text{pH}_m \approx 3$ and in 0.5, 2.0 and 5.0 M NaCl systems at $\text{pH}_m \approx 11$. These sharp patterns match those of $\text{SnO}(\text{cr})$ (JCPDS file Nr. 72–1012) very well in both investigated pH conditions, as shown in detail in Figure 4.7. These observations are also in line with experimental results obtained in our research group using different radionuclides but with Sn(II) as reducing chemical, *e.g.* Tc [144] or Pu [145].

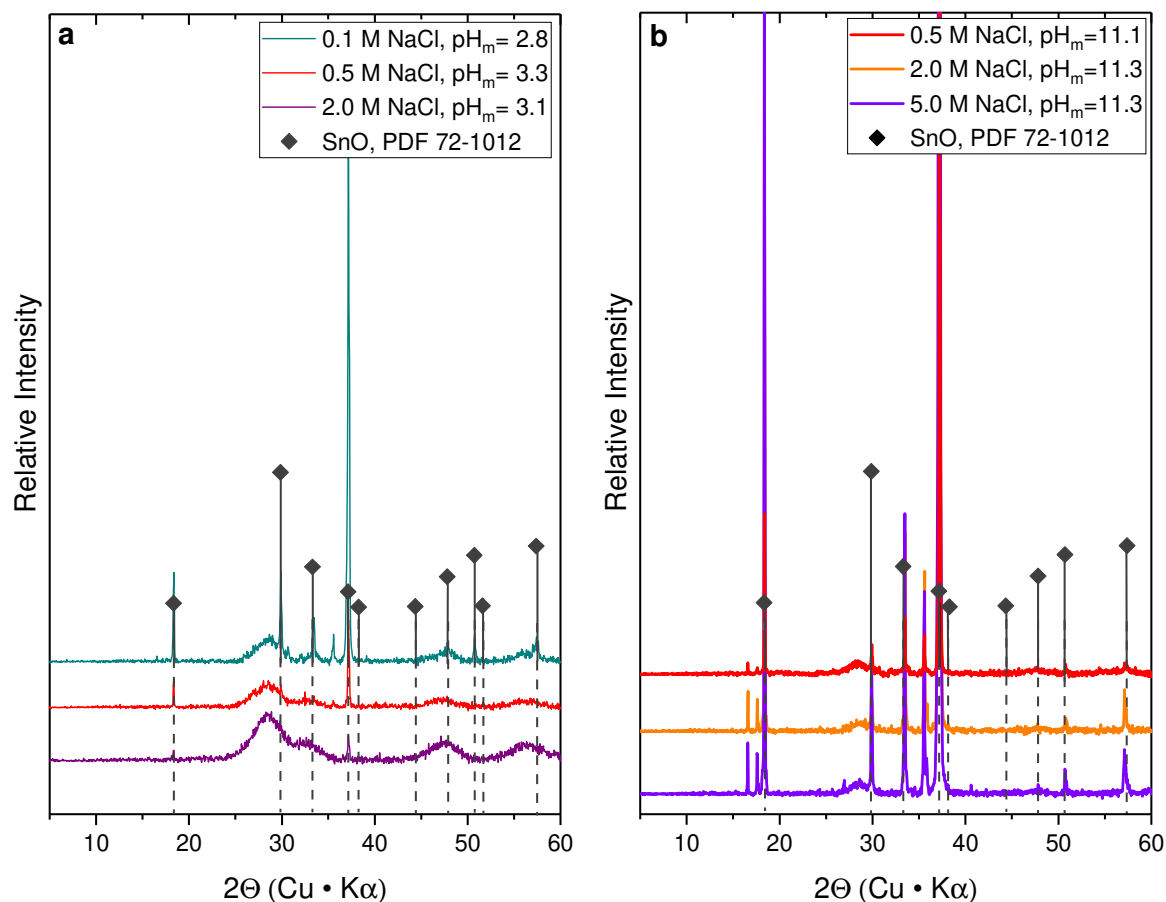


Figure 4.7. Comparison of XRD diffractograms of solid phases collected from selected solubility samples in NaCl systems a. in acidic pH_m conditions and, b. in alkaline pH_m conditions, with reference data available for SnO(cr) (JCPDS file Nr. 72–1012).

Figure 4.8 shows the SEM image of the U(IV) “starting material”, where an aggregated solid phase composed of very small particles (in the nanoscale range) can be observed. EDS results summarized in Table 4.1 for this solid indicate the presence of a small fraction of Na in the solid, in good agreement with results obtained by quantitative chemical analysis (ICP–OES). This observation likely arises from the insufficient washing of Na₂S₂O₄ (or its degradation products) present in the “starting material” suspension, although may also result from the sorption of Na on the surface of the solid phase and/or incorporation to the solid phases, as reported previously for Th(IV) hydrous oxide [146].

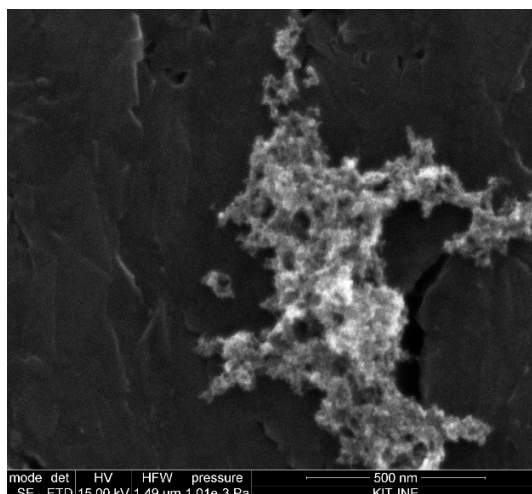


Figure 4.8. SEM image of the “starting material” at $pH_m = 12.1$.

SEM pictures of solid phases recovered from NaCl systems with Sn(II) as reducing chemical** show similar uranium aggregates as the “starting material” (Figure 4.9), but in this case together with additional, more crystalline structures (Figures 4.9 c and d). EDS analyses indicate that these crystalline compounds mostly contain Sn, in agreement with the XRD patterns obtained for these samples. Indeed, the platelet-like units observed in Figure 4.9c (sample equilibrated in 0.1 M NaCl at $pH_m = 2.8$) show a great similarity with the SnO(cr) particles aged under acidic conditions as reported elsewhere [147]. Note that, in contrast to the “starting material” prepared and stored in $Na_2S_2O_4$, no (or very small fraction of) Na is determined by EDS and quantitative chemical analysis in the solubility samples equilibrated in the presence of Sn(II). This observation supports that the Na-content identified in the “starting material” is likely resulting from the deposition of $Na_2S_2O_4$ (or its degradation product) in the surface of the uranium solid, rather than from Na sorption or incorporation in the UO_2 structure.

** $Na_2S_2O_4$ was only used as reducing system in the U(IV) “starting material”.

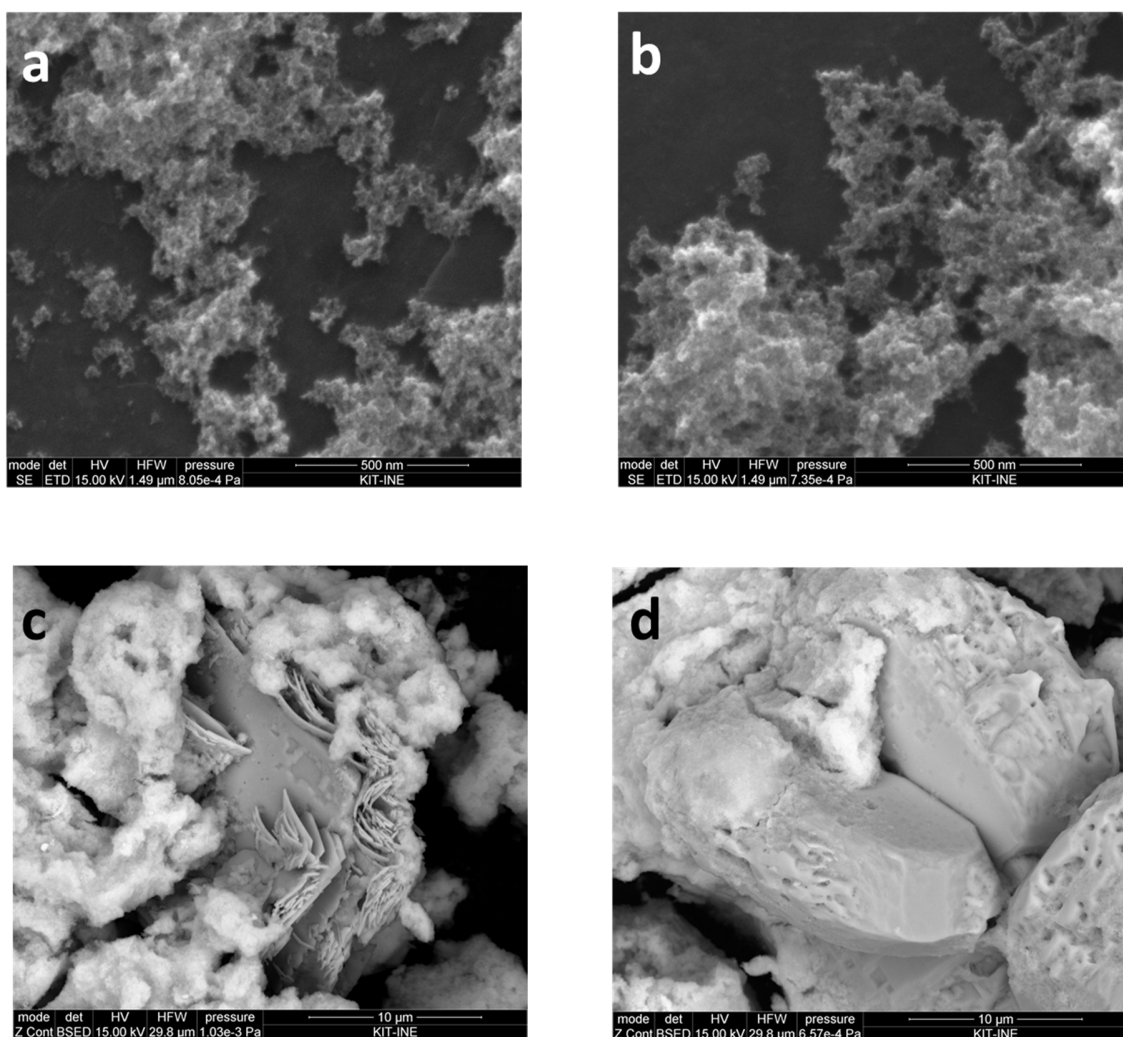


Figure 4.9. SEM images of selected solid samples equilibrated in a. 0.1 M NaCl at $pH_m = 11.4$; b. 5.0 M NaCl at $pH_m = 3.3$; c. 0.1 M NaCl at $pH_m = 2.8$; and d. 5.0 M NaCl at $pH_m = 11.3$.

Aliquots of the U(IV) “starting material” were collected after different equilibration times (30, 365, 418 and 798 days) and characterized by TG-DTA in order to quantify the number of hydration waters present. Samples were washed 3-5 times with ethanol and dried under Ar atmosphere before the measurement. The weight loss in the four investigated samples indicated the presence of 0.9, 1.4, 0.8 and 1.0 water molecules, respectively. No clear trend in the number of hydration waters was observed with increasing equilibration time, and the unweighted average of all measurements (1.0 ± 0.5 , with uncertainty calculated as 3 times the standard deviation) is taken as the water content in the investigated $UO_2(\text{ncr, hyd})$ material.

Based on the combination of all solid characterization techniques, the solid phase used in this solubility study is identified as $\text{UO}_2\cdot\text{H}_2\text{O}(\text{ncr})$. To the best of the author's knowledge, this is the most accurate characterization of " $\text{UO}_2(\text{s})$ " used in solubility experiments at ambient temperature conditions.

4.2.2 EXAFS

EXAFS measurements were performed at the INE-beamline [122] at the KIT synchrotron light source. Reduction and fit of EXAFS data were performed using ATHENA/ARTEMIS programs of the Demeter 0.9.26 package [124]. Figure 4.9 shows the k^2 -weighted uranium L_{III} EXAFS data and corresponding Fourier transforms of the two investigated samples: (i) the "starting material" $\text{UO}_2\cdot\text{H}_2\text{O}(\text{ncr})$ in the presence of 20 mM $\text{Na}_2\text{S}_2\text{O}_4$ ($t = 293$ days), and (ii) the solid phase $\text{UO}_2\cdot\text{H}_2\text{O}(\text{ncr})$ equilibrated in 0.1 M NaCl at $\text{pH}_m = 8.5$ in the presence of 5 mM SnCl_2 ($t = 455$ days). Table 4.2 summarizes the structural parameters derived from the EXAFS fit: coordination numbers (N), distances (R), Debye-Waller factors (σ^2) and energy shift parameter (ΔE^0). The goodness of the fit is given in terms of the percentage misfit between data and theory (R-factor). Fits are performed in R-space simultaneously in k^1 -, k^2 - and k^3 -weighted data. The k - and R-ranges used for the fit are given in Table 4.2. The overall intensity factor (S_0^2) was set to 0.65 in the fit.

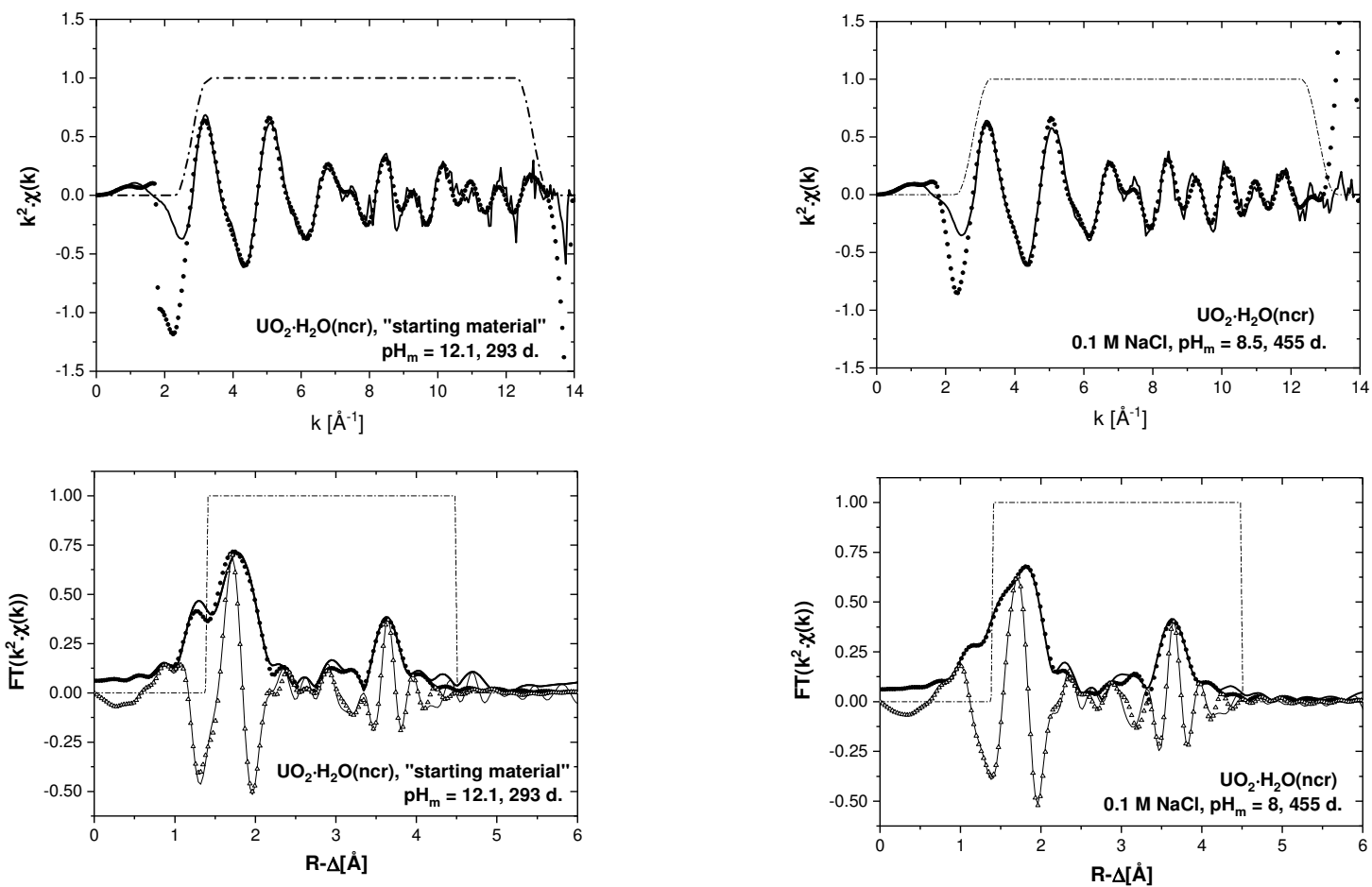


Figure 4.10. $U L_{III}$ -edge EXAFS results for $UO_2 \cdot H_2O(ncr)$ “starting material” at $pH_m = 12.1$ (left) and $UO_2 \cdot H_2O(ncr)$ in 0.1 M NaCl at $pH_m = 8.5$ (right). k^2 -weighted EXAFS spectra (upper panel) and Fourier Transform (lower panel); experimental data are depicted as solid lines, whereas fits are shown as circles and triangles (modulus and imaginary parts, respectively). Dashed lines correspond to the FT hanging windows used in the EXAFS fit.

Table 4.2. Structural parameters obtained from the EXAFS evaluation of $\text{UO}_2\cdot\text{H}_2\text{O}(\text{ncr})$ "starting material" at $\text{pH}_m = 12.1$ and $\text{UO}_2\cdot\text{H}_2\text{O}(\text{ncr})$ in 0.1 M NaCl at $\text{pH}_m = 8.5$.

Sample	Eq. time (days)	Path	CN	R(Å)	σ^2 (Å ²)	ΔE_0	R-factor
$\text{UO}_2\cdot\text{H}_2\text{O}(\text{ncr})$ "starting mat.", $\text{pH}_m = 12.1$	293	U-O ₁	6.5	2.33	0.007	-1.38	0.02
R-space (1.4-4.5 Å)		U-U	12*	3.86	0.010		
k-Range (2.8-12.8 Å ⁻¹)		U-O ₂	24*	4.44	0.008		
$\text{UO}_2\cdot\text{H}_2\text{O}(\text{ncr})$, 0.1 M NaCl, $\text{pH}_m = 8.5$	455	U-O ₁	8.0	2.33	0.010	-2.66	0.03
R-space (1.4-4.5 Å)		U-U	12*	3.86	0.009		
k-Range (2.8-12.8 Å ⁻¹)		U-O ₂	24*	4.45	0.008		

Fit errors: CN: $\pm 20\%$, R: 0.01 Å, σ^2 : 0.001 Å².

*parameter fixed during the fit (coordination number from the UO_2 crystal structure)

EXAFS spectra and Fourier Transforms of the two investigated samples show great similarities (see Figure 4.10), denoting that the structure of the starting material $\text{UO}_2\cdot\text{H}_2\text{O}(\text{ncr})$ is mostly retained throughout the solubility experiments (up to $t = 455$ days). Fourier Transforms in Figure 4.10 show two well-defined shells at $R-\Delta \approx 1.8$ and 3.7 Å corresponding to the backscattering of O and U atoms, respectively. The prominent U-U backscattering at $R-\Delta \approx 3.7$ Å observed in both samples supports the presence of a well-ordered, (nano-)crystalline solid phase. The good quality (signal-to-noise ratio) of the EXAFS data collected allowed the fit within $2.8 \leq k \text{ (Å}^{-1}\text{)} \leq 12.8$ and $1.5 \leq R \text{ (Å)} \leq 4.5$. The fit was performed using as starting structure $\text{UO}_2(\text{cr})$ as reported in [148], and included the shells U-O₁ and U-U, but also a distant U-O₂ shell. In order to limit the number of free parameters in the fit and avoid a too strong correlation between fit parameter, the coordination numbers of U-U and U-O₂ shells were fixed to 12 and 24 as reported for the original $\text{UO}_2(\text{cr})$ structure.

Virtually the same distances U-O₁ ($R_{\text{U-O}_1}$), U-U ($R_{\text{U-U}}$) and U-O₂ ($R_{\text{U-O}_2}$) were determined for the two solid phases investigated (Table 4.1), strongly supporting that both solid phases hold the same structure. Furthermore, the distances determined in this work for $R_{\text{U-O}_1} = 2.33$ Å and $R_{\text{U-U}} = 3.86$ Å are in good agreement with data reported in the literature for $\text{UO}_{2.00}(\text{cr})$, *i.e.* Cooper [148] ($R_{\text{U-O}_1} = 2.37$ Å and $R_{\text{U-U}} = 3.87$ Å) and Conradson *et al.* (2004) [149] ($R_{\text{U-O}_1} = 2.36$ Å and $R_{\text{U-U}} = 3.87$ Å). Conradson and co-workers [149] investigated also the impact of x in $\text{UO}_{2+x}(\text{cr})$ (with $x = 0.05, 0.08, 0.12, 0.17$ and 0.20) in the original structural parameters of $\text{UO}_{2.00}(\text{cr})$, and thus the comparison with experimental data determined in this work is of special relevance. Hence, these authors observed a clear increase in $R_{\text{U-O}_1}$ when going from $\text{UO}_{2.00}(\text{cr})$ ($R_{\text{U-O}_1} = 2.36$ Å) to $\text{UO}_{2.20}(\text{cr})$ ($R_{\text{U-O}_1} = 2.42$ Å). As indicated above, an invariant value of $R_{\text{U-O}_1}$

was determined in the present work for the two investigated samples ($R_{U-O1} = 2.36 \text{ \AA}$), thus supporting the presence of a stoichiometric UO_2 solid phase with $x \rightarrow 0$ in both cases.

Conradson *et al.* [149] observed also a significant impact of an increasing x in the U-U backscattering. Hence, the authors reported a decrease in the coordination number of U, from 10.6 in $UO_{2.00}(cr)$ to 2.5 in $UO_{2.20}(cr)$, in both cases holding the same distance $R_{U-U} = 3.88 \text{ \AA}$. Coordination numbers U-U were set constant in the present work (12), but the fit resulted in virtually the same R_{U-U} and Debye-Waller factors for both investigated samples. This observation supports again the presence of an structure close to ideal $UO_{2.00}(cr)$ in the two solid phases characterized in the present work. It is also interesting to note the differences observed in CN_{O1} for the $UO_2 \cdot H_2O(ncr)$ samples investigated in this study. Hence, the solid phase equilibrated for a longer time ($t = 455$ days) shows $CN_{O1} = 7.95$, a value very close to the ideal $CN_{O1} = 8$ in $UO_{2.00}(cr)$. On the other hand, a slightly lower value, $CN_{O1} = 6.53$, is determined for the solid phase aged 293 days. This observation possibly hints towards an increased order in the structure of $UO_2 \cdot H_2O(ncr)$ with increasing equilibration time.

EXAFS results obtained in the present work complement and further extend the characterization of the solid phase achieved by XRD, SEM-EDS, quantitative chemical analysis and TG-DTA. Structural parameters derived from EXAFS data evaluation strongly support the presence of stoichiometric $UO_{2.00} \cdot H_2O(ncr)$. Uranium is thus predominantly found as +IV, as expected on the basis of the very reducing conditions imposed by Sn(II) ($pe + pH_m \approx 2$) and in agreement with the low solubility observed within the complete pH_m -range investigated.

4.3 Chemical, thermodynamic and SIT activity models of the system U^{4+} – Na^+ – Mg^{2+} – Ca^{2+} – H^+ – OH^- – Cl^- – $H_2O(l)$

The chemical model of the system controlling the solubility of U(IV) in the absence of complexing ligands other than water is, *a priori*, well-defined and includes the solid phase $UO_2 \cdot H_2O(ncr)$ and the aqueous species UOH^{3+} , $U(OH)_2^{2+}$, $U(OH)_3^+$ and $U(OH)_4(aq)$. Accordingly, data evaluation in this work is restricted to these hydrolysis species and the solid phase $UO_2 \cdot H_2O(ncr)$. Due to the large number of parameters controlling the solubility in the investigated systems ($\log^* K_{s,0}^o$, $\log^* \beta_{(1,1)}^o$, $\log^* \beta_{(1,2)}^o$, $\log^* \beta_{(1,3)}^o$, $\log^* \beta_{(1,4)}^o$) and corresponding SIT coefficients for UOH^{3+} , $U(OH)_2^{2+}$ and $U(OH)_3^+$, the following modelling approach is considered in the context of this PhD thesis.

The approach used is based on the fit of only three parameters, namely $\log {}^*K_{s,0}^{\circ}$, $\log {}^*\beta_{(1,2)}^{\circ}$ and $\log {}^*\beta_{(1,3)}^{\circ}$. The values of $\log {}^*\beta_{(1,1)}^{\circ}$, $\log {}^*\beta_{(1,4)}^{\circ}$ are kept constant as selected in the NEA-TDB [41], whereas SIT coefficients of all charged species are either taken from NEA-TDB [41] or from the charge analogy reported in Neck and Kim (2001) [42].

Five different datasets are considered for the fit of the three parameters indicated above: 0.1, 0.5, 2.0, 5.0 M NaCl and 0.25 M MgCl₂. Data collected so far in 2.0 and 4.5 M MgCl₂ solutions are disregarded in the fit due to the absence of thermodynamic equilibrium within the considered timeframe ($t \leq 351$ days, see Section 4.1.2). Because of the considerably larger number of experimental data points at $\text{pH}_m \leq 5$, a weighting factor of 4 has been given to the limited data collected in the near-neutral to hyperalkaline pH_m -range using micro-injection ICP–MS (data only available for 0.1 and 0.5 M NaCl solutions). Additional measurements will be conducted after the completion of this PhD thesis to compensate the lack of experimental data in this pH_m -region, and thus to avoid the use of any weighting scheme.

The five datasets are simultaneously fitted by minimizing the function $\sum((\log [U]_{\text{exp}} - \log [U]_{\text{calc}})^2)^{1/2}$. The value of $[U]_{\text{calc}}$ is the sum of $[U\text{OH}^{3+}]$, $[U(\text{OH})_2^{2+}]$, $[U(\text{OH})_3^+]$ and $[U(\text{OH})_4(\text{aq})]$, and can be calculated based on equations (4.1) – (4.4) and using equation (4.5):



$${}^*K_{s,0}^{\circ} = a_{\text{U}^{4+}} a_w^3 / a_{\text{H}^+}^4 \quad (4.2)$$

and



$${}^*\beta_{(1,n)}^{\circ} = a_{\text{U}(\text{OH})_n^{(4-n)}} a_{\text{H}^+}^n / a_{\text{U}^{4+}} a_w^n \quad (4.4)$$

with

$$[U]_{\text{calc}} = {}^*K_{s,0}^{\circ} \gamma_{\text{H}^+} m_{\text{H}^+}^4 a_w^{-3} (1 + \sum {}^*\beta_{(1,n)}^{\circ} \gamma_{\text{H}^+} m_{\text{H}^+}^{-n} a_w^n) \quad (4.5)$$

where $a_i = \gamma_i \cdot m_i$, γ_i is the activity coefficient calculated by SIT as described in Section 1.2.2.5, and m_i is the concentration in molal units. The outcome of this modelling exercise is summarized in Table 4.3, whereas Table 4.4 shows the SIT interaction coefficients used in the fit. As observed in the discussion of the experimental data, the value of $\log {}^*K_{s,0}^{\circ}\{\text{UO}_2 \cdot \text{H}_2\text{O}(\text{ncr})\}$ determined in this work is clearly lower than $\log {}^*K_{s,0}^{\circ}\{\text{UO}_2(\text{am, hyd})\}$ reported in Neck and Kim (2001) [42] and selected in the NEA–TDB [41]. This result reflects the differences in the observed solubility, and highlights the larger particle size of the solid phase used in the present solubility study. Note that the currently used solid phase was

equilibrated at $T = 22$ °C but for significantly longer time periods than in previous solubility studies. Accordingly, the value of $\log {}^*K_{s,0}^{\circ}\{\text{UO}_2\cdot\text{H}_2\text{O}(\text{ncr})\}$ is possibly more representative of the U(IV) solubility expected under repository conditions, if such a oxy-hydroxide is formed as secondary phase. A different behaviour should be expected for $\text{UO}_2(\text{cr})$ present in spent fuel.

The fit of the experimental solubility data derived in this work results in a very similar $\log {}^*\beta_{(1,3)}^{\circ}$ to the equilibrium constant estimated by Neck and Kim (2001). On the contrary, the fit results in a very low value of $\log {}^*\beta_{(1,2)}^{\circ}$ indicating a negligible contribution of this species to the overall solubility. The incorporation of this species to the solubility calculation using the hydrolysis constant estimated by Neck and Kim (2001) [42] results in a significantly worse fit (quality parameter $\sum((\log [\text{U}]_{\text{exp}} - \log [\text{U}]_{\text{calc}})^2)^{1/2}$) equal to 72, compared with 41 for the set of constants summarized in Table 4.3). The model together with the experimental data are shown in Figures 4.11 and 4.12 for 0.1-5.0 M NaCl and 0.25 M MgCl_2 systems, respectively.

Table 4.3. Equilibrium constants for U(IV) solubility and hydrolysis as determined in the present work and reported in the NEA–TDB [41], Neck and Kim (2001) [42] and Fellhauer *et al.* (2010) [79]

	$\log {}^*K^{\circ}$			
	[p.w.]	NEA–TDB	Neck and Kim	Fellhauer <i>et al.</i>
Solubility				
$\text{UO}_2\cdot\text{H}_2\text{O}(\text{ncr}) + 4\text{H}^+ \rightleftharpoons \text{U}^{4+} + 4\text{H}_2\text{O}(\text{l})$	$-(0.32 \pm 0.60)$	$(1.5 \pm 1.0)^{\text{a}}$	$(1.5 \pm 1.0)^{\text{a}}$	
Hydrolysis				
$\text{U}^{4+} + \text{H}_2\text{O}(\text{l}) \rightleftharpoons \text{UOH}^{3+} + \text{H}^+$	$-(0.54 \pm 0.06)^{\text{b}}$	$-(0.54 \pm 0.06)$	$-(0.40 \pm 0.20)$	
$\text{U}^{4+} + 2\text{H}_2\text{O}(\text{l}) \rightleftharpoons \text{U}(\text{OH})_2^{2+} + 2\text{H}^+$	$-(8.6 \pm 0.5)$	–	$-(1.10 \pm 1.00)$	
$\text{U}^{4+} + 3\text{H}_2\text{O}(\text{l}) \rightleftharpoons \text{U}(\text{OH})_3^+ + 3\text{H}^+$	$-(4.2 \pm 0.5)$	–	$-(4.70 \pm 1.00)$	
$\text{U}^{4+} + 4\text{H}_2\text{O}(\text{l}) \rightleftharpoons \text{U}(\text{OH})_4(\text{aq}) + 4\text{H}^+$	$-(10.0 \pm 1.4)^{\text{b}}$	$-(10.0 \pm 1.4)$	$-(10.0 \pm 1.4)$	
Ternary Ca(II)–U(IV)–OH complexes				
$4\text{Ca}^{2+} + \text{U}^{4+} + 8\text{H}_2\text{O}(\text{l}) \rightleftharpoons \text{Ca}_4[\text{U}(\text{OH})_8]^{4+} + 8\text{H}^+$	$\leq -58.4^{\text{c}}$			$-(58.7 \pm 1.0)^{\text{d}}$

a. value reported for $\text{UO}_2(\text{am, hyd})$; b. set constant in the fit. Value taken as reported in NEA–TDB; c. extrapolated to $I = 0$ considering $\epsilon(\text{Ca}_4[\text{U}(\text{OH})_8]^{4+}, \text{Cl}^-) = \epsilon(\text{Ca}_4[\text{Th}(\text{OH})_8]^{4+}, \text{Cl}^-)$ as reported in Altmaier *et al.* (2008) [85] and Fellhauer *et al.* (2010) [79]; d. estimated from LFER.

Table 4.4. SIT interaction coefficients (in kg mol^{-1}) used in the present work for the modelling of U(IV) experimental solubility data in 0.1, 0.5, 2.0 and 5.0 M NaCl solutions.

<i>i</i>	<i>j</i>	$\epsilon(i,j)$	Reference
U(IV) species			
U ⁴⁺	Cl ⁻	(0.36 ± 0.10)	[42]
U(OH) ³⁺	Cl ⁻	(0.20 ± 0.10)	[42]
U(OH) ₂ ²⁺	Cl ⁻	(0.10 ± 0.10)	[42]
U(OH) ₃ ⁺	Cl ⁻	(0.05 ± 0.10)	[42]
U(OH) ₄ (aq)	Na ⁺ , Cl ⁻	0	a
	Mg ²⁺ , Cl ⁻	0	a
	Ca ²⁺ , Cl ⁻	0	a
Ca ₄ [U(OH) ₈] ⁴⁺	Cl ⁻	-(0.01 ± 0.10) ^b	[79, 85]

a. by definition in SIT; b. in analogy to $\epsilon(\text{Ca}_4[\text{Th}(\text{OH})_8]^{4+}, \text{Cl}^-)$ as reported in Altmaier *et al.* (2008) [85] and Fellhauer *et al.* (2010) [79]

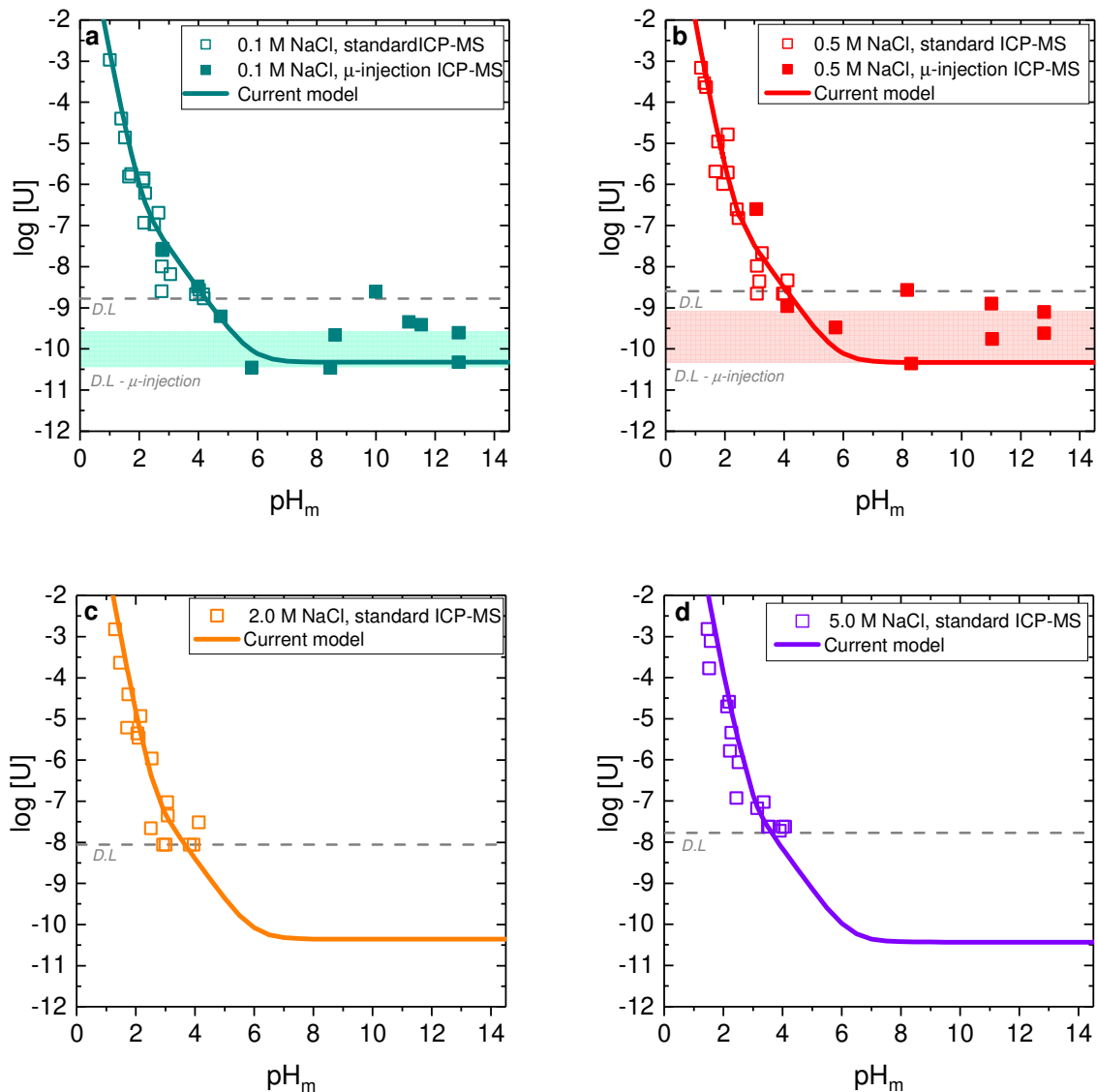


Figure 4.11. Comparison of experimental $U(IV)$ solubility data determined in 0.1 M, 0.5 M, 2.0 M and 5.0 M NaCl solutions with solubility calculations using the thermodynamic model derived in the present work (see Tables 4.3 and 4.4) and activity model reported by Neck and Kim (2001) [42]. Detection limits for μ -injection ICP-MS measurements are shown as shadowed areas in light cyan and light red in 0.1 and 0.5 M NaCl systems involving detection limits from different measurements (calculated as 3σ of the blank). Gray dashed lines show the detection limit of standard ICP-MS measurements.

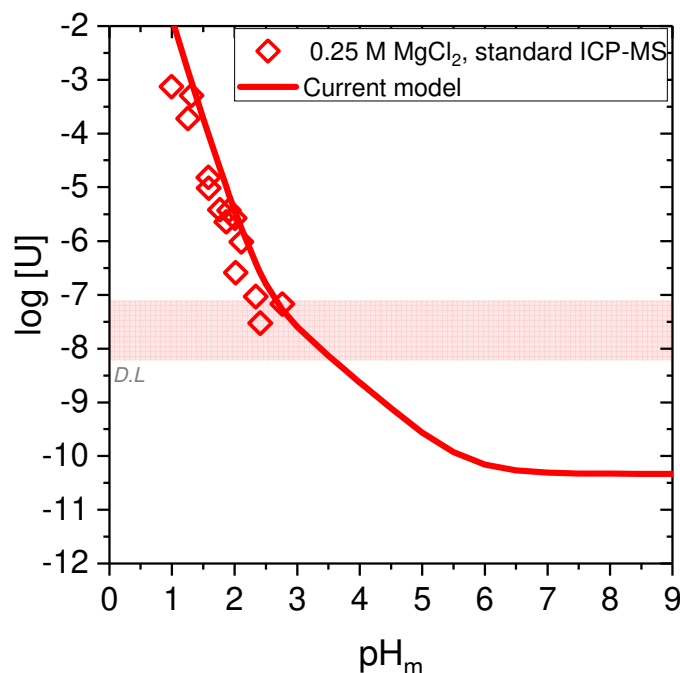


Figure 4.12. Comparison of experimental $U(IV)$ solubility data determined in 0.25 M $MgCl_2$ solutions with solubility calculations using the thermodynamic model derived in the present work (see Table 4.3) and activity model reported by Neck and Kim (2001) [42]. Detection limit is shown as a light red area, involving several different detection limits from different standard ICP-MS measurements (calculated as 3σ of the blank).

4.3.1 Application of the thermodynamic model derived to $CaCl_2$ systems

All solubility data determined in alkaline, dilute to concentrated $CaCl_2$ systems resulted in concentrations of uranium below the detection limit of ICP-MS (for the given salt concentrations). The combination of the solubility and hydrolysis constants in Table 4.3 with $\log^* \beta^{\circ}_{(4,1,8)}$ reported in Fellhauer *et al.* (2010) [79] results in the calculated solid lines in Figure 4.13. In contrast to the solubility calculations using $\log^* K^{\circ}_{s,0}$ reported in Neck and Kim (2001) [42] (Figure 4.4), the updated thermodynamic model results in a calculated solubility below / at the detection limit of ICP-MS. Note that upper limits estimated in this work for $\log^* \beta'_{(4,1,8)}(I = 2.0 \text{ M } CaCl_2)$ and $\log^* \beta'_{(4,1,8)}(I = 4.5 \text{ M } CaCl_2)$ based on the detection limits of ICP-MS for these salt concentrations are of the same order of the conditional equilibrium constants calculated with thermodynamic data reported in Fellhauer *et al.* (2010) [79]:

$$\log^* \beta'_{(4,1,8)}(I = 2.0 \text{ M } CaCl_2) \leq -61.0 \text{ [p.w.]}$$

$$\log^* \beta'_{(4,1,8)}(I = 4.5 \text{ M } CaCl_2) \leq -63.9 \text{ [p.w.]}$$

and

$$\log {}^*\beta'_{(4,1,8)}(I = 2.0 \text{ M CaCl}_2) = -(61.53 \pm 1.00) \text{ calculated from Fellhauer } et al. (2010) [79]$$

$$\log {}^*\beta'_{(4,1,8)}(I = 4.5 \text{ M CaCl}_2) = -(64.01 \pm 1.00) \text{ calculated from Fellhauer } et al. (2010) [79]$$

The extrapolation to $I = 0$ of the upper limits determined in this work for $\log {}^*\beta'_{(4,1,8)}$ in 2.0 and 4.5 M CaCl_2 can be performed considering $\epsilon(\text{Ca}_4[\text{U}(\text{OH})_8]^{4+}, \text{Cl}^-) = \epsilon(\text{Ca}_4[\text{Th}(\text{OH})_8]^{4+}, \text{Cl}^-) = -(0.01 \pm 0.10) \text{ kg}\cdot\text{mol}^{-1}$ [79, 85]. The resulting value, $\log {}^*\beta^\circ_{(4,1,8)} \leq -58.4$, is not in contradiction with the estimate reported by Fellhauer and co-workers from LFER. A final experimental “proof-of-concept” confirming the existence of such ternary species of U(IV) is still missing.

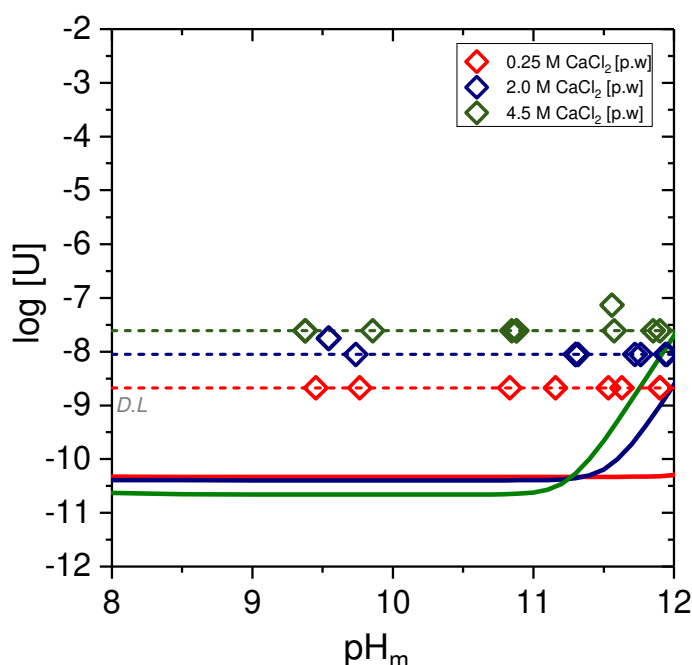


Figure 4.13. U(IV) solubility calculations in 0.25 M, 2.0 M and 4.5 M CaCl_2 using thermodynamic and activity models summarized in Table 4.3 and Table 4.4, and including the formation of the ternary complex $\text{Ca}_4[\text{U}(\text{OH})_8]^{4+}$ as estimated in Fellhauer *et al.* (2010) [79]. Symbols represent experimental solubility data determined in the present work, all of them at the detection limit of ICP–MS (dashed lines, calculated as 3σ of the blank).

4.3.2 Systematic trends on An(IV) solubility: new insights arising from the present work

New solubility data determined in the present work for U(IV) shows significantly lower $\log {}^*K_{s,0}^\circ\{\text{UO}_2\cdot\text{H}_2\text{O}(\text{ncr})\}$ and $\log {}^*K_{s,(1,4)}^\circ$ than previously reported data available in the literature and selected in the NEA–TDB. As discussed before in this chapter and in the introduction,

systematic trends are expected in the solution chemistry of An(IV) (with An= Th, U, Np and Pu) due to their same charge but decreasing ionic radii ($r_{\text{Th}^{4+}} = 1.08 \text{ \AA}$; $r_{\text{U}^{4+}} = 1.04 \text{ \AA}$; $r_{\text{Np}^{4+}} = 1.02 \text{ \AA}$; $r_{\text{Pu}^{4+}} = 1.01 \text{ \AA}$) as reported in Neck and Kim (2001) [42]. Figure 4.14 shows the correlation of solubility constants with ionic radii for (a) $\log^* K_{s,0}^\circ$ and (b) $\log^* K_{s,(1,4)}^\circ$, as selected in the NEA–TDB for Th(IV), U(IV), Np(IV) and Pu(IV) (NEA-TDB) [40, 41, 150] and determined experimentally in this work for U(IV). Figure 4.14a includes data reported for crystalline and amorphous phases. Figure 4.14b figure includes also values of $\log^* K_{s,(1,4)}^\circ$ recently reported for Np(IV) by Fellhauer *et al.*, (2014) [151] and Schepperle *et al.*, (2016) [152].

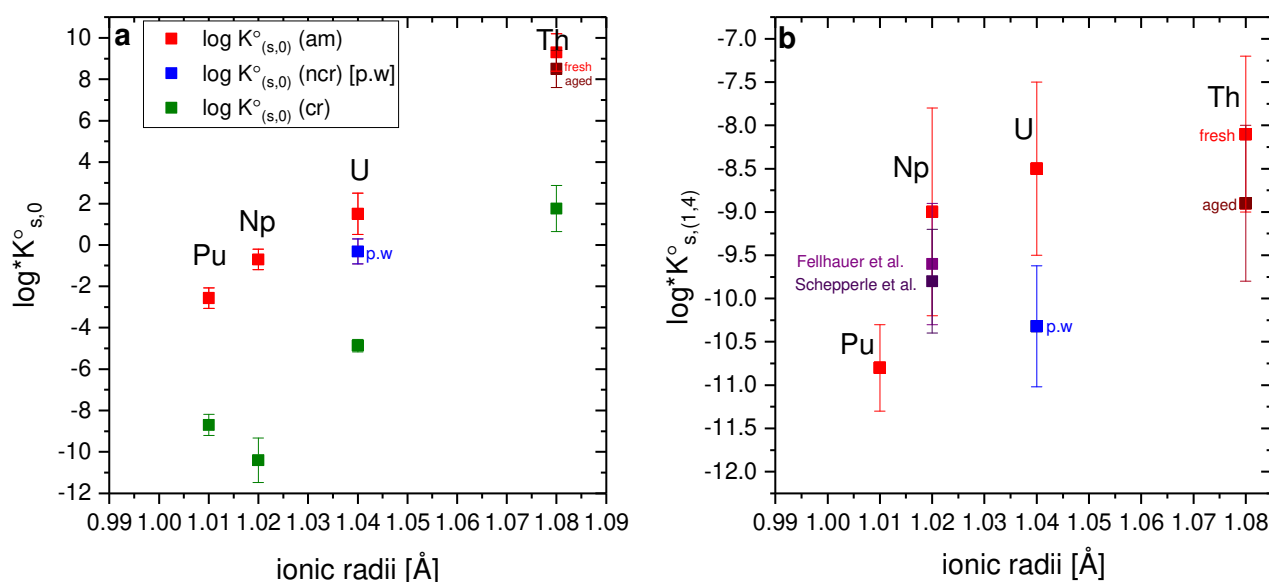


Figure 4.14. Comparison between the solubility constants available for An(IV): a. $\log K_{s,0}^\circ$ as selected in the NEA-TDB for $\text{AnO}_2(\text{am, hyd})$ and $\text{AnO}_2(\text{cr})$, and determined experimentally in this work for $\text{UO}_2 \cdot \text{H}_2\text{O}(\text{ncr})$; b. $\log^* K_{s,(1,4)}^\circ$ as selected in the NEA-TDB (Th, U, Np, Pu), reported in Fellhauer *et al.* (2014) [151] and Schepperle *et al.* (2015) [152] (Np) and determined experimentally in the present work (U).

Figure 4.14a shows that $\log^* K_{s,0}^\circ$ determined in this work for $\text{UO}_2 \cdot \text{H}_2\text{O}(\text{ncr})$ is clearly below $\log^* K_{s,0}^\circ\{\text{UO}_2(\text{am, hyd})\}$ selected in the NEA–TDB, but (as expected) several orders of magnitude greater than $\log^* K_{s,0}^\circ\{\text{UO}_2(\text{cr})\}$. The value of $\log^* K_{s,0}^\circ\{\text{UO}_2 \cdot \text{H}_2\text{O}(\text{ncr})\}$ is somehow out of the trend of $\log^* K_{s,0}^\circ\{\text{AnO}_2(\text{am, hyd})\}$ for An = Th, Np and Pu, although this observation is likely related with the nanocrystalline character of the solid phase investigated

in the present work, with the consequent impact on the solubility. Similar conclusions can be extracted from Figure 4.14b for $\log {}^*K_{s,(1,4)}^{\circ}$: the value determined in the present work is clearly lower than the one selected in the NEA–TDB for $\text{UO}_2(\text{am}, \text{hyd})$. Note however that lower values of $\log {}^*K_{s,(1,4)}^{\circ}$ were recently reported for Np(IV) by Fellhauer *et al.*, (2014) [151] and Schepperle *et al.*, (2015) [152] compared to the value currently selected in the NEA–TDB. Some considerations need to be accounted for when comparing the available solubility data:

- The correlation of An(IV) equilibrium constants with the ionic radii of An^{4+} is straight forward for aqueous complexes, but includes additional parameters in the case of solid phases. This is especially true for amorphous compounds, where slight variations of the particle size can have a large impact on the solubility. In spite of the extensive work on the solubility of amorphous oxo-hydroxides of An(IV), the information available on the particle size of these solid phases is virtually inexistent. Very recently, Tasi *et al.* (2018) [145] provided insights into the particle size dependency of the solubility of a $\text{PuO}_2(\text{ncr}, \text{hyd})$ solid phase (aged *ca.* 8 years) used in their experiments. Based on their XRD data (see Figure 4.15, compared to XRD collected in present work for $\text{UO}_2 \cdot \text{H}_2\text{O}(\text{ncr})$), the authors reported an average crystal (domain) size of (4 ± 1) nm calculated using Rietveld refinement of their diffraction data. This value compares well with the average crystal (domain) size of (3 ± 1) nm determined in the present work for $\text{UO}_2 \cdot \text{H}_2\text{O}(\text{ncr})$. The absence of such information for other An(IV) solid phases / solubility studies hinders an adequate comparison of the available $\log {}^*K_{s,0}^{\circ}$ and $\log {}^*K_{s,(1,4)}^{\circ}$ values.

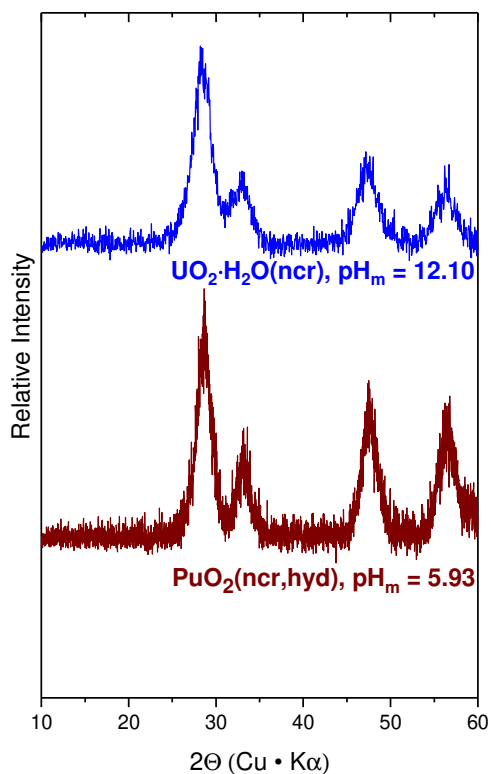


Figure 4.15. Comparison of XRD diffractograms obtained in this work for $\text{UO}_2\cdot\text{H}_2\text{O}(\text{ncr})$ and reported by Tasi et al. (2018) [145] for $\text{PuO}_2(\text{ncr, hyd})$.

- Neck and Kim (2001) (among other authors) proposed that crystalline $\text{AnO}_2(\text{cr})$ phases controlling the solubility in acidic conditions are covered by an amorphous layer in the alkaline pH conditions, which is therefore responsible of the solubility control in this pH-region. This interpretation is mostly based in indirect observations, *i.e.* change in the solubility behavior, from $\log {}^*K_{\text{s},0}^{\circ}\{\text{AnO}_2(\text{cr})\}$ in acidic conditions to $\log {}^*K_{\text{s},0}^{\circ}\{\text{AnO}_2(\text{am, hyd})\}$ in alkaline systems. It is unclear, though, if such a mechanism applies to nanocrystalline solid phases as those investigated in the present work. Note that both XRD diffractograms and SEM pictures show very similar characteristics for U(IV) solid phases equilibrated in acidic and alkaline pH conditions (see Section 4.2.1).
- An(IV) are characterized by very low solubility in alkaline pH conditions, which in many cases is close to the detection limit used for the quantification of $[\text{An}]_{\text{aq}}$. In the present study, the use of standard ICP–MS was insufficient to properly characterize the solubility of $\text{UO}_2\cdot\text{H}_2\text{O}(\text{ncr})$ above $\text{pH}_m \approx 5$. It is unclear how these limitations may have affected previous solubility experiments with U(IV). The detection limit of LSC for

^{237}Np lies approximately at $\approx 10^{-9}$ M (depending upon equipment and dilution steps). This concentration is indeed in the same order of $\log {}^*K'_{s,(1,4)}$ selected in the NEA–TDB (-9 ± 1) for the equilibrium reaction:



$$\log {}^*K'_{s,(1,4)} = \log {}^*K'_{s,(1,4)} = \log [\text{Np}(\text{OH})_4(\text{aq})] = (-9 \pm 1)$$

However, using SF–ICP–MS, Fellhauer, Schepperle and co-workers were able to quantify lower neptunium concentrations characterizing the solubility of $\text{NpO}_2(\text{am, hyd})$ in alkaline pH conditions (see Figure 4.14b).

The dependency of the solubility constant (or rather $\Delta_f G^\circ_m$) of a given solid phase with the particle size can be quantitatively evaluated through the (adapted) Schindler equation [91]:

$$\Delta_f G^\circ_m\{\text{AnO}_2(\text{am/col})\} = \Delta_f G^\circ_m\{\text{AnO}_2(\text{cr})\} + 2/3\gamma S \quad (4.7)$$

where S is the surface area per mole of solid ($S = M\alpha / \rho d$) and γ is the mean free surface energy per unit of surface area:

$$\gamma = \frac{3\Delta_f G^\circ_m(S \rightarrow 0)}{2N_A \sum 4\pi r_i^2} \quad (4.8)$$

where M is the molecular weight of the solid, ρ is the density of the crystalline phase, d is the particle size (diameter), α the geometry factor (6, in spherical particles), N_A is the Avogadro number and r_i is the ionic radii. Figure 4.16 shows the application of this relationship to the cases of Th(IV) and Pu(IV) (based on data reported in [39, 150]), and for U(IV) using $\Delta_f G^\circ_m\{\text{UO}_2(\text{cr})\}$ reported in the NEA–TDB as anchoring point in the calculation. Figure 4.16 shows also $\Delta_f G^\circ_m\{\text{UO}_2(\text{ncr})\}$ calculated from the value of $\log {}^*K'_{s,0}\{\text{UO}_2 \cdot \text{H}_2\text{O}(\text{ncr})\}$ determined in this work from experimental solubility data, and using $\Delta_f G^\circ_m\{\text{U}^{4+}\} = -(529.860 \pm 1.765) \text{ kJ} \cdot \text{mol}^{-1}$ and $\Delta_f G^\circ_m\{\text{H}_2\text{O}(\text{l})\} = -(237.140 \pm 0.041) \text{ kJ} \cdot \text{mol}^{-1}$ as reported in the NEA–TDB. Note that in order to allow such exercise, $\Delta_f G^\circ_m\{\text{UO}_2(\text{ncr})\}$ instead of $\Delta_f G^\circ_m\{\text{UO}_2 \cdot \text{H}_2\text{O}(\text{ncr})\}$ must be used in the comparison. In the same way, Neck and co-workers calculated $\Delta_f G^\circ_m$ of Pu(IV) and Th(IV) hydrated amorphous / colloidal phases of unknown number of hydration waters using the general stoichiometry AnO_2 [42]. Note further that, as already indicated in the NEA–TDB reviews [41], the contribution of structural water to the Gibbs energy of formation of a given solid phase is similar to that of the free liquid water.

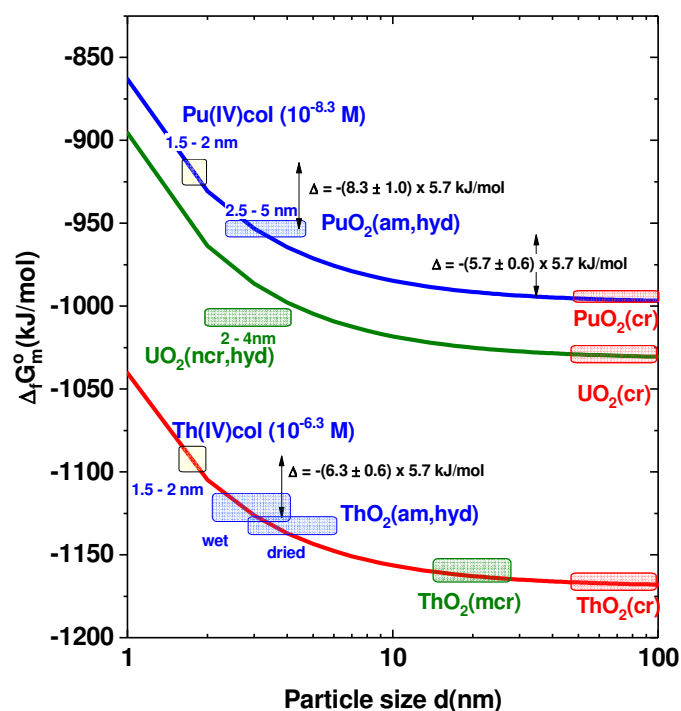


Figure 4.16. Application of the Schindler equation to $\text{ThO}_2(\text{cr}/\text{am}/\text{col})$, $\text{PuO}_2(\text{cr}/\text{am}/\text{col})$ and $\text{UO}_2(\text{ncr}/\text{cr})$ systems. $\Delta_f G^\circ_m$ data for $\text{ThO}_2(\text{cr})$ and $\text{ThO}_2(\text{am})$ calculated from [10]. $\Delta_f G^\circ_m$ data for $\text{PuO}_2(\text{cr})$ and $\text{PuO}_2(\text{am})$ calculated from [5]. $\Delta_f G^\circ_m$ data for $\text{ThO}_2(\text{col})$ and $\text{PuO}_2(\text{col})$ as determined in Neck et al (2007). $\Delta_f G^\circ_m$ data for $\text{UO}_2(\text{cr})$ and $\text{UO}_2\cdot\text{H}_2\text{O}(\text{ncr})$ as selected in [41] and calculated from experimental data determined in this work, respectively.

The experimentally determined $\Delta_f G^\circ_m$ for $\text{UO}_2(\text{ncr})$ in the present study is in moderate agreement with the theoretical calculation obtained using the Schindler equation and data for $\text{UO}_2(\text{cr})$ as reported in the NEA–TDB. To the best of the author’s knowledge, this is the first time that such approach is applied to U(IV), especially using experimentally determined values of particle size.

This exercise provides relevant insights to understand the role of particle size in the solubility of tetravalent actinides, in this case U(IV). Because of the amorphous nature of the oxo-hydroxide phases usually formed by tetravalent actinides, slight variations of the particle size as a result of aging and ripening can lead to very significant changes in the solubility and, consequently, in the concentration upper limits of these actinides in solution. A better understanding of these phenomena can contribute to a more accurate estimation of the source

term, and thus represents an important input to the Safety Case of repositories for radioactive waste.

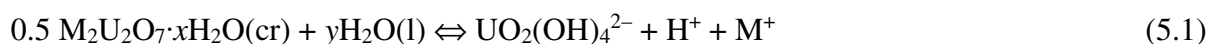
5 Solubility and hydrolysis of U(VI) in alkaline, dilute to concentrated KCl solutions

Undersaturation batch experiments were performed in order to investigate the solubility of U(VI) in 0.1, 0.5, 1.0, 3.0 and 4.0 M KCl solutions at $7.5 \leq \text{pH}_m \leq 14.6$. A potassium uranate solid phase was precipitated in alkaline conditions, aged for two months and characterized using several techniques before the preparation of the solubility samples. pH_m values and uranium concentrations were measured regularly from 6 up to 250 days. Solid phases of selected solubility samples were characterized after attaining equilibrium conditions using XRD, SEM–EDS, quantitative chemical analysis and TG–DTA. Chemical, thermodynamic and SIT activity models for the system $\text{UO}_2^{2+}\text{--H}^+\text{--K}^+\text{--Na}^+\text{--Cl}^-\text{--OH}^-\text{--H}_2\text{O(l)}$ were derived based on the newly generated solubility data in alkaline conditions, previous solubility studies in acidic KCl systems and U(VI) hydrolysis constants reported in Altmaier *et al.* (2017) [43].

5.1 U(VI) solubility in dilute to concentrated KCl–KOH solutions

Uranium(VI) solubility data determined in 0.1, 0.5, 1.0, 3.0 and 4.0 M KCl–KOH solutions are shown in Figure 5.1 For comparative purposes, the figure includes also U(VI) solubility data reported by Altmaier *et al.* [43] in NaCl solutions of analogous ionic strength.

An increase of the solubility following a well-defined slope of +1 was observed at pH_m above ≈ 11 in all KCl systems. This result is in excellent agreement with the solubility data reported by Altmaier and co-workers in NaCl solutions (empty triangles in Figure 5.1), although the overall U(VI) solubility in KCl systems is slightly lower for the same MCl concentration. A slope of +1 in a $\log [\text{U}]$ vs. pH_m diagram indicates the release of one H^+ in the equilibrium reaction between the solid phase and aqueous species predominating under hyperalkaline conditions. This is consistent with the solubility equilibrium (5.1):

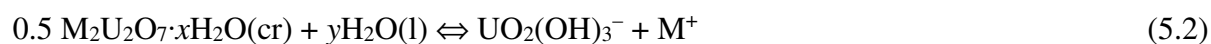


with $x + 2y = 5$, and $\text{M} = \text{Li}, \text{Na}, \text{K}$, etc.

Reaction (5.1) agrees also well with the the known aqueous speciation of U(VI) for these pH_m conditions [40, 41, 43]. In this pH_m -region, a decrease of approximately 1.5 orders of magnitude in the solubility was observed when increasing the concentration of KCl from 0.1 to 4.0 M. Such a behaviour reflects the impact of K^+ concentration in the equilibrium reaction (5.1), but also accounts for ion interaction processes between the negatively charged species $\text{UO}_2(\text{OH})_4^{2-}$

and K^+ . Similar observations were reported by Altmaier and co-workers for U(VI) in alkaline NaCl solutions [43].

At pH_m below ≈ 11 , the solubility of U(VI) remains pH_m -independent for all investigated KCl concentrations (Figure 5.1). This is in excellent agreement with analogous solubility experiments performed by Altmaier and co-authors in NaCl systems [43]. The observed trend is consistent with the equilibrium reaction (5.2):



with $x + 2y = 3$, and $M = Li, Na, K$, etc.

Experimental solubility data in this pH_m -region show a large scattering of up to one order of magnitude, most likely as a result of the low concentration of uranium close to or at the detection limit. A similar behaviour was reported for the solubility of U(VI) in weakly alkaline, dilute to concentrated NaCl solutions [43, 153].

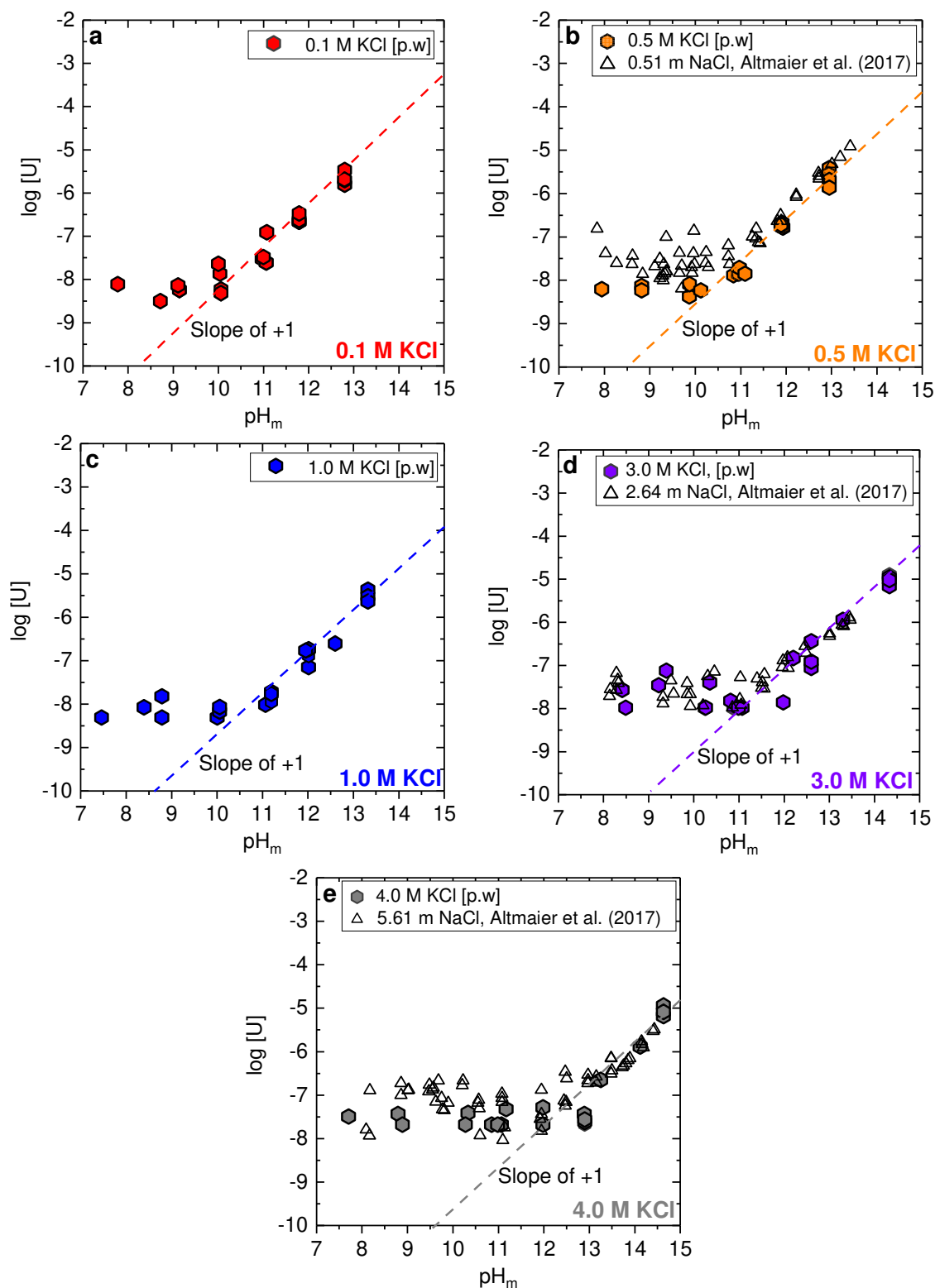


Figure 5.1. Experimental solubility data of U(VI) obtained in this work in a. 0.1 M, b. 0.5 M, c. 1.0 M d. 3.0 M and e. 4.0 M KCl systems (colored symbols). Empty triangles show the solubility of U(VI) in dilute to concentrated NaCl solutions as reported in Altmaier et al. (2017) [43]. Dashed lines indicate a slope of +1.

5.2 Solid phase characterization

Table 5.1 summarizes the main outcome of the solid phase characterization using XRD, SEM-EDS, quantitative chemical analysis and DT-TGA. Figure 5.2 shows the diffraction patterns of the initial solid phase (“starting material”) and solid phases from selected solubility experiments at each ionic strength. Figure 5.2a compares the XRD pattern of the “starting material” with reference spectra of several U(VI) solid phases, namely $\text{UO}_3 \cdot 2\text{H}_2\text{O}(\text{cr})$, $\text{Na}_2\text{U}_2\text{O}_7 \cdot \text{H}_2\text{O}(\text{cr})$, $\text{K}_2\text{U}_6\text{O}_{19} \cdot 11\text{H}_2\text{O}(\text{cr})$, $\text{K}_2\text{U}_4\text{O}_{13}(\text{cr})$, $\text{K}_2\text{U}_2\text{O}_7(\text{cr})$ and $\text{K}_2\text{UO}_4(\text{cr})$ [43, 120]. Due to the less crystalline character of the solid phase synthesized at room temperature in the present work, the sharper peak observed at small angles was used as fingerprint for the identification of the U(VI) “starting material” [43, 105, 154-156]. Hence, the peak found at $2\Theta = 13.1$ is very different from the values reported for $\text{UO}_3 \cdot 2\text{H}_2\text{O}(\text{cr})$ ($2\Theta = 12.0$) or $\text{Na}_2\text{U}_2\text{O}_7 \cdot \text{H}_2\text{O}(\text{cr})$ ($2\Theta = 14.9$) [43], and in moderate agreement with the value of $2\Theta = 13.4$ reported for $\text{K}_2\text{U}_2\text{O}_7(\text{cr})$ (JCPDS file Nr. 29–1058). EDS and quantitative chemical analysis data summarized in Table 5.1 confirm a ratio $\text{K}:\text{U} \approx 1$ in the “starting material”, further supporting that $\text{K}_2\text{U}_2\text{O}_7 \cdot x\text{H}_2\text{O}(\text{cr})$ was the solid phase used in the solubility experiments.

Figures 5.2b and 5.2c show XRD diffractograms collected for U(VI) solid phases equilibrated in 0.1, 0.5, 1.0, 3.0 and 4.0 M KCl solutions at $7.7 \leq \text{pH}_m \leq 10.3$ and $12.9 \leq \text{pH}_m \leq 13.3$, respectively. The same XRD pattern as for the “starting material” are retained in all cases (except one, see below), indicating that no transformation of the solid phase occurred during the equilibration time in these systems regardless of the pH_m and KCl concentration. A clear shift in the position of the first peak was observed for the solid phase equilibrated in 0.1 M KCl at $\text{pH}_m = 7.7$ ($2\Theta \approx 12.8$, see Figure 5.2b), hinting towards a possible solid phase transformation occurring at this pH_m and salt concentration. The shift of 2Θ values to lower angles is possibly related to a decrease in the $\text{K}:\text{U}$ ratio of the solid phase, as deduced from the trend observed for the reference compounds $\text{K}_2\text{U}_2\text{O}_7(\text{cr})$, $\text{K}_2\text{U}_4\text{O}_{13}(\text{cr})$ and $\text{K}_2\text{U}_6\text{O}_{19} \cdot 11\text{H}_2\text{O}(\text{cr})$ (see Table 5.1). A similar behaviour was previously reported for U(VI) and Np(VI) in NaCl systems [92, 153, 157].

In combination with XRD evidences, the ratio $\text{K}:\text{U} \approx 1$ determined by EDS and quantitative chemical analysis for most of the solubility samples supports that the solid phase $\text{K}_2\text{U}_2\text{O}_7 \cdot x\text{H}_2\text{O}(\text{cr})$ was responsible of the solubility-control (see Table 5.1). The high $\text{K}:\text{U}$ ratio (1.3) observed for the sample at $\text{pH}_m = 10.2$ in 4.0 M KCl is most likely due to the insufficient washing steps for such high KCl concentration.

SEM images of selected solid phases equilibrated in 0.1, 0.5, 1.0, 3.0 and 4.0 M KCl at $\text{pH}_m \approx 10$ are shown in Figure 5.3. All images show solid phases with platelet-like structures of similar size. Results on TG-DTA analysis summarized in Table 5.1 indicate that the number of hydration waters in the investigated potassium uranate phase is (1.5 ± 0.3) .

Based on all experimental evidences collected, the solid phase investigated in this series of solubility experiments was identified as $\text{K}_2\text{U}_2\text{O}_7 \cdot 1.5\text{H}_2\text{O}(\text{cr})$.

Table 5.1. Summary of the main results obtained in the solid phase characterization of the “starting material” and selected solubility samples equilibrated in KCl systems using XRD, SEM–EDS, quantitative chemical analysis (K:U ratio) and TG–DTA (number of hydration waters, *x*). Position of the first diffraction peak reported in the literature for some layered U(VI) structures is provided for comparison.

Background electrolyte	pH _m ^a	XRD (2 θ)	K:U ratio SEM–EDS	K:U ratio Chemical analysis	TG–DTA (number of hyd. H ₂ O)
2.5 M KCl “starting material”	12.7	13.1	1.0	0.9	1.4
0.1 M KCl	7.7	12.8	n.m.	n.m.	n.m.
0.1 M KCl	9.9	13.1	1.0	0.9	1.3
0.1 M KCl	12.9	13.2	n.m.	0.9	1.7
0.5 M KCl	10.0	13.2	0.9	0.9	1.3
0.5 M KCl	12.9	13.2	n.m.	0.9	1.7
1.0 M KCl	9.8	13.1	1.0	0.9	1.3
1.0 M KCl	13.3	13.2	n.m.	1.0	1.7
3.0 M KCl	10.3	13.0	0.9	0.9	1.3
3.0 M KCl	13.3	13.2	n.m.	1.0	1.7
4.0 M KCl	10.2	13.0	1.0	1.3	1.3
4.0 M KCl	13.2	13.1	n.m.	1.0	1.7
average^b			(1.0 ± 0.1)	(0.9 ± 0.1)^c	(1.5 ± 0.3)
UO₃·2H₂O(cr) Altmaier <i>et al.</i> (2017) [43]		12.0			
Na₂U₂O₇·H₂O(cr) Altmaier <i>et al.</i> (2017) [43]		14.9			
K₂UO₄(cr) JCPDS file Nr. 72–2228 [120]		13.5			
K₂U₂O₇(cr) JCPDS file Nr. 29–1058 [120]		13.4			
K₂U₄O₁₃(cr) JCPDS file Nr. 29–1059 [120]		12.6			
K₂U₆O₁₉·11H₂O(cr) JCPDS file Nr. 33–1049 Nipruk <i>et al.</i> (2017) [120, 154]		11.9			

a. ± 0.05; **b.** uncertainty calculated as 2 σ ; **c.** results obtained in 4.0 M KCl at pH_m = 10.2 disregarded for calculating average and uncertainty; **n.m.** = not measured.

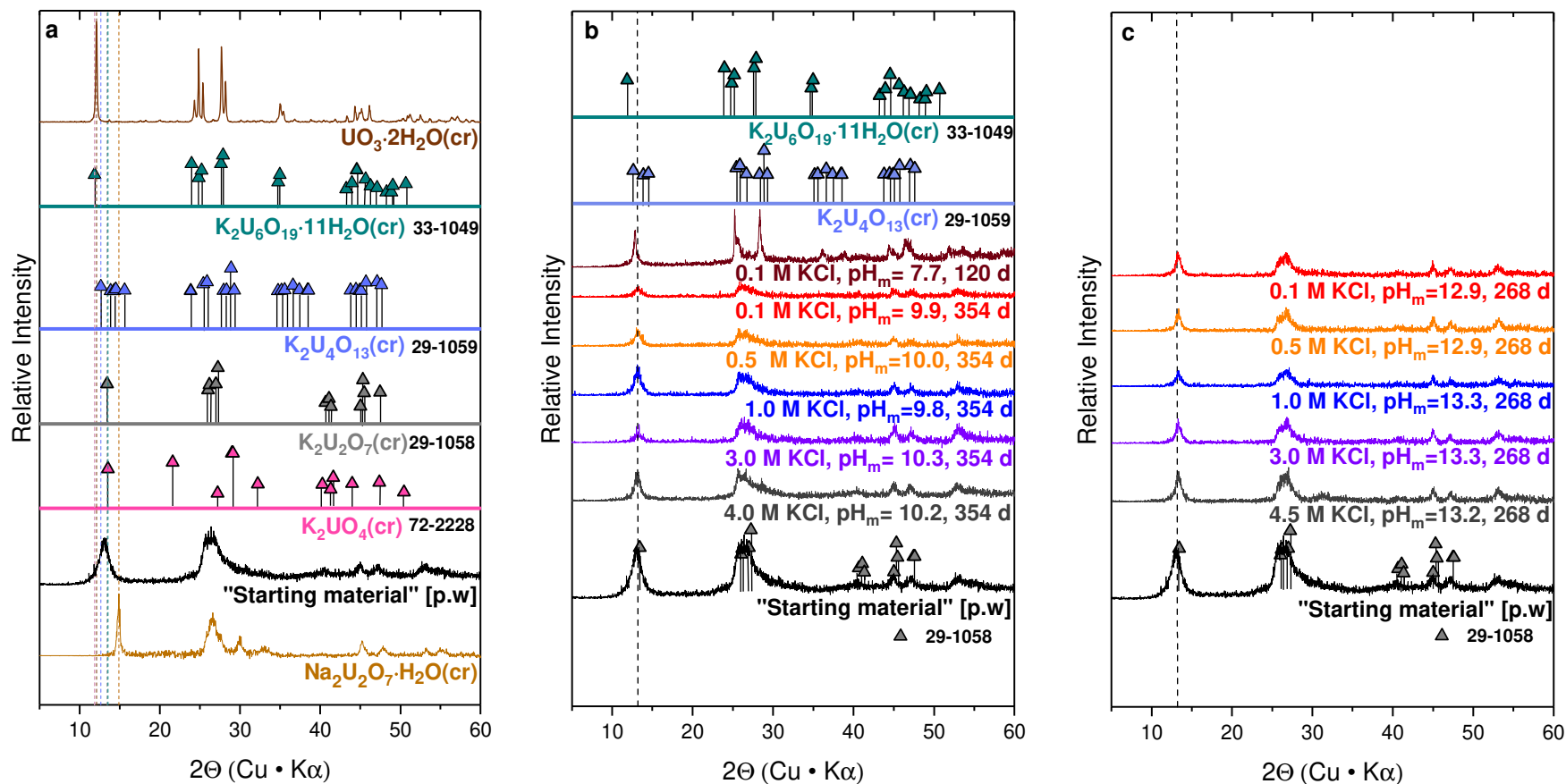


Figure 5.2. XRD pattern of solid phases of selected solubility samples in dilute to concentrated KCl systems: a. comparison between “starting material” and XRD patterns reported by Altmaier et al. (2017) for Na₂U₂O₇·H₂O(cr) and UO₃·2H₂O(cr), and reference data reported in the JCPDS database [120] for K₂U₆O₁₉·11H₂O(cr) (JCPDS file Nr. 33–1049), K₂U₄O₁₃(cr) (JCPDS file Nr. 29–1059), K₂U₂O₇(cr) (JCPDS file Nr. 29–1058) and K₂UO₄(cr) (JPDS file Nr. 72–2228); b. comparison between “starting material” and solid phases at pH_m = 7.7–10.3. Diffractograms of K₂U₂O₇(cr) (JCPDS file Nr. 29–1058), K₂U₄O₁₃(cr) (JCPDS file Nr. 29–1059) and K₂U₆O₁₉·11H₂O(cr) (JCPDS file Nr. 33–1049) provided for comparison; c. comparison between “starting material” and solid phases recovered from solubility experiments at pH_m=12.9–13.3 after t = 268 days. Diffractogram of K₂U₂O₇(cr) (JCPDS file Nr. 29–1058) provided for comparison.

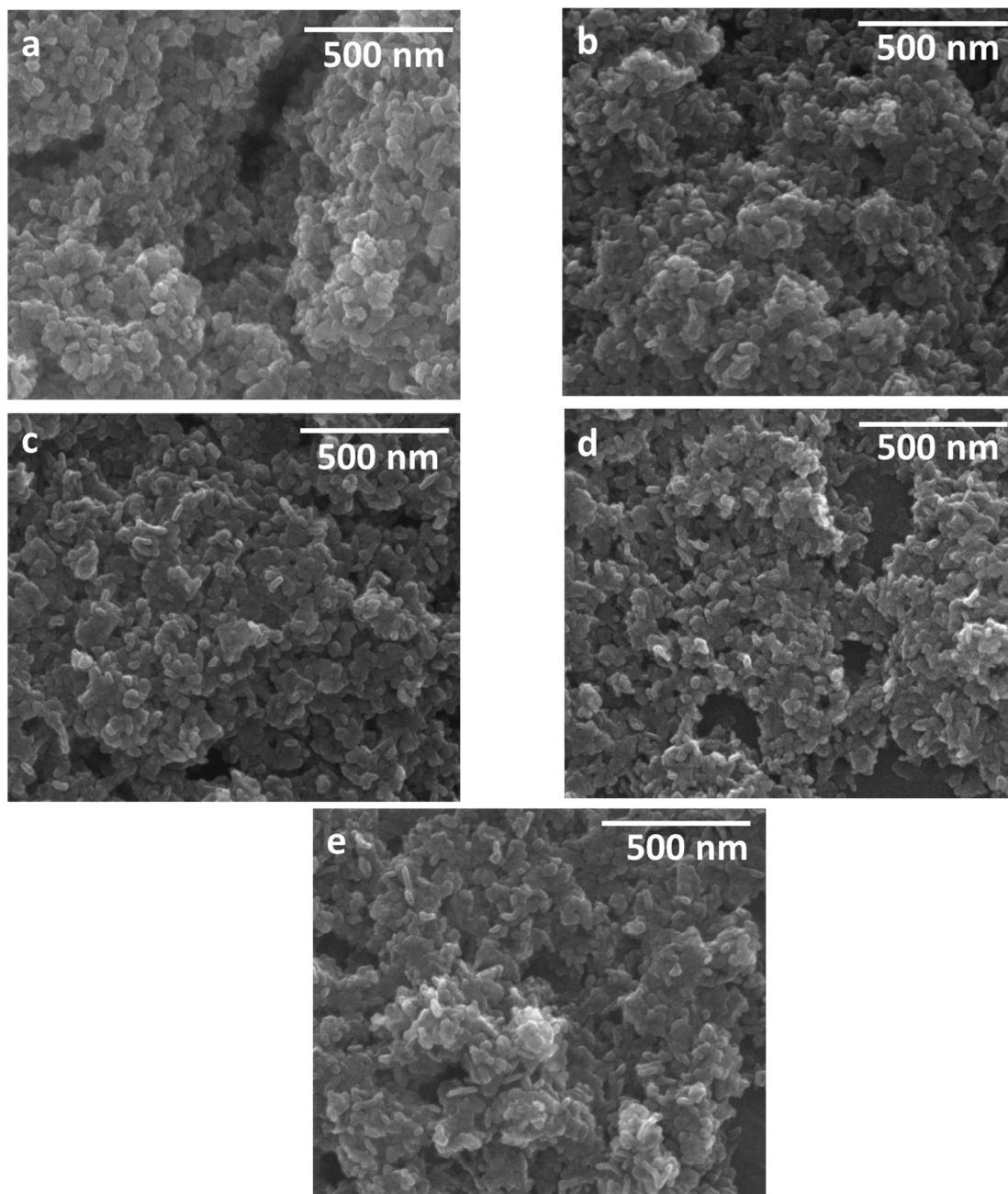


Figure 5.3. SEM images of $K_2U_2O_7 \cdot 1.5H_2O(cr)$ solid phases equilibrated at $pH_m \approx 10$ in a. 0.1 M KCl, b. 0.5 M KCl, c. 1.0 M KCl, d. 3.0 M KCl and e. 4.0 M KCl.

5.3 Chemical, thermodynamic and SIT activity models for the system $\text{UO}_2^{2+}\text{-H}^+\text{-K}^+\text{-Na}^+\text{-Cl}^-\text{-OH}^-\text{-H}_2\text{O(l)}$

Chemical models defining the solution chemistry of U(VI) in alkaline KCl systems were determined based on the slope analysis of the solubility data at $\text{pH}_m \geq 11$ and solid phase characterization. Thermodynamic and activity models were accordingly derived based on these chemical models and considering experimental solubility data summarized in Section 5.1.1. Conditional solubility constants $\log {}^*K'_{s,(1,4)}$ were determined for 0.1–4.0 M systems, and $\log {}^*K^\circ_{s,(1,4)}$ and $\epsilon(\text{UO}_2(\text{OH})_4^{2-}, \text{K}^+)$ were obtained following the SIT approach and considering $\epsilon(\text{K}^+, \text{Cl}^-)$, $\epsilon(\text{H}^+, \text{Cl}^-)$ and a_w as reported in the NEA-TDB [41]. The value of $\log {}^*K^\circ_{s,0}\{0.5 \text{K}_2\text{U}_2\text{O}_7 \cdot 1.5\text{H}_2\text{O}(\text{cr})\}$ was calculated using the combination of $\log {}^*K^\circ_{s,(1,4)}$ with the hydrolysis constant, $\log {}^*\beta_{(1,4)}$ reported in Altmaier *et al.* [43]. No modelling attempt was performed for the data collected at $\text{pH}_m \leq 11$, but these data were compared to the solubility calculated using $\log {}^*K^\circ_{s,0}\{0.5 \text{K}_2\text{U}_2\text{O}_7 \cdot 1.5\text{H}_2\text{O}(\text{cr})\}$ derived in this study. Solubility data reported previously by Sandino and Grambow [99] for $\text{K}_2\text{U}_6\text{O}_{19} \cdot 11\text{H}_2\text{O}(\text{cr})$ (compreignacite) solid phase were re-evaluated (Section 5.3.2) consistently with the current model for U(VI) speciation in the investigated systems (Section 5.3.3). In Section 5.3.4, the role of Na- and K-uranates in controlling the solubility of U(VI) in alkaline, cementitious environments was investigated using the updated thermodynamic model for the system $\text{UO}_2^{2+}\text{-H}^+\text{-K}^+\text{-Na}^+\text{-Cl}^-\text{-OH}^-\text{-H}_2\text{O(l)}$.

5.3.1 Thermodynamic data derived using U(VI) solubility experiments in alkaline, dilute to concentrated KCl solutions

The equilibrium reaction (5.3) is responsible for the solubility control of U(VI) at $\text{pH}_m \geq 11$, as determined considering the slope analysis (slope of +1) and solid phase characterization ($\text{K}_2\text{U}_2\text{O}_7 \cdot 1.5\text{H}_2\text{O}(\text{cr})$):



The values of $\log {}^*K'_{s,(1,4)}$ and $\log {}^*K^\circ_{s,(1,4)}$ can be accordingly defined as:

$$\log {}^*K'_{s,(1,4)} = \log [\text{UO}_2(\text{OH})_4^{2-}] + \log [\text{H}^+] + \log [\text{K}^+] \quad (5.4)$$

$$\begin{aligned} \log {}^*K^\circ_{s,(1,4)} = \log {}^*K'_{s,(1,4)} + \log \gamma_{\text{UO}_2(\text{OH})_4^{2-}} + \log \gamma_{\text{H}^+} \\ + \log \gamma_{\text{K}^+} - 1.75 \log a_w \end{aligned} \quad (5.5)$$

Solubility data obtained in 0.1, 0.5, 1.0, 3.0 and 4.0 M KCl solutions with $\text{pH}_m \geq 11$ were evaluated separately in order to determine the corresponding conditional constants, $\log^* K'_{s,(1,4)}$. The resulting values of $\log^* K'_{s,(1,4)}$ were considered in a SIT-plot to derive $\log^* K^{\circ}_{s,(1,4)}$ (intercept) and $-\Delta\epsilon$ (slope). The SIT interaction coefficient $\epsilon(\text{UO}_2(\text{OH})_4^{2-}, \text{K}^+)$ was calculated from $-\Delta\epsilon$ and using the values of $\epsilon(\text{H}^+, \text{Cl}^-)$ and $\epsilon(\text{K}^+, \text{Cl}^-)$ reported in the NEA-TDB [41]. The SIT-plot $\log^* K'_{s,(1,4)} - 6D - 1.75 \log a_w$ vs. $[\text{KCl}]$ is shown in Figure 5.3 together with the SIT-plot for the analogous solubility equilibrium in NaCl systems with $\text{Na}_2\text{U}_2\text{O}_7 \cdot \text{H}_2\text{O}(\text{cr})$ (with $\log^* K'_{s,(1,4)} - 6D - 2 \log a_w$ vs. $[\text{NaCl}]$), as reported by Altmaier *et al.* (2017) [43].

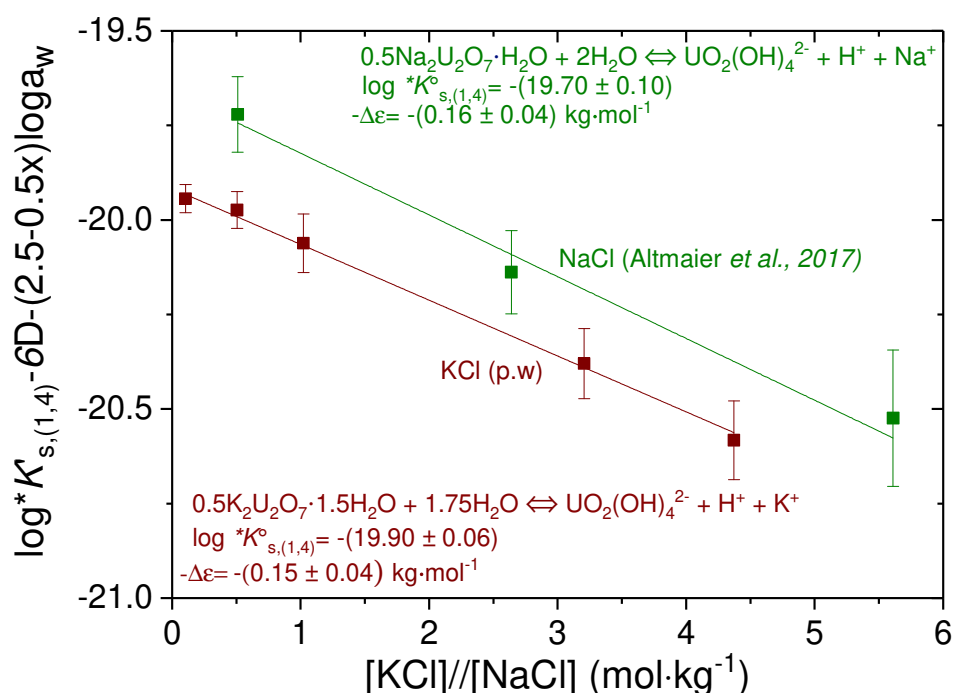
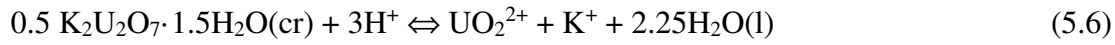


Figure 5.4. SIT-plot for the solubility reactions $0.5 M_2\text{U}_2\text{O}_7 \cdot x\text{H}_2\text{O}(\text{cr}) + (2.5 - 0.5x) \text{H}_2\text{O}(\text{l}) \Leftrightarrow \text{UO}_2(\text{OH})_4^{2-} + \text{H}^+ + \text{M}^+$ (with $M = \text{K}$ and Na) using experimental $\log^* K'_{s,(1,4)}$ values determined in dilute to concentrated KCl (present work) and NaCl solutions [43].

The intercept and slope of the linear SIT regression result in $\log^* K^{\circ}_{s,(1,4)} = -(19.90 \pm 0.06)$ and $-\Delta\epsilon = -(0.15 \pm 0.04) \text{ kg}\cdot\text{mol}^{-1}$ with $-\Delta\epsilon = -[\epsilon(\text{UO}_2(\text{OH})_4^{2-}, \text{K}^+) + \epsilon(\text{H}^+, \text{Cl}^-) + \epsilon(\text{K}^+, \text{Cl}^-)]$, respectively. The SIT interaction coefficient for $\text{UO}_2(\text{OH})_4^{2-}$ with K^+ is accordingly calculated as $\epsilon(\text{UO}_2(\text{OH})_4^{2-}, \text{K}^+) = (0.03 \pm 0.04) \text{ kg}\cdot\text{mol}^{-1}$. Based on their solubility data in alkaline NaCl systems, Altmaier and co-workers [43] reported $\epsilon(\text{UO}_2(\text{OH})_4^{2-}, \text{Na}^+) = (0.01 \pm 0.04) \text{ kg}\cdot\text{mol}^{-1}$, which is in excellent agreement with the value determined in the present work for KCl systems and highlights the similar behaviour of U(VI) in both salt systems.

The solubility product $\log {}^*K_{s,0}^{\circ}\{0.5 \text{ K}_2\text{U}_2\text{O}_7 \cdot 1.5\text{H}_2\text{O}(\text{cr})\}$ according to reaction (5.6) was calculated considering $\log {}^*K_{s,(1,4)}^{\circ} = -(19.90 \pm 0.06)$ determined in the present work and $\log {}^*\beta_{(1,4)}^{\circ} = -(31.9 \pm 0.2)$ reported by Altmaier *et al.* [43]:

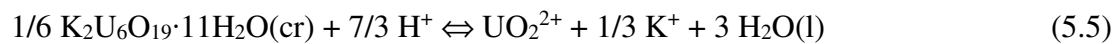


The combination of $\log {}^*K_{s,(1,4)}^{\circ}$ and $\log {}^*\beta_{(1,4)}^{\circ}$ results in $\log {}^*K_{s,0}^{\circ}\{0.5 \text{ K}_2\text{U}_2\text{O}_7 \cdot 1.5\text{H}_2\text{O}(\text{cr})\} = \log {}^*K_{s,(1,4)}^{\circ} - \log {}^*\beta_{(1,4)}^{\circ} = (12.0 \pm 0.2)$. Note that this value is in good agreement although slightly lower than $\log {}^*K_{s,0}^{\circ}\{0.5 \text{ Na}_2\text{U}_2\text{O}_7 \cdot \text{H}_2\text{O}(\text{cr})\} = (12.2 \pm 0.2)$ reported by Altmaier and co-authors for NaCl systems [43].

Solubility data at $\text{pH}_m \leq 11$ were not used to derive any thermodynamic quantity. Instead, $\log {}^*K_{s,0}^{\circ}\{0.5 \text{ K}_2\text{U}_2\text{O}_7 \cdot 1.5\text{H}_2\text{O}(\text{cr})\}$ determined from solubility data at $\text{pH}_m \geq 11$ and hydrolysis constants reported by Altmaier *et al.* [43] were considered to reproduce the solubility of U(VI) in this pH_m -region. Ion interaction coefficients for $\text{UO}_2(\text{OH})_3^-$ (13) and $(\text{UO}_2)_3(\text{OH})_7^-$ (37) species (expected to prevail within $8 \leq \text{pH}_m \leq 11$) with K^+ were taken as $\epsilon(\text{UO}_2(\text{OH})_3^-, \text{K}^+) = \epsilon(\text{UO}_2(\text{OH})_3^-, \text{Na}^+) = -(0.24 \pm 0.09) \text{ kg} \cdot \text{mol}^{-1}$ and $\epsilon((\text{UO}_2)_3(\text{OH})_7^-, \text{K}^+) = \epsilon((\text{UO}_2)_3(\text{OH})_7^-, \text{Na}^+) = -(0.24 \pm 0.09) \text{ kg} \cdot \text{mol}^{-1}$, considering the close similarities between $\epsilon(\text{UO}_2(\text{OH})_4^{2-}, \text{Na}^+)$ and $\epsilon(\text{UO}_2(\text{OH})_4^{2-}, \text{K}^+)$.

5.3.2 Re-evaluation of $\log {}^*K_{s,0}^{\circ}\{1/6 \text{ K}_2\text{U}_6\text{O}_{19} \cdot 11\text{H}_2\text{O}(\text{cr})\}$ (compreignacite) in 1 m KCl reported in the literature

Sandino and Grambow [99] and Gorman-Lewis and co-authors [101] previously investigated the solubility of compreignacite, $\text{K}_2\text{U}_6\text{O}_{19} \cdot 11\text{H}_2\text{O}(\text{cr})$, in acidic KCl solutions conditions ($3.5 \leq \text{pH} \leq 5$). Solubility data reported by Gorman-Lewis *et al.* [101] are characterized by large variations in the ionic strength between different samples and by short equilibration times. Accordingly, only data reported by Sandino and Grambow were re-evaluated in the present work, consistently with hydrolysis constants and SIT interaction coefficients reported by Altmaier *et al.* [43] (see Table 5.2 and 5.3). The only unknown parameter required for the parametrization of the solubility data is $\log {}^*K_{s,0}^{\circ}\{1/6 \text{ K}_2\text{U}_6\text{O}_{19} \cdot 11\text{H}_2\text{O}(\text{cr})\}$ corresponding to the equilibrium reaction (5.5):



with

$$\log {}^*K'_{s,0} = \log [\text{UO}_2^{2+}] - \frac{7}{3} \log [\text{H}^+] + \frac{1}{3} \log [\text{K}^+] \quad (5.6)$$

$$\begin{aligned} \log {}^*K_{s,0}^{\circ} &= \log {}^*K'_{s,0} + \log \gamma_{\text{UO}_2^{2+}} - \frac{7}{3} \log \gamma_{\text{H}^+} \\ &\quad + \frac{1}{3} \log \gamma_{\text{K}^+} + 3 \log a_w \end{aligned} \quad (5.7)$$

The value of $\log {}^*K_{s,0}^{\circ}\{1/6 \text{K}_2\text{U}_6\text{O}_{19} \cdot 11\text{H}_2\text{O}(\text{cr})\}$ was determined based upon two independent datasets (run K1 and K2), corresponding to a different preparation approach of the original $\text{K}_2\text{U}_6\text{O}_{19} \cdot 11\text{H}_2\text{O}(\text{cr})$ solid phase. The use of the minimization function $\sum((\log [\text{U}]_{\text{exp}} - \log [\text{U}]_{\text{calc}})^2)^{1/2}$ resulted in:

$$\log {}^*K_{s,0}^{\circ}(\text{run K1}) = (6.0 \pm 0.1)$$

$$\log {}^*K_{s,0}^{\circ}(\text{run K2}) = (6.4 \pm 0.1)$$

The average of these two values, $\log {}^*K_{s,0}^{\circ}\{1/6 \text{K}_2\text{U}_6\text{O}_{19} \cdot 11\text{H}_2\text{O}(\text{cr})\} = (6.2 \pm 0.1)$ agrees within the uncertainties with the data selected in NEA-TDB [41] based on the same solubility dataset ($\log {}^*K_{s,0}^{\circ} = (6.18 \pm 0.09)$), but it is now internally consistent with the hydrolysis constants and SIT interaction coefficients considered in the present work. Figure 5.5 shows the original experimental data reported in Sandino and Grambow [99] and the solubility curve of $\text{K}_2\text{U}_6\text{O}_{19} \cdot 11\text{H}_2\text{O}(\text{cr})$ calculated using thermodynamic data selected in the present work.

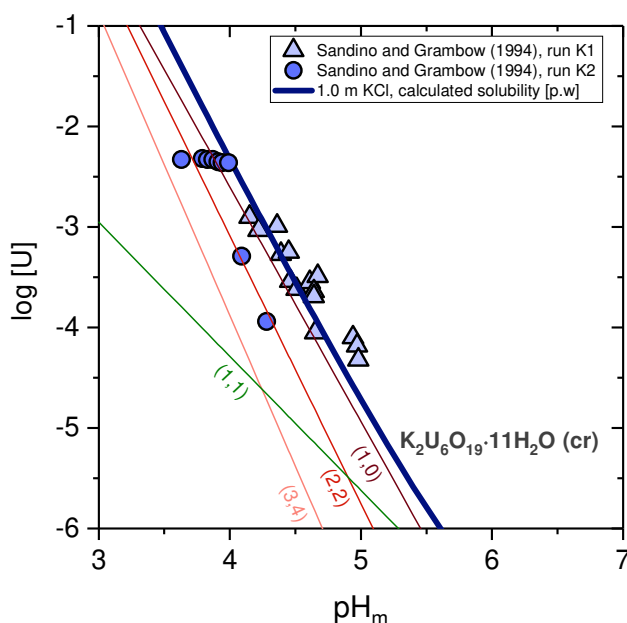


Figure 5.5. Solubility data of U(VI) in 1 m KCl solutions at $3 \leq \text{pH}_m \leq 6$ as reported by Sandino and Grambow (1994) [99] (runs K1 and K2 in the original publication, see discussion in text). Solid lines correspond to the solubility of $\text{K}_2\text{U}_6\text{O}_{19} \cdot 11\text{H}_2\text{O}(\text{cr})$ (thick blue line) and underlying aqueous speciation (thin lines) calculated with the thermodynamic and SIT activity models summarized in Tables 5.2 and 5.3.

5.3.3 Summary of the improved thermodynamic model for the system $\text{UO}_2^{2+}\text{-H}^+\text{-K}^+\text{-Na}^+\text{-Cl}^-\text{-OH}^-\text{-H}_2\text{O(l)}$

Tables 5.2 and 5.3 summarize chemical, thermodynamic and SIT activity models for the system $\text{UO}_2^{2+}\text{-H}^+\text{-K}^+\text{-Na}^+\text{-Cl}^-\text{-OH}^-\text{-H}_2\text{O(l)}$, as derived in the present work and reported in the NEA-TDB [41] and Altmaier *et al.* [43]. Solubility calculations using these thermodynamic data are compared in Figure 5.6 with experimental solubility data determined in this work in 0.1–4.0 M KCl solutions at $7 \leq \text{pH}_m \leq 14.5$.

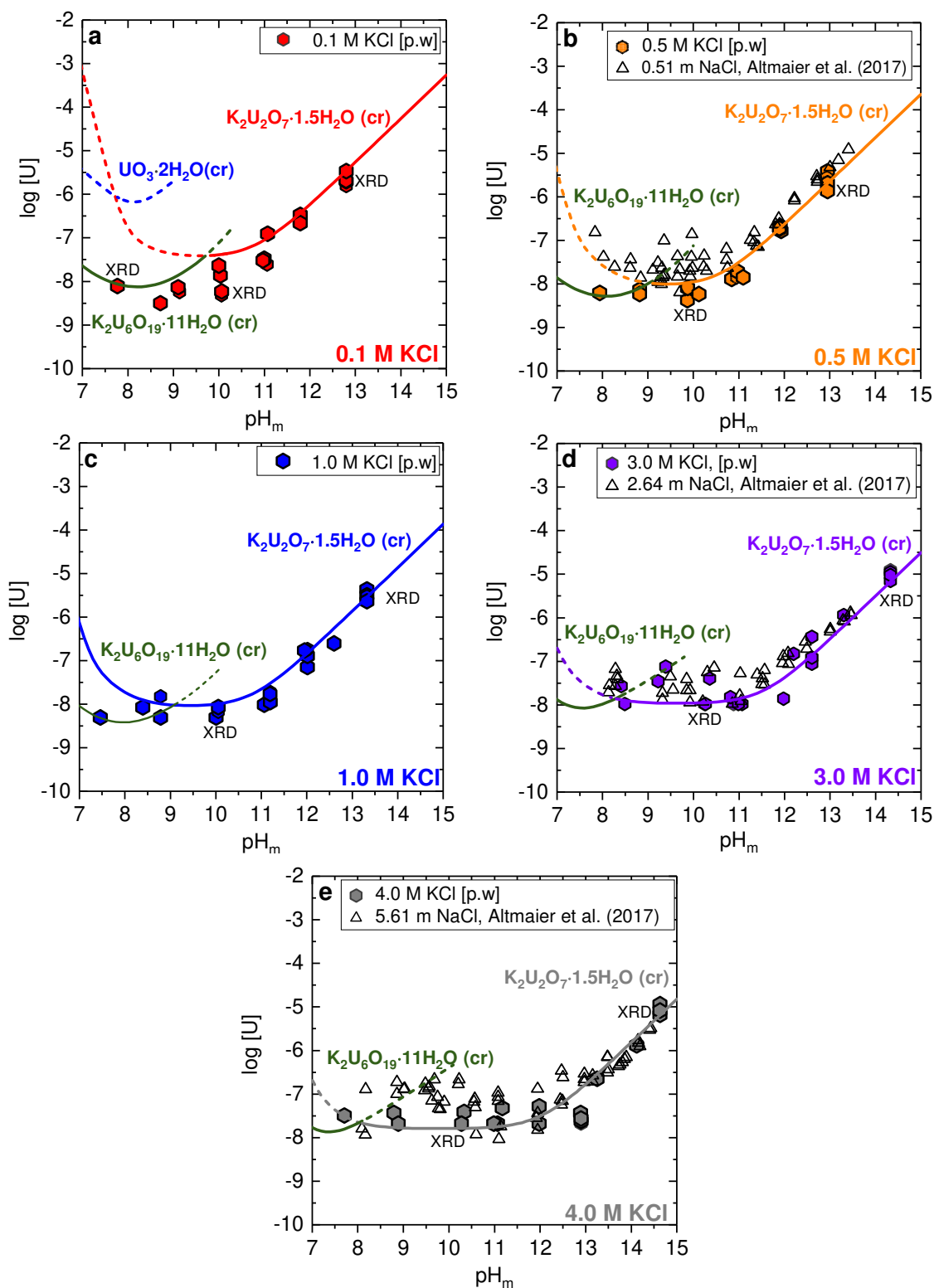


Figure 5.6. Solubility of U(VI) in alkaline KCl solutions: a. 0.1 M; b. 0.5 M, c. 1.0 M, d. 3.0 M and e. 4.0 M. Empty triangles correspond to the solubility of $\text{Na}_2\text{U}_2\text{O}_7 \cdot \text{H}_2\text{O}(\text{cr})$ reported by Altmaier et al. [43] in 0.5, 2.64 and 5.61 m NaCl systems. Lines are solubilities of $\text{UO}_3 \cdot 2\text{H}_2\text{O}(\text{cr})$, $\text{K}_2\text{U}_6\text{O}_{19} \cdot 11\text{H}_2\text{O}(\text{cr})$ and $\text{K}_2\text{U}_2\text{O}_7 \cdot 1.5\text{H}_2\text{O}(\text{cr})$ calculated with thermodynamic and SIT activity models summarized in Tables 5.2 and 5.3.

Figure 5.6 shows that the calculated solubility is in good agreement with the experimental data in most of the investigated cases. Solubility calculations support that $K_2U_2O_7 \cdot 1.5H_2O(cr)$ is the solid phase controlling the solubility of U(VI) in KCl solutions with $pH_m \geq 8 - 9$ (depending upon KCl concentration). Below this pH_m , thermodynamic calculations predict a solid phase transformation into $K_2U_6O_{19} \cdot 11H_2O(cr)$. This result is in line with results obtained by XRD (see Section 5.2), which hinted towards a solid phase transformation in the solubility sample equilibrated in 0.1 M KCl at $pH_m = 7.7$. Although the collected XRD pattern did not perfectly match those of compregnecite, the position of the first peak clearly hinted to a solid phase transformation towards a uranate phase with K:U < 1.

Table 5.2. Solubility and hydrolysis constants at $I = 0$ selected in the present work for the system

$UO_2^{2+} - H^+ - K^+ - Na^+ - Cl^- - OH^- - H_2O(l)$.

Solid phases		$\log^* K_{s,0}^\circ$	References
0.5K ₂ U ₂ O ₇ ·1.5H ₂ O(cr)		(12.0 ± 0.2)	(p.w.)
1/6K ₂ U ₆ O ₁₉ ·11H ₂ O(cr)		(6.2 ± 0.1)	(p.w.), a
0.5Na ₂ U ₂ O ₇ ·H ₂ O(cr)		(12.2 ± 0.2)	[43]
Hydrolysis species	(xy)	$\log^* \beta_{(x,y)}^\circ$	
UO ₂ OH ⁺	(11)	−(5.25 ± 0.24)	[41]
UO ₂ (OH) ₂ (aq)	(12)	−(12.15 ± 0.17)	[41]
UO ₂ (OH) ₃ [−]	(13)	−(20.7 ± 0.40)	[43]
UO ₂ (OH) ₄ ^{2−}	(14)	−(31.9 ± 0.2)	[43]
(UO ₂) ₂ (OH) ₂ ²⁺	(22)	−(5.62 ± 0.04)	[41]
(UO ₂) ₃ (OH) ₄ ²⁺	(34)	−(11.9 ± 0.3)	[41]
(UO ₂) ₃ (OH) ₅ ⁺	(35)	−(15.55 ± 0.12)	[41]
(UO ₂) ₃ (OH) ₇ [−]	(37)	−(32.20 ± 0.80)	[41]
(UO ₂) ₄ (OH) ₇ ⁺	(47)	−(21.9 ± 1.0)	[41]

a. re-evaluated in this work from experimental data reported in Sandino and Grambow (1994).

Table 5.3. SIT ion interaction coefficients for UO_2^{2+} and U(VI) hydrolysis species derived in the present work and reported in the literature for NaCl and KCl systems.

U(VI) species		SIT coefficients	
<i>I</i>	<i>J</i>	$\epsilon(i,j)$	References
UO_2^{2+}	Cl^-	(0.21 ± 0.02)	[82]
UO_2OH^+	Cl^-	(0.10 ± 0.10)	[43]
$(UO_2)_2(OH)_2^{2+}$	Cl^-	(0.30 ± 0.06)	[43]
$(UO_2)_3(OH)_4^{2+}$	Cl^-	$-(0.07 \pm 0.17)$	[43]
$(UO_2)_3(OH)_5^+$	Cl^-	(0.24 ± 0.15)	[43]
$(UO_2)_4(OH)_7^+$	Cl^-	(0.17 ± 0.18)	[43]
$UO_2(OH)_3^-$	Na^+	$-(0.24 \pm 0.09)$	[43]
$UO_2(OH)_4^{2-}$	K^+	$-(0.24 \pm 0.09)$	(p.w.), a
	Na^+	(0.01 ± 0.04)	[43]
$(UO_2)_3(OH)_7^-$	K^+	(0.03 ± 0.04)	(p.w.)
	Na^+	$-(0.24 \pm 0.09)$	[43]
$UO_2(OH)_2(aq)$	K^+	$-(0.24 \pm 0.09)$	(p.w.), a
	K^+, Na^+, Cl^-	0	b

a. set equal to the ion interaction coefficient of the same species with Na^+ ; b. by definition in SIT.

5.3.4 Role of ternary Na-U(VI)-OH and K-U(VI)-OH solid phases in cementitious systems

The dissolution of Na_2O and K_2O within the degradation stage I of cement buffers the pH in the hyperalkaline region, whilst retaining rather high concentrations of Na^+ and K^+ (0.1–0.2 M) in solution [8, 9, 11, 158]. Mixed salt systems containing both NaCl and KCl in different concentrations are also expected in different concepts and scenarios of relevance in the context of nuclear waste disposal. In these conditions, the solid phases $K_2U_2O_7 \cdot 1.5H_2O(cr)$ and / or $Na_2U_2O_7 \cdot H_2O(cr)$ may form, eventually controlling the solubility of U(VI) in such environments. Based on the thermodynamic and activity models summarized above, this section aims at evaluating the role of $K_2U_2O_7 \cdot 1.5H_2O(cr)$ and $Na_2U_2O_7 \cdot H_2O(cr)$ solid phases in controlling the solubility of U(VI) in the systems:

- i. Solutions containing 0.1 m Na^+ and 0.1 m K^+ at $pH_m \approx 13.2$, representing the degradation phase I of cement in dilute porewater systems (Figure 5.6a)
- ii. Solutions containing 5.641 m Na^+ + 0.614 m K^+ . This porewater composition was calculated by Bube *et al.* [4] as a simulation of cemented wastes in concentrated NaCl brine solutions^{††}.

^{††} Salt concentrations reported in Bube *et al.* (2013) were decreased by 10% to avoid precipitation of saturated salts.

Figure 5.7 shows the solubility of U(VI) within $10 \leq \text{pH}_m \leq 13.5$ for the porewater composition described in (i) and (ii) and using thermodynamic data summarized in Tables 5.2 and 5.3.

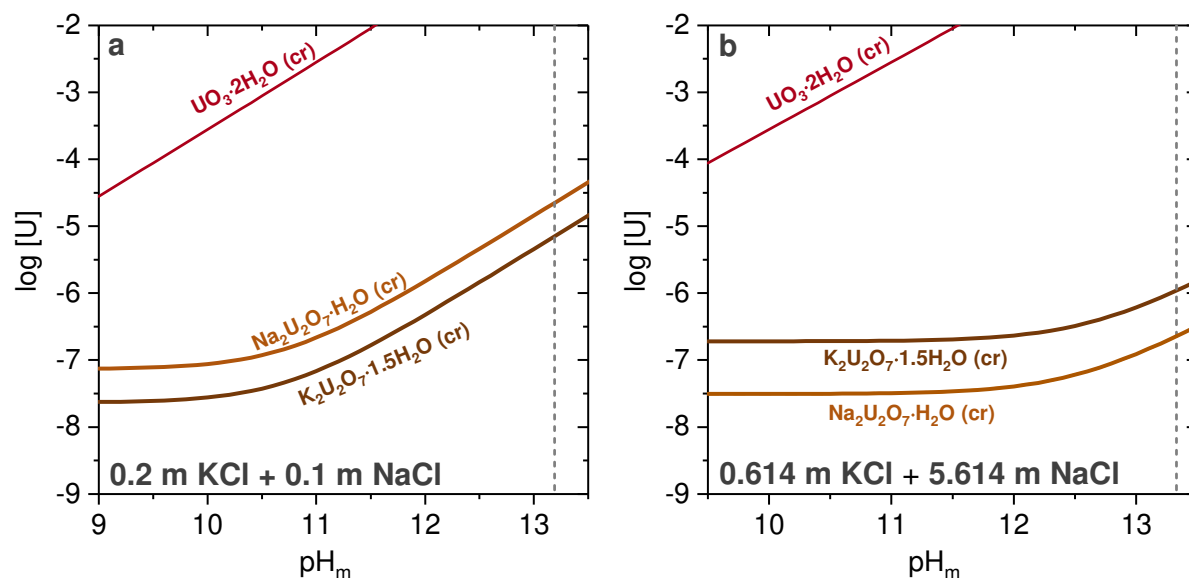


Figure 5.7. Solubility of $\text{UO}_3 \cdot 2\text{H}_2\text{O (cr)}$, $\text{K}_2\text{U}_2\text{O}_7 \cdot 1.5\text{H}_2\text{O (cr)}$ and $\text{Na}_2\text{U}_2\text{O}_7 \cdot \text{H}_2\text{O (cr)}$ at $10 \leq \text{pH}_m \leq 13.5$ in a. 0.2 m KCl + 0.1 m NaCl solutions; b. 0.614 m KCl + 5.614 m NaCl solutions. Calculations performed using thermodynamic and activity models summarized in Tables 2 and 3. Vertical dashed line corresponding to the pH_m of the original composition.

Figure 5.7a shows that $\text{K}_2\text{U}_2\text{O}_7 \cdot 1.5\text{H}_2\text{O (cr)}$ is expected to control the solubility of U(VI) in the dilute system, whereas the solubility of U(VI) in 5.614 m NaCl + 0.614 m is controlled by $\text{Na}_2\text{U}_2\text{O}_7 \cdot \text{H}_2\text{O (cr)}$ due to the significantly higher concentration of Na^+ compared to K^+ (Figure 5.7b). In both cases and for the same pH_m -range, the calculated solubility of $\text{UO}_3 \cdot 2\text{H}_2\text{O (cr)}$ is several orders of magnitude higher. These results highlight that both ternary Na/K–U(VI)–OH solid phases must be accounted for a correct evaluation of U(VI) solubility in alkaline to hyperalkaline systems. Although only simple salt systems were investigated in this work and in Altmaier *et al.* (2017) (accordingly resulting in the formation of $\text{K}_2\text{U}_2\text{O}_7 \cdot 1.5\text{H}_2\text{O (cr)}$ and $\text{Na}_2\text{U}_2\text{O}_7 \cdot \text{H}_2\text{O (cr)}$), the layered structure of such uranates phases is expected to accommodate both cations in mixed NaCl–KCl systems. The formation of mixed phases $\text{Na}_x\text{K}_{2-x}\text{U}_2\text{O}_7 \cdot x\text{H}_2\text{O (cr)}$ should be possibly expected in these conditions. Based on the similarity of the solubility constants determined for the pure $\text{K}_2\text{U}_2\text{O}_7 \cdot 1.5\text{H}_2\text{O (cr)}$ and $\text{Na}_2\text{U}_2\text{O}_7 \cdot \text{H}_2\text{O (cr)}$ phases ($\log^* K_{s,0}^\circ = 12.0 \pm 0.2$ and 12.2 ± 0.2 , respectively), $\log^* K_{s,0}^\circ \{ \text{Na}_x\text{K}_{2-x}\text{U}_2\text{O}_7 \cdot x\text{H}_2\text{O (cr)} \}$ should be also expected to be of the same order.

This work contributes to close an important thermodynamic gap affecting the solution chemistry of U(VI) in the hyperalkaline pH_m conditions representative of cementitious systems. The presented results highlight also the importance of having complete thermodynamic databases (TDB) for the correct interpretation of a given (radionuclide) system. The absence of relevant solid phases or aqueous complexes in the available TDB may result in totally unrealistic thermodynamic calculations (*e.g.* solubility limits, aqueous speciation, etc.). Neither $\text{K}_2\text{U}_2\text{O}_7 \cdot 1.5\text{H}_2\text{O}(\text{cr})$ nor $\text{Na}_2\text{U}_2\text{O}_7 \cdot \text{H}_2\text{O}(\text{cr})$ are currently selected in the NEA–TDB reviews. This fact can be taken as evidence of the importance that thermodynamic studies still have in the context of nuclear waste disposal.

6 Summary and conclusions

This PhD thesis aimed at providing a fundamental understanding on the solution chemistry of uranium, with focus on three main parts aspects, namely redox behavior, solubility and hydrolysis. The boundary conditions investigated range from very acidic to hyperalkaline pH values, from very reducing to oxidizing, and from dilute to concentrated salt systems. In this context, focus is given to conditions for which relevant data gaps or controversial discussion is provided in the literature. Some of these conditions are representative of different repository concepts (*e.g.* crystalline, clay, salt-rock) and wasteforms (*e.g.* cementitious systems), and thus can provide relevant inputs in the context of nuclear waste disposal.

The redox behaviour of uranium was investigated in reducing, dilute to concentrated NaCl solutions from acidic to hyperalkaline pH_m conditions. Uranium(VI) was added to NaCl solutions of given pH_m values containing individual and mixed reducing systems (Sn(II), $Na_2S_2O_4$, Sn(II) + Fe(0), Sn(II) + TiO_2 and Sn(II) + Fe_3O_4). According to thermodynamic calculations in the form of *Pourbaix* diagrams, the reducing conditions set by these systems (with $pe + pH_m \leq 4$) were expected to promote the reduction of U(VI) to U(IV). The large difference in solubility between solid phases of U(VI) ($UO_3 \cdot 2H_2O(cr)$ and $Na_2U_2O_7 \cdot H_2O(cr)$) and U(IV) ($UO_2(am, hyd)$) expected to form in these conditions was taken as main indicator to follow the reduction to U(IV). Solubility data, in combination with solvent extraction and XANES confirm that a complete reduction of U(VI) to U(IV) took place in most of the investigated systems. The reduction occurs in two steps, involving a first, fast precipitation of a U(VI) solid phase, and a second, slower reaction with the transformation of this solid phase into $UO_2(am, hyd)$. The main parameters affecting the reduction kinetics are identified as $[U(VI)]_0$, pH_m , E_h , concentration of the reducing chemicals, presence of redox-active surfaces and $[NaCl]$ (in alkaline systems). In the less favoured conditions, a complete reduction is only observed after 635 days. The pH-independent solubility observed (after attaining equilibrium conditions) from weakly acidic to hyperalkaline conditions (up to $pH_m \approx 14.5$) confirms the predominance of $U(OH)_4(aq)$ in the aqueous phase, in equilibrium with $UO_2(am, hyd)$. These results preclude a predominant role of anionic hydrolysis species ($U(OH)_5^-$ and $U(OH)_6^{2-}$) in the solution chemistry of U(IV). Furthermore, experimental observations obtained within this work support that previous studies reporting the formation of such anionic species of U(IV) are affected by insufficient equilibration time, and that the increased uranium concentrations measured in previous publications correspond indeed to a solubility-control by $Na_2U_2O_7 \cdot H_2O(cr)$.

The excellent agreement between experimental observations obtained in this work and thermodynamic calculations (*Pourbaix* and solubility diagrams) supports the use of (pe + pH_m) measurements as an accurate tool to predict the redox behaviour of uranium in dilute to concentrated saline systems under repository relevant boundary conditions.

U(IV) solubility was investigated in reducing, dilute to concentrated NaCl, MgCl₂ and CaCl₂ solutions under acidic to hyperalkaline pH_m conditions. A U(IV) solid phase was precipitated in alkaline, reducing conditions and aged for three months before further use in solubility experiments. A thorough characterization of this solid using XRD, EXAFS, SEM-EDS, TG-DTA and quantitative chemical analysis confirmed the formation of a (nano-)crystalline UO₂·H₂O(ncr) phase with an average crystal (domain) size of (3 ± 1) nm. The well-characterized solid was used in a series of undersaturation solubility experiments in 0.1–5.0 M NaCl at 1 ≤ pH_m ≤ 14.5, 0.25–4.5 M MgCl₂ at 1 ≤ pH_m ≤ 9, and 0.25–4.5 M CaCl₂ at 9 ≤ pH_m ≤ 12. Solid phase characterization performed after completing the solubility experiments confirmed that UO₂·H₂O(ncr) remained unaltered in the course of the solubility study.

In acidic NaCl and MgCl₂ solutions, the solubility of UO₂·H₂O(ncr) shows a steep decrease with increasing pH_m. Although following a very similar trend in terms of log [U] vs. pH_m, solubility data determined in this work is approximately two orders of magnitude lower than most of the previous solubility studies with UO₂(am, hyd). This observation highlights the more crystalline character of the solid phase compared to previous solubility studies. All solubility data measured above pH_m ≈ 4 / 5 (depending upon ionic strength) resulted in values below the detection limit of standard ICP–MS. The use of μ-injection ICP–MS for the quantification of [U] in 0.1 and 0.5 M NaCl systems allowed a significantly reduced detection limit, showing that solubility is pH_m-independent and significantly lower than previous studies with UO₂(am, hyd). As in the case of oversaturation / redox experiments, these results support the predominance of U(OH)₄(aq) in solution for this pH_m-range, thus ruling out a predominant role of anionic hydrolysis species of U(IV) in hyperalkaline systems. Solubility data measured at pH_m ≥ 3 without using any phase separation technique resulted in uranium concentrations 2–3 orders of magnitude higher than those measured after 10 kD ultrafiltration. This observation is likely related to the presence of U(IV) intrinsic colloids as those previously described for Th(IV) and Pu(IV). However, a trend to decreasing the concentration of the colloidal fraction with time may hint towards aggregation phenomena, and opens the question of the long-term stability of such colloids.

All solubility measurements in CaCl₂ solutions resulted below the detection limit of standard ICP–MS. Although unable to confirm the formation of the ternary complex Ca₄[U(OH)₈]⁴⁺ expected in analogy to the previously reported species for Th(IV), Np(IV) and Pu(IV), upper limits derived in this work for log *β[∞]_(4,1,8) are consistent with the estimates provided in Fellhauer *et al.* (2010) based upon linear free energy relationships.

The combination of solubility data determined in the present work, solid phase characterization and thermodynamic data reported in the NEA–TDB and Neck and Kim (2001) for U(IV) hydrolysis species allowed deriving accurate thermodynamic and activity models for the system U⁴⁺–Na⁺–Mg²⁺–Ca²⁺–H⁺–Cl[–]–OH[–]–H₂O(l). To the author’s knowledge, this is the most comprehensive thermodynamic study undertaken so far for U(IV) and, especially, involving the most accurate solid phase characterization of the solubility-controlling oxo-hydroxide phase of U(IV).

In the last part of this PhD study, **the solubility of U(VI) was investigated in dilute to concentrated KCl systems under near neutral to hyperalkaline pH_m conditions.** A solid phase precipitated in an alkaline KCl solution was characterized using XRD, SEM-EDS, TG-DTA and quantitative chemical analysis, and identified as K₂U₂O₇·1.5H₂O(cr). This solid phase was used in a systematic series of solubility experiments in 0.1–4.0 M KCl at 7.5 ≤ pH_m ≤ 14.6. Characterization of selected solid samples after the solubility experiments confirmed that K₂U₂O₇·1.5H₂O(cr) remained unaltered in the course of the experiments, except in less alkaline, dilute KCl solutions where the formation of a solid phase with a ratio U:K < 1 was hinted by XRD. Slope analysis of the solubility data confirms the predominance of UO₂(OH)₃[–] and UO₂(OH)₄^{2–} below and above pH_m ≈ 11, in excellent agreement with previous solubility experiments in analogous alkaline NaCl systems. Chemical, thermodynamic and SIT activity models for the system UO₂²⁺–H⁺–K⁺–Na⁺–Cl[–]–OH[–]–H₂O(l) were derived based on the newly generated solubility data in alkaline conditions, previous solubility studies in acidic KCl systems and U(VI) hydrolysis constants reported in Altmaier *et al.* (2017). This work contributes to close an important thermodynamic gap affecting the solution chemistry of U(VI) in the hyperalkaline pH_m conditions representative of cementitious systems.

This PhD thesis provides new insights on the solution chemistry of uranium with focus in the +IV and +VI oxidation states. Thermodynamic constants derived in the standard state and (SIT) ion interaction coefficients obtained can be implemented in thermodynamic databases and used in geochemical calculations under a variety of boundary conditions. This covers dilute to concentrated salt systems, thus allowing thermodynamic calculations under conditions

representative of the different host-rocks foreseen for repositories for nuclear waste disposal. The important effort undertaken to attain an accurate characterization of the solid phase/s controlling the solubility in the investigated systems represents in itself an important achievement, especially in the case of U(IV) where amorphous, ill-defined oxo-hydroxides phases control the solution chemistry of uranium over a very broad range of geochemical conditions.

References

- [1] Bundesanstalt für Geowissenschaften und Rohstoffe; Final disposal of radioactive waste- Nuclear Waste Disposal in Germany. Investigation and evaluation of regions with potentially suitable host rock formations for a geologic nucleus repository; Available from: <https://www.bgr.bund.de/>, (2013).
- [2] Metz, V., Kienzler, B., Schüßler, W., Geochemical evaluation of different groundwater-host rock systems for radioactive waste disposal, *Journal of Contamination Hydrology*, 61, 265-279, (2003).
- [3] Metz, V., Geckeis, H., González-Robles, E., Loida, A., Bube, C., Kienzler, B., Radionuclide behaviour in the near-field of a geological repository for spent nuclear fuel, *Radiochimica Acta*, 100, 699-713, (2012).
- [4] Bube, C., Metz, V., Bohnert, E., Garbev, K., Schild, D., Kienzler, B., Long-term cement corrosion in chloride-rich solutions relevant to radioactive waste disposal in rock salt – Leaching experiments and thermodynamic simulations, *Physics Chemistry of the Earth*, 64, 87–94, (2013).
- [5] Kim, J.I., Grambow, B., Geochemical assessment of actinide isolation in a German salt repository environment, *Engineering Geology*, 52, 221-230, (1999).
- [6] Frapé, S.K., Fritz, P., McNutt, R.H., Water Rock Interaction and Chemistry of Groundwaters from the Canadian Shield, *Geochimica Et Cosmochimica Acta*, 48, 1617-1627, (1984).
- [7] Brewitz, W., F + E Programm zur Eignungsprüfung der Schachanlage Konrad für die Einlagerung radioaktiver Abfälle - Zusammenfassender Zwischenbericht, GSF-T 114, Braunschweig (1981).
- [8] Ochs, M., Dirk, M., Wang, L., Radionuclide and Metal Sorption on Cement and Concrete, Springer, Switzerland, (2016).
- [9] Berner, U.R., Thermodynamic Modeling of Cement Degradation - Impact of Redox Conditions on Radionuclide Release, *Cement and Concrete Research*, 22, 465-475, (1992).
- [10] Wieland, E., Van Loon, L., Cementitious Near-Field Sorption Data Base for Performance Assessment of an ILW Repository in Opalinus Clay. Technical report, Paul Scherrer Institut, Villigen, Switzerland., in, 2003.
- [11] Taylor, H.F.W., Cement Chemistry, second ed. Thomas Telford, London, (1997).
- [12] Greenwood, N.N., Earnshaw, A., Chemistry of the Elements, 2nd Edition, Butterworth-Heinemann, Oxford, (1997).

- [13] Hahn, O., Strassman, F., Über den Nachweis und das Verhalten bei der Bestrahlung des Urans mittels Neutronen entstehenden Erdalkalimetalle, *Naturwissenschaften*, 27, 11-15, (1939).
- [14] How the first chain reaction changed science; Available from: <http://www.uchigaco.edu>.
- [15] Frondel, J.W., Fleischer, M., Glossary of Uranium and Thorium-Bearing Minerals, third ed. Report, Geological Survey Bulletin 1009-F, USA, (1954).
- [16] Abdelouas, A., Grambow, B., Aquatic chemistry of long-lived mobile fission and activation products in the context of deep geological disposal. *Aquatic chemistry in the context of deep geological disposal*. ed. P. Christophe and G. Horst, Cambridge, UK, Woodhead Publishing, (2012).
- [17] Altmaier, M., Gaona, X., Fanghanel, T., Recent Advances in Aqueous Actinide Chemistry and Thermodynamics, *Chemical Reviews*, 113, 901-943, (2013).
- [18] Choppin, G.R., Solution Chemistry of the Actinides, *Radiochimica Acta*, 32, 43-53, (1983).
- [19] Mizuguchi, K., Park, Y.Y., Tomiyasu, H., Ikeda, Y., Electrochemical and Spectroelectrochemical Studies on Uranyl Carbonato and Aqua Complexes, *Journal of Nuclear Science and Technology*, 30, 542-548, (1993).
- [20] Capdevila, H., Vitorge, P., Redox potentials of M(VI)/M(V) limiting carbonate complexes (M = U or Pu) at different ionic strengths and temperatures. Entropy and heat capacity., *Czechoslovak Journal of Physics*, 49, 603-609, (1999).
- [21] Miyake, C., Yamana, Y., Imoto, S., Ohyanishiguchi, H., Direct Evidence of Uranium(V) Intermediates by Electron-Spin Resonance in Photo-Reduction and Electrolytic Reduction Processes of Uranyl Complexes in Organic Solutions, *Inorganica Chimica Acta-F-Block Elements Articles and Letters*, 95, 17-21, (1984).
- [22] Miyake, C., Kondo, T., Imoto, S., Ohyanishiguchi, H., Direct Evidence of Uranium(V) Intermediates by Electron-Spin-Resonance in Photolytic and Electrolytic Reduction Processes of Uranyl Complexes in Organic Solutions, *Journal of the Less-Common Metals*, 122, 313-317, (1986).
- [23] Berthet, J.C., Nierlich, M., Ephritikhine, M., Isolation of a Uranyl $[\text{UO}_2]^+$ Species: Crystallographic Comparison of the Dioxouranium(V) and (VI) Compounds $[\text{UO}_2(\text{OPPh}_3)_4(\text{OTf})_n]$ (n=1, 2), *Angewandte Chemie-International Edition*, 42, 1952-1954, (2003).
- [24] Natrajan, L., Burdet, F., Pecaut, J., Mazzanti, M., Synthesis and Structure of a Stable Pentavalent-Uranyl Coordination Polymer, *Journal of the American Chemical Society*, 128, 7152-7153, (2006).

- [25] Shannon, J.C., Database of ionic radii. Available from: <http://abulafia.mt.ic.ac.uk/shannon/ptable.php> (accessed 02.03.2018).
- [26] Niinisto, L., Toivonen, J., Valkonen, J., Uranyl(VI) compounds. II. Crystal-Structure of Potassium Uranyl Sulfate Dihydrate, $K_2UO_2(SO_4)_2 \cdot 2H_2O$, Acta Chemica Scandinavica Series a-Physical and Inorganic Chemistry, 33, 621-624, (1979).
- [27] Burns, P.C., Hayden, L.A., A uranyl sulfate cluster in $Na_{10}[(UO_2)(SO_4)_4](SO_4)_2 \cdot 3H_2O$, Acta Crystallographica Section C-Crystal Structure Communications, 58, I121-I123, (2002).
- [28] Anderson, A., Chieh, C., Irish, D.E., Tong, J.P.K., An X-Ray Crystallographic, Raman, and Infrared Spectral Study of Crystalline Potassium Uranyl Carbonate, $K_4UO_2(CO_3)_3$, Canadian Journal of Chemistry-Revue Canadienne De Chimie, 58, 1651-1658, (1980).
- [29] Zalkin, A., Templeton, L.K., Templeton, D.H., Structure of Rubidium Uranyl(VI) Trinitrate, Acta Crystallographica Section C-Crystal Structure Communications, 45, 810-811, (1989).
- [30] Navaza, A., Charpin, P., Vigner, D., Heger, G., Single-crystal neutron diffraction: structure of sodium tris(acetato)dioxouranate(1-), Acta Crystallographica Section C-Crystal Structure Communications, 47, 1842-1845, (1991).
- [31] Clark, D.L., Conradson, S.D., Donohoe, R.J., Keogh, D.W., Morris, D.E., Palmer, P.D., Rogers, R.D., Tait, C.D., Chemical speciation of the uranyl ion under highly alkaline conditions. Synthesis, structures, and oxo ligand exchange dynamics, Inorganic Chemistry, 38, 1456-1466, (1999).
- [32] Wahlgren, U., Moll, H., Grenthe, I., Schimmelpfennig, B., Maron, L., Vallet, V., Gropen, O., Structure of uranium(VI) in strong alkaline solutions. A combined theoretical and experimental investigation, Journal of Physical Chemistry A, 103, 8257-8264, (1999).
- [33] Moll, H., Reich, T., Szabó, Z., The hydrolysis of dioxouranium(VI) investigated using EXAFS and O-17-NMR, Radiochimica Acta, 88, 411-415, (2000).
- [34] Zachariasen, W.H., Crystal Chemical Studies of the 5f-Series of Elements .23. On the Crystal Chemistry of Uranyl Compounds and of Related Compounds of Transuranic Elements, Acta Crystallographica, 7, 795-799, (1954).
- [35] Grenthe, I., Drożdżyński, J., Fujino, T., Buck, E.C., Albrecht-Schmitt, T.E., Wolf, S.F., Uranium in: Morss L.R., Edelstein N.M., Fuger, J., The Chemistry of the Actinide and Transactinide Elements. Springer, Dordrecht, pp 253-698, (2006).
- [36] Lundgren, G., The Crystal Structure of $U(OH)_2SO_4$, Arkiv for Kemi, 4, 421-428, (1952).
- [37] Fuchs, L.H., Gebert, E., X-Ray Studies of Synthetic Coffinite, Thorite and Uranothorites, American Mineralogist, 43, 243-248, (1958).

- [38] Crawford, M.J., Ellern, A., Mayer, P., UN₂₁³⁻: A structurally characterized binary actinide heptaazide anion, *Angewandte Chemie-International Edition*, 44, 7874-7878, (2005).
- [39] Neck, V., Altmaier, M., Fanghanel, T., Solubility of plutonium hydroxides/hydrous oxides under reducing conditions and in the presence of oxygen, *Comptes Rendus Chimie*, 10, 959-977, (2007).
- [40] Grenthe, I., Fuger, J., Konings, R.J.M., J., L.R., Müller, A.B., Nguyen-Trung, C., Wanner, H., *Chemical Thermodynamics of Uranium*, Vol 1 of *Chemical Thermodynamics*, Elsevier Science Publishers, Amsterdam, (1992).
- [41] Guillaumont, R., Fanghanel, T., Fuger, J., Grenthe, I., Neck, V., Palmer, D.A., Rand, M.H., Update on the Chemical Thermodynamics of Uranium, Neptunium, Plutonium, Americium and Technetium, Vol.5 of *Chemical Thermodynamics*, in, Elsevier Science Publishers, Amsterdam, (2003).
- [42] Neck, V., Kim, J.I., Solubility and hydrolysis of tetravalent actinides, *Radiochimica Acta*, 89, 1-16, (2001).
- [43] Altmaier, M., Yalcintas, E., Gaona, X., Neck, V., Müller, R., Schlieker, M., Fanghanel, T., Solubility of U(VI) in chloride solutions. I. The stable oxides/hydroxides in NaCl systems solubility products, hydrolysis constants and SIT coefficients, *Journal of Chemical Thermodynamics*, 114, 2-13, (2017).
- [44] Gayer, K.H., Leider, H., The solubility of uranium(IV) hydroxide in solutions of sodium hydroxide and perchloric acid at 25 °C, *Canadian Journal of Chemistry*, 35, 5-7, (1957).
- [45] Galkin, N.P., Stepanov, M.A., Solubility of uranium (IV) hydroxide in sodium hydroxide, *Soviet Journal of Atomic Energy*, 8, 258-261, (1960).
- [46] Tremaine, P.R., Chen, J.D., Wallace, G.J., Boivin, W.A., Solubility of Uranium (IV) Oxide in Alkaline Aqueous-Solutions to 300 °C, *Journal of Solution Chemistry*, 10, 221-230, (1981).
- [47] Ryan, J.L., Rai, D., The solubility of uranium(IV) hydrous oxide in sodium-hydroxide solutions under reducing conditions, *Polyhedron*, 2, 947-952, (1983).
- [48] Bruno, J., Ferri, D., Grenthe, I., Salvatore, F., Studies on Metal Carbonate Equilibria.13. On the Solubility of Uranium(IV) Dioxide, UO₂(s), *Acta Chemica Scandinavica Series a-Physical and Inorganic Chemistry*, 40, 428-434, (1986).
- [49] Parks, G.A., Pohl, D.C., Hydrothermal solubility of uraninite, *Geochimica Et Cosmochimica Acta*, 52, 863-875, (1988).
- [50] Rai, D., Felmy, A.R., Ryan, J.L., Uranium(IV) Hydrolysis Constants and Solubility Product of UO₂·xH₂O(am), *Inorganic Chemistry*, 29, 260-264, (1990).

- [51] Fujiwara, K., Yamana, H., Fujii, T., Moriyama, H., Determination of uranium(IV) hydrolysis constants and solubility product of $\text{UO}_2 \cdot x\text{H}_2\text{O}$, *Radiochimica Acta*, 91, 345-350, (2003).
- [52] Fujiwara, K., Yamana, H., Fujii, T., Kawamoto, K., Sasaki, T., Moriyama, H., Solubility of uranium(IV) hydrous oxide in high pH solution under reducing condition, *Radiochimica Acta*, 93, 347-350, (2005).
- [53] Yajima, T., Kawamura, Y., Ueta, S., Uranium(IV) Solubility and Hydrolysis Constants under Reduced conditions *Materials Research Society Symposium Proceedings* 353, 1137, (1995).
- [54] Zhao, R., Wang, L., Gu, Z.J., Yuan, L.Y., Xiao, C.L., Zhao, Y.L., Chai, Z.F., Shi, W.Q., A facile additive-free method for tunable fabrication of UO_2 and U_3O_8 nanoparticles in aqueous solution, *Crystengcomm*, 16, 2645-2651, (2014).
- [55] Casas, I., de Pablo, J., Giménez, J., Torrero, M.E., Bruno, J., Cera, E., Finch, R.J., Ewing, R.C., The role of pe, pH, and carbonate on the solubility of UO_2 and uraninite under nominally reducing conditions, *Geochimica Et Cosmochimica Acta*, 62, 2223-2231, (1998).
- [56] Bruno, J., Casas, I., Lagerman, B., Munoz, M., The determination of the solubility of amorphous $\text{UO}_2(\text{s})$ and the mononuclear hydrolysis constants of uranium(IV) at 25 °C, *Materials Research Society Proceedings*, 84, (1986).
- [57] Morel, M.M.F., Hering, J.G., *Principals and applications of aquatic chemistry*, John Wiley & Sons, New York, (1996).
- [58] Stumm, W., Morgan, J.J., *Aquatic Chemistry*, third ed. John Wiley & Sons, New York, (1996).
- [59] Altmaier, M., Gaona, X., D., F., Buckau, G., Intercomparison of Redox Determination Methods on Designed and Near Neutral Aqueous Systems, KIT SR 7572. Karlsruhe Institute of Tehcnology, Karlsruhe, 34., in, 2011.
- [60] Bruno, J., Trace element modelling in: Grenthe, I. and Puigdomenech, I. *Modelling in aquatic chemistry*. OECD, NEA, pp 593-621, (1997).
- [61] Spahiu, K., Werme, L., Eklund, U.B., The influence of near field hydrogen on actinide solubilities and spent fuel leaching, *Radiochimica Acta*, 88, 507-511, (2000).
- [62] Spahiu, K., Devoy, J., Cui, D.Q., Lundstrom, M., The reduction of U(VI) by near field hydrogen in the presence of $\text{UO}_2(\text{s})$, *Radiochimica Acta*, 92, 597-601, (2004).
- [63] Duro, L., El Aamrani, S., Rovira, M., de Pablo, J., Bruno, J., Study of the interaction between U(VI) and the anoxic corrosion products of carbon steel, *Applied Geochemistry*, 23, 1094-1100, (2008).

- [64] El Aamrani, F.Z., Casas, I., De Pablo, J., Duro, L., Grivé, M., Bruno, J., Experimental and modeling study of the interaction between Uranium(VI) and magnetite. KB Technical Report TR-99-21. Swedish Nuclear Fuel and Waste Management Co., Stockholm, Sweden, in, (1999).
- [65] Grambow, B., Smailos, E., Geckeis, H., Müller, R., Hentschel, H., Sorption and Reduction of Uranium(VI) on Iron Corrosion Products under Reducing Saline Conditions, *Radiochimica Acta*, 74, 149–154, (1996).
- [66] Huber, F., Schild, D., Vitova, T., Rothe, J., Kirsch, R., Schäfer, T., U(VI) removal kinetics in presence of synthetic magnetite nanoparticles, *Geochimica Et Cosmochimica Acta*, 96, 154-173, (2012).
- [67] Ilton, E.S., Boily, J.F., Buck, E.C., Skomurski, F.N., Rosso, K.M., Cahill, C.L., Bargar, J.R., Felmy, A.R., Influence of Dynamical Conditions on the Reduction of U^{VI} at the Magnetite-Solution Interface, *Environmental Science Technology*, 44, 170-176, (2010).
- [68] Latta, D.E., Gorski, C.A., Boyanov, M.I., O'Loughlin, E.J., Kemner, K.M., Scherer, M.M., Influence of Magnetite Stoichiometry on U^{VI} Reduction, *Environmental Science Technology*, 46, 778–786, (2012).
- [69] Liger, E., Charlet, L., Van Cappellen, P., Surface catalysis of uranium(VI) reduction by iron(II), *Geochimica Et Cosmochimica Acta*, 63, 2939-2955, (1999).
- [70] Missana, T., Maffiotte, U., García-Gutiérrez, M., Surface reactions kinetics between nanocrystalline magnetite and uranyl, *Journal of Colloid Interface Science*, 261, 154-160, (2003).
- [71] O'Loughlin, E.J., Kelly, S.D., Cook, R.E., Csencsits, R., Kemner, K.M., Reduction of Uranium(VI) by Mixed Iron(II)/Iron(III) Hydroxide (green rust): Formation of UO₂ Nanoparticles, *Environmental Science Technology*, 37, 721-727, (2003).
- [72] Scott, T.B., Allen, G.C., Heard, P.J., Randell, M.G., Reduction of U(VI) to U(IV) on the surface of magnetite, *Geochimica Et Cosmochimica Acta*, 69, 5639-5646, (2005).
- [73] Scott, T.B., Allen, G.C., Heard, P.J., Lewis, A.C., Lee, D.F., The extraction of uranium from groundwaters on iron surfaces, *Proceedings of the Royal Society a-Mathematical Physical and Engineering Sciences*, 461, 1247-1259, (2005).
- [74] Huber, F., Schild, D., Vitova, T., Rothe, J., Kirsch, R., Schafer, T., U(VI) removal kinetics in presence of synthetic magnetite nanoparticles, *Geochimica Et Cosmochimica Acta*, 96, 154-173, (2012).
- [75] Cantrell, K.J., Kaplan, D.I., Wietsma, T.W., Zero-valent iron for the in-situ remediation of selected metals in groundwater, *Journal of Hazardous Materials*, 42, 201-212, (1995).

- [76] Fiedor, J.N., Bostick, W.D., Jarabek, R.J., Farrell, J., Understanding the Mechanism of Uranium Removal from Groundwater by Zero-Valent Iron Using X-ray Photoelectron Spectroscopy, *Environ. Sci. Technol.*, 32, 1466-1473, (1998).
- [77] Farrell, J., Bostick, W.D., Jarabek, R.J., Fiedor, J.N., Uranium Removal from Ground Water Using Zero Valent Iron media, *Ground Water*, 37, 618-624, (1999).
- [78] Grenthe, I., Wanner, H., Östhols, M., Guidelines for the extrapolation to zero ionic strength, Nuclear Energy Agency, OECD, (2000).
- [79] Fellhauer, D., Neck, V., Altmaier, M., Lutzenkirchen, J., Fanghanel, T., Solubility of tetravalent actinides in alkaline CaCl_2 solutions and formation of $\text{Ca}_4[\text{An}(\text{OH})_8]^{4+}$ complexes: A study of Np(IV) and Pu(IV) under reducing conditions and the systematic trend in the An(IV) series, *Radiochimica Acta*, 98, 541–548, (2010).
- [80] Neck, V., Altmaier, M., Rabung, T., Lutzenkirchen, J., Fanghanel, T., Thermodynamics of trivalent actinides and neodymium in NaCl, MgCl_2 , and CaCl_2 solutions: Solubility, hydrolysis, and ternary Ca–M(III)–OH complexes, *Pure and Applied Chemistry*, 81, 1555–1568, (2009).
- [81] Brendebach, B., Altmaier, M., Rothe, J., Neck, V., Denecke, M.A., EXAFS study of aqueous Zr-IV and Th-IV complexes in alkaline CaCl_2 solutions: $\text{Ca}_3[\text{Zr}(\text{OH})_6]^{4+}$ and $\text{Ca}_4[\text{Th}(\text{OH})_8]^{4+}$, *Inorganic Chemistry*, 46, 6804-6810, (2007).
- [82] Ciavatta, L., The Specific Interaction Theory in Evaluating Ionic Equilibria, *Annali Di Chimica*, 70, 551–567, (1980).
- [83] Kraus, K.A., Nelson, F., Hydrolytic behavior of metal Ions .1. The acid constants of uranium (IV) and plutonium (IV), *Journal of the American Chemical Society*, 72, 3901-3906, (1950).
- [84] Rai, D., Felmy, A.R., Sterner, S.M., Moore, D.A., Mason, M.J., Novak, C.F., The solubility of Th(IV) and U(IV) hydrous oxides in concentrated NaCl and MgCl_2 solutions, *Radiochimica Acta*, 79, 239-247, (1997).
- [85] Altmaier, M., Neck, V., Fanghanel, T., Solubility of Zr(IV), Th(IV) and Pu(IV) hydrous oxides in CaCl_2 solutions and the formation of ternary Ca-M(IV)-OH complexes, *Radiochimica Acta*, 96, 541-550, (2008).
- [86] Rakitskaya, E.M., Tsyplenkova, V.L., S., P.A., Interaction of uranium dioxide with water, *Russian Journal of Inorganic Chemistry*, 41, 1893-1894, (1996).
- [87] Torrero, M.E., Baraj, E., DePablo, J., Gimenez, J., Casas, I., Kinetics of corrosion and dissolution of uranium dioxide as a function of pH, *International Journal of Chemical Kinetics*, 29, 261-267, (1997).

- [88] Neck, V., Altmaier, M., Fanghanel, T., Thermodynamic data for hydrous and anhydrous $\text{PuO}_{2+x}(\text{s})$, *Journal of Alloys and Compounds*, 444, 464-469, (2007).
- [89] Neck, V., Altmaier, M., Seibert, A., Yun, J.I., Marquardt, C.M., Fanghanel, T., Solubility and redox reactions of Pu(IV) hydrous oxide: Evidence for the formation of $\text{PuO}_{2+x}(\text{s, hyd})$, *Radiochimica Acta*, 95, 193-207, (2007).
- [90] Haschke, J.M., Allen, T.H., Morales, L.A., Reactions of plutonium dioxide with water and hydrogen-oxygen mixtures: Mechanisms for corrosion of uranium and plutonium, *Journal of Alloys and Compounds*, 314, 78-91, (2001).
- [91] Schindler, P.W., Heterogeneous Equilibria Involving Oxides Hydroxides Carbonates and Hydroxide Carbonates, *Advances in Chemistry Series*, 67, 196-221, (1967).
- [92] Diaz-Arocas, P., Grambow, B., Solid-liquid phase equilibria of U(VI) in NaCl solutions, *Geochimica Et Cosmochimica Acta*, 62, 245-263, (1998).
- [93] Gorman-Lewis, D., Fein, J.B., Burns, P.C., Szymanowski, J.E.S., Converse, J., Solubility measurements of the uranyl oxide hydrate phases metaschoepite, compreignacite, Na-compreignacite, becquerelite, and clarkeite, *Journal of Chemical Thermodynamics*, 40, 980-990, (2008).
- [94] Meinrath, G., Fischer, S., Köhncke, W., Voigt, W., Solubility behaviour of uranium (VI) in alkaline solution, *Uranium Mining and Hydrogeology*, (1998).
- [95] Rai, B.D., Felmy, A.R., Hess, N.J., LeGore, V.L., McCready, D.E., Thermodynamics of the U(VI)- Ca^{2+} -Cl-OH-H₂O system: Solubility product of becquerelite, *Radiochimica Acta*, 90, 495-503, (2002).
- [96] Valsami-Jones, E., Ragnarsdottir, K.V., Solubility of Uranium Oxide and Calcium Uranate in Water, and Ca(OH)₂-bearing Solutions, *Radiochimica Acta*, 79, 249-257, (1997).
- [97] Yamamura, T., Kitamura, A., Fukui, A., Nishikawa, S., Yamamoto, T., Moriyama, H., Solubility of U(VI) in highly basic solutions, *Radiochimica Acta*, 83, 139-146, (1998).
- [98] Yamazaki, H., Lagerman, B., Symeopoulos, V., Choppin, G.R., Solubility of uranyl in brine, *American Society of Civil Engineers*, 2, 1607-1611, (1992).
- [99] Sandino, M.C.A., Grambow, B., Solubility equilibria in the U(VI)-Ca-K-Cl-H₂O system: Transformation of Schoepite into Becquerelite and Compreignacite, *Radiochimica Acta*, 66-7, 37-43, (1994).
- [100] Hummel, W., Anderegg, G., Puigdoménech, I., Rao, I., Tochiyama, O., Chemical Thermodynamics of U, Np, U, An, Tc, Se, Ni and Zr with selected organic ligands, Vol.9 of chemical thermodynamics, Elsevier Science Publishers, Amsterdam, (2005).

- [101] Gorman-Lewis, D., Burns, P.C., Fein, J.B., Review of uranyl mineral solubility measurements, *Journal of Chemical Thermodynamics*, 40, 335-352, (2008).
- [102] O'Hare, P.A.G., Hoekstra, H.R., Thermochemistry of uranium compounds V. standard enthalpies of formation of monouranates of lithium, potassium, and rubidium, *Journal of Chemical Thermodynamics*, 6, 1161–1169, (1974).
- [103] Cordfunke, E.H.P., Ouweltjes, W., Standard enthalpies of formation of uranium compounds VI. MUO_3 (M= Li, Na, K and Rb), *Journal of Chemical Thermodynamics*, 13, 187–192, (1981).
- [104] Fuger, J., Thermochemistry of the Alkali Metal and Alkaline Earth-Actinide Complex Oxides, *Journal of Nuclear Materials*, 130, 253–265, (1985).
- [105] Van Egmond, A.B., Cordfunke, E.H.P., Investigations on Potassium and Rubidium Uranates, *Journal of Inorganic and Nuclear Chemistry*, 38, 2245–2247, (1976).
- [106] Neck, V., Kim, J.I., An electrostatic approach for the prediction of actinide complexation constants with inorganic ligands-application to carbonate complexes, *Radiochimica Acta*, 88, 815-822, (2000).
- [107] Grenthe, I., Puigdoménech, I., Modelling in Aquatic Chemistry, OECD Nuclear Energy Agency Paris, (1997).
- [108] Schwertmann, U., Cornell, R.M., Iron oxides in the laboratory: preparation and characterization., in, Wiley-VCH, Weinheim, New York, (2000).
- [109] Sørensen, S., Linderstrøm-Lang, K., On the determination and values of π_0 in electromotoric measurements of hydrogen ion concentrations., *C.R. Lab. Carlsberg*, 15, 1-40, (1924).
- [110] Bates, R.G., Definitions of Ph Scales, *Chemical Reviews*, 42, 1-61, (1948).
- [111] Covington, A.K., Bates, R.G., Durst, R.A., Definition of Ph Scales, Standard Reference Values, Measurement of Ph and Related Terminology (Recommendation 1984), *Pure and Applied Chemistry*, 57, 531-542, (1985).
- [112] Buck, R.P., Rondinini, S., Covington, A.K., Baucke, F.G.K., Brett, C.M.A., Camoes, M.F., Milton, M.J.T., Mussini, T., Naumann, R., Pratt, K.W., Spitzer, P., Wilson, G.S., Measurement of pH. Definition, standards, and procedures, *Pure and Applied Chemistry*, 74, 2169-2200, (2002).
- [113] Butler, J.N., Ionic equilibrium: solubility and pH calculations, John Wiley & Sons, New York, (1998).

- [114] Knauss, K.G., Wolery, T.J., Jackson, K.J., A New Approach to Measuring Ph in Brines and Other Concentrated Electrolytes, *Geochimica Et Cosmochimica Acta*, 54, 1519-1523, (1990).
- [115] Altmaier, M., Metz, V., Neck, V., Muller, R., Fanghänel, T., Solid-liquid equilibria of $\text{Mg}(\text{OH})_2(\text{cr})$ and $\text{Mg}_2(\text{OH})_3\text{Cl}\cdot 4\text{H}_2\text{O}(\text{cr})$ in the system $\text{Mg}-\text{Na}-\text{H}-\text{OH}-\text{O}-\text{Cl}-\text{H}_2\text{O}$ at 25°C, *Geochimica Et Cosmochimica Acta*, 67, 3595-3601, (2003).
- [116] Baumann, A., Yalcintas, E., Gaona, X., Altmaier, M., Geckeis, H., Solubility and hydrolysis of Tc(IV) in dilute to concentrated KCl solutions: an extended thermodynamic model for $\text{Tc}^{4+}-\text{H}^+-\text{K}^+-\text{Na}^+-\text{Mg}^{2+}-\text{Ca}^{2+}-\text{OH}^--\text{Cl}^--\text{H}_2\text{O}(\text{l})$ mixed systems, *New J. Chem.*, 41, 9077-9086, (2017).
- [117] Fellhauer, D., Untersuchungen zur Redoxchemie und Löslichkeit von Neptunium und Plutonium, PhD thesis, University of Heidelberg, Germany, (2013).
- [118] Coronel, F.T., Mareva, S., Yordanov, N., Extraction of Uranium(IV) from Phosphoric-Acid Solutions with 1-Phenyl-3-Methyl-4-Benzoylpyrazolone-5 (PMBP), *Talanta*, 29, 119-123, (1982).
- [119] Nagar, M.S., Ruikar, P.B., Subramanian, M.S., Complexes of Tetravalent Plutonium, Uranium and Thorium with Acylpyrazolones, *Inorganica Chimica Acta*, 141, 309-312, (1988).
- [120] JCPDS, Powder diffraction files, in: Joint Committee on Powder Diffraction Standards, Swarthmore, USA, (2001).
- [121] Zimina, A., Dardenne, K., Denecke, M.A., Huttel, E., Lichtenberg, H., Mangold, S., Prüßmann, T., Rothe, J., Spangenberg, T., Steininger, R., Vitova, T., Geckeis, H., Grunwaldt, J.-D., CAT-ACT a new highly versatile X-ray spectroscopy beamline for catalysis and radionuclide science at the KIT synchrotron light facility ANKA, *Review of Scientific Instruments*, (in print), (2017).
- [122] Rothe, J., Butorin, S., Dardenne, K., Denecke, M.A., Kienzler, B., Loble, M., Metz, V., Seibert, A., Steppert, M., Vitova, T., Walther, C., Geckeis, H., The INE-Beamline for actinide science at ANKA, *Rev. Sci. Instrum.*, 83, (2012).
- [123] Zimina, A., Dardenne, K., Denecke, M.A., Doronkin, D.E., Huttel, E., Lichtenberg, H., Mangold, S., Pruessmann, T., Rothe, J., Spangenberg, T., Steininger, R., Vitova, T., Geckeis, H., Grunwaldt, J.D., CAT-ACT-A new highly versatile x-ray spectroscopy beamline for catalysis and radionuclide science at the KIT synchrotron light facility ANKA, *Review of Scientific Instruments*, 88, (2017).
- [124] Ravel, B., Newville, M., ATHENA, ARTEMIS, HEPHAESTUS: data analysis for X-ray absorption spectroscopy using IFEFFIT, *Journal of Synchrotron Radiation*, 12, 537-541, (2005).

- [125] Cohen, D., Carnall, W.T., Absorption spectra of uranium(III) and uranium(IV) in DClO_4 solution, *Journal of Physical Chemistry*, 64, 1933-1936, (1960).
- [126] Lem, W.J., Wayman, M., Decomposition of aqueous dithionite 1. kinetics of decomposition of aqueous sodium dithionite, *Canadian Journal of Chemistry*, 48, 776-&, (1970).
- [127] Wayman, M., Lem, W.J., Decomposition of aqueous dithionite 2. a reaction mechanism for decomposition of aqueous sodium dithionite, *Canadian Journal of Chemistry*, 48, 782-&, (1970).
- [128] Puigdomenech, I., HYDRA and MEDUSA chemical equilibrium software. Software and documentation. <http://web.telia.com/~u15651596/>. in, (2004).
- [129] Kobayashi, T., Scheinost, A.C., Fellhauer, D., Gaona, X., Altmaier, M., Redox behavior of Tc(VII)/Tc(IV) under various reducing conditions in 0.1 M NaCl solutions, *Radiochimica Acta*, 101, 323-332, (2013).
- [130] Yalcintas, E., Gaona, X., Scheinost, A.C., Kobayashi, T., Altmaier, M., Geckeis, H., Redox chemistry of Tc(VII)/Tc(IV) in dilute to concentrated NaCl and MgCl_2 solutions, *Radiochimica Acta*, 103, 57-72, (2015).
- [131] Amadelli, R., Maldotti, A., Sostero, S., Carassiti, V., Photodeposition of uranium oxides onto TiO_2 from aqueous uranyl solutions, *Journal of Chemical Society Faraday Transactions*, 87, 3267-3273, (1991).
- [132] Tan, T.T.Y., Beydoun, D., Amal, R., Photocatalytic reduction of Se(VI) in aqueous solutions in UV/ TiO_2 system: Kinetic modeling and reaction mechanism, *Journal of Physical Chemistry B*, 107, 4296-4303, (2003).
- [133] Wehrli, B., Sulzberger, B., Stumm, W., Redox processes catalyzed by hydrous oxide surfaces, *Chemical Geology*, 78, 167-179, (1989).
- [134] Comarmond, M.J., Payne, T.E., Harrison, J.J., Thiruvoth, S., Wong, H.K., Aughterson, R.D., Lumpkin, G.R., Müller, K., Foerstendorf, H., Uranium Sorption on Various Forms of Titanium Dioxide - Influence of Surface Area, Surface Charge, and Impurities, *Environmental Science Technology*, 45, 5536-5542, (2011).
- [135] Den Auwer, C., Drot, R., Simoni, E., Conradson, S.D., Gailhanou, M., de Leon, J.M., Grazing incidence XAFS spectroscopy of uranyl sorbed onto TiO_2 rutile surfaces, *New Journal of Chemistry*, 27, 648-655, (2003).
- [136] Eliet, V., Bidoglio, G., Kinetics of the Laser-Induced Photoreduction of U(VI) in Aqueous Suspensions of TiO_2 Particles, *Environmental Science and Technology* 32, 3155-3161, (1998).

- [137] Lefevre, G., Kneppers, J., Fédoroff, M., Sorption of uranyl ions on titanium oxide studied by ATR-IR spectroscopy, *Journal of Colloid and Interface Science*, 327, 15-20, (2008).
- [138] Schmidt, J., Vogelsberger, W., Aqueous Long-Term Solubility of Titania Nanoparticles and Titanium(IV) Hydrolysis in a Sodium Chloride System Studied by Adsorptive Stripping Voltammetry, *Journal of Solution Chemistry*, 38, 1267-1282, (2009).
- [139] Felmy, A.R., Rai, D., Schramke, J.A., Ryan, J.L., The Solubility of Plutonium Hydroxide in Dilute-Solution and in High-Ionic-Strength Chloride Brines, *Radiochimica Acta*, 48, 29-35, (1989).
- [140] González-Siso, M.R., Gaona, X., Duro, L., Schild, D., Fellhauer, D., Pidchenko, I., Vitova, T., Altmaier, M., Bruno, J., Interaction of Pu, U and Tc with iron corrosion products under hyperalkaline reducing conditions, in: *Migration Conference*, Santa Fe, USA, (2015).
- [141] Gaona, X., Tits, J., Dardenne, K., Liu, X., Rothe, J., Denecke, M.A., Wieland, E., Altmaier, M., Spectroscopic investigations of Np(V/VI) redox speciation in hyperalkaline TMA-(OH, Cl) solutions, *Radiochimica Acta*, 100, 759-770, (2012).
- [142] Altmaier, M., Neck, V., Fanghanel, T., Solubility and colloid formation of Th(IV) in concentrated NaCl and MgCl₂ solution, *Radiochimica Acta*, 92, 537-543, (2004).
- [143] Altmaier, M., Yalcintas, E., Gaona, X., Neck, V., Müller, R., Schlieker, M., Fanghanel, T., Solubility of U(VI) in chloride solutions. I. The stable oxides/hydroxides in NaCl systems, solubility products, hydrolysis constants and SIT coefficients, *Journal of Chemical Thermodynamics*, 114, 2–13, (2017).
- [144] Yalcintas, E., Redox, solubility and sorption chemistry of technetium in dilute to concentrated saline systems, PhD thesis, Karlsruhe Institute of Technology, (2015).
- [145] Tasi, A., Gaona, X., Fellhauer, D., Böttle, M., Rothe, J., Dardenne, K., Schild, D., Grivé, M., Colàs, E., Bruno, J., Källström, K., Altmaier, M., Geckeis, H., Redox behaviour and solubility of plutonium under alkaline reducing conditions, *Radiochimica Acta*, 106, 259-281, (2017).
- [146] Felmy, A.R., Rai, D., Mason, M.J., The Solubility of Hydrated Thorium(IV) Oxide in Chloride Media: Development of an Aqueous Ion-Interaction Model, *Radiochimica Acta*, 55, 177-185, (1991).
- [147] Uchiyama, H., Nakanishi, S., Kozuka, H., Biomimetic synthesis of nanostructured SnO particles from Sn₆O₄OH₄ in aqueous solution of gelatin, *Crystengcomm*, 17, 628-632, (2015).
- [148] Cooper, M.J., The Analysis of Powder Diffraction Data, *Acta Crystallographica Section A*, 38, 264-269, (1982).

- [149] Conradson, S.D., Manara, D., Wastin, F., Clark, D.L., Lander, G.H., Morales, L.A., Rebizant, J., Rondinella, V.V., Local structure and charge distribution in the $\text{UO}_2\text{-U}_4\text{O}_9$ system, *Inorganic Chemistry*, 43, 6922-6935, (2004).
- [150] Fuger, J., Grenthe, I., Neck, V., Rai, D., *Chemical Thermodynamics of Thorium*, Vol 11 of *Chemical Thermodynamics*, Elsevier Science Publishers, Amsterdam, (2008).
- [151] Fellhauer, D., Altmaier, M., Gaona, X., Neck, V., Lagos, M., Wiss, T., Runke, J., Fanghänel, T., Comparison of plutonium and neptunium redox behaviour in reducing aqueous solution, *Plutonium Futures-The Science 2014*, Las Vegas, USA, (2014).
- [152] Schepperle, J., Fellhauer, D., Gaona, X., Altmaier, M., Geckeis, H., Investigation of the solubility and hydrolysis of $\text{NpO}_2(\text{am, hyd})$ and $\text{PuO}_2(\text{am, hyd})$ in dilute to concentrated NaCl brines, *ABC-Salt IV*, Heidelberg, (2015).
- [153] Endrizzi, F., Gaona, X., Fernandes, M.M., Baeyens, B., Altmaier, M., Solubility and hydrolysis of U(VI) in 0.5 mol/kg NaCl solutions at $T=22$ and 80 degrees C, *Journal of Chemical Thermodynamics*, 120, 45-53, (2018).
- [154] Nipruk, O.V., Chernorukov, G.N., Abrazheev, R.V., Kostrova, E.L., Synthesis and Characterization of Sodium and Potassium Uranates with the Compositions $\text{Na}_2[(\text{UO}_2)_6\text{O}_4(\text{OH})_6]\cdot 8\text{H}_2\text{O}$ and $\text{K}_2[(\text{UO}_2)_6\text{O}_4(\text{OH})_6]\cdot 8\text{H}_2\text{O}$, *Inorganic Materials*, 53, 816-819, (2017).
- [155] Nipruk, O.V., Chernorukov, N.G., Kostrova, E.L., Chernorukov, G.N., Synthesis and Study of Potassium Uranates $\text{K}_2\text{U}_6\text{O}_{19}$ and $\text{K}_2\text{U}_4\text{O}_{13}\cdot 2.2\text{H}_2\text{O}$, *Radiochemistry*, 57, 580-583, (2015).
- [156] Saine, M.C., Synthesis and structure of monoclinic $\text{K}_2\text{U}_2\text{O}_7$, *Journal of Less Common Materials*, 154, 361-365, (1989).
- [157] Gaona, X., Fellhauer, D., Altmaier, M., Thermodynamic description of Np(VI) solubility, hydrolysis, and redox behavior in dilute to concentrated alkaline NaCl solutions, *Pure Applied Chemistry*, 85, 2027-2049, (2013).
- [158] Wieland, E., Van Loon, L.R., *Cementitious Near-Field Sorption Data Base for Performance Assessment of an ILW Repository in Opalinus Clay*. Nagra Technical Report NTB 02-20: Nagra, Wettingen, Switzerland, (2002).

